

---

---

# Development, Validation and Optimization of a Speed Steering System

---

---

Master Thesis  
Kenia Labata Lezaun

Aalborg University  
Electro-Mechanical System Design





**AALBORG UNIVERSITY**  
STUDENT REPORT

**School of Engineering  
and Science**

Fibigerstræde 16

DK - 9220 Aalborg Øst

Tel. 99 40 93 09

lft@mp.aau.dk

<http://www.ses.aau.dk/>

**Title:** Development, Validation and Optimization of a Speed Steering System

**Project:** Master Project

**Project duration:** 01-09-2019 to 03-06-2020

**ECTS:** 50

**Supervisor:** Torben Ole Andersen

**Project members:**

---

Kenia Labata Lezaun

**Report pages:** 67

**Appendix:** 3

**Abstract:**

The purpose of this project is to find a solution to reduce or remove the unwanted vibrations obtained when turning the steering wheel leftwards for an asymmetrical steering unit. In order to find the solution, a mathematical model of the system has been obtained and validated. With this mathematical model, a state space model has been formulated and solved for different key pressure points. With these linearized models a sensitivity analysis has been conducted in order to find the influence of each one of the components in the overall stability and response of the system. The findings provided by this sensitivity analysis have been implemented in an improved model, which does not present the unwanted vibrations.

*By signing this document, each member of the group confirms that everyone has participated in the project work equally and that everyone thus is liable for the content of the report. The content of the report is freely available, but publication (with source) may only be in agreement with the authors.*



# Preface

The report has been composed by one student through the course of the third and fourth semester of the Master's program in Electro-Mechanical System Design at Aalborg University. The models, calculations and graphs in the report are made in either MATLAB, SIMULINK, Microsoft Excel or Origin.

## Reading guide

Prerequisites for reading the report are some knowledge of hydraulic and mechanics, as well other engineering contexts and terminology. The report can be read independently of appendices that serve as additional material for reference. Appendices are named and sorted chronologically the order in which they are referred. Figures and tables are numbered according to chapter, i.e. the first figure and table in chapter 1 has number 1.1, the second, number 1.2, etc. The explanatory text for figures and tables is found under the given figures and tables. Unless otherwise noted, all values are given in SI-units. Sources are all to be found in a list at the end of the report, where books are given by author, title, edition and publisher, while web pages are given by author, title and URL-address. When referring to the sources, the Harvard method is used (referenced in the text with [Surname, Year]).



# Nomenclature

## Greek

Symbol	Description	Unit
$\alpha_{GS}$	Angular displacement of the Gear Set	rad
$\alpha_{SW}$	Angular displacement of the Steering Wheel	rad
$\omega_{GS}$	Angular velocity of the Gear Set	rad/s
$\omega_{SW}$	Angular velocity of the Steering Wheel	rad/s
$\rho_{local}$	Local Mass Density	kg/m <sup>3</sup>

## Latin

Symbol	Description	Unit
$A_{CF}$	Area of the Control Flow Orifice	m <sup>2</sup>
$A_{EF}$	Equivalent area of the Excess Flow Orifices	m <sup>2</sup>
$P_B$	Steering Cylinder pressure	Pa
$P_{CF}$	Control Flow Pressure	Pa
$P_{DYN}$	Dynamic Orifice Pressure	Pa
$P_{EF}$	Excess Flow Pressure	Pa
$P_{GS}$	Gear Set Pressure	Pa
$P_{LS'}$	Pressure after the Load Sensor Orifice	Pa
$P_{LS}$	Load Sensor Pressure	Pa
$P_{PP}$	Pilot Pressure	Pa
$P_P$	Pump Pressure	Pa
$P_{sut}$	Steering Unit to tank pressure	Pa
$P_T$	Tank Pressure	Pa
$Q_{A1,A2R,A2L...}$	Flow through Orifice $A_1, A_{2R}, A_{2L}, A_{3R}, A_{3L}$	m <sup>3</sup> /s
$Q_{CF}$	Control Flow	m <sup>3</sup> /s
$Q_{DYN}$	Dynamic orifice Flow	m <sup>3</sup> /s
$Q_{EF}$	Excess Flow	m <sup>3</sup> /s
$Q_{LS}$	Load Sensor Flow	m <sup>3</sup> /s

---

$Q_{PP}$	Pilot Pressure Flow	$\text{m}^3/\text{s}$
$Q_T$	Flow through Orifice $A_{10}$ to tank	$\text{m}^3/\text{s}$
$T_{GS}$	Gear Set Torque	N m
$T_{SW}$	Steering Wheel Torque	N m

# Contents

<b>1</b>	<b>Introduction</b>	<b>1</b>
1.1	Danfoss Group . . . . .	1
1.2	Steering Unit . . . . .	1
1.2.1	OSPB ON . . . . .	1
1.2.2	OSPS . . . . .	3
1.3	OLS 40 . . . . .	4
1.4	Example of symmetric steering system: OSPF . . . . .	5
1.5	The assembled OSPS LS . . . . .	6
1.6	The Problem . . . . .	8
<b>2</b>	<b>Problem Description</b>	<b>9</b>
<b>3</b>	<b>Methodology</b>	<b>11</b>
<b>4</b>	<b>Mathematical model</b>	<b>13</b>
4.1	Pump . . . . .	14
4.2	OSP 40 Flow Equations . . . . .	14
4.3	Steering unit Flow Equations . . . . .	16
4.4	Displacement of the spool in the priority valve . . . . .	18
4.5	Angular displacement of the steering unit . . . . .	19
4.6	Flows in the Gear Set . . . . .	20
4.7	Steering Cylinder . . . . .	21
4.8	Bulk modulus . . . . .	21
4.9	Equation Summary . . . . .	22
4.9.1	Priority valve . . . . .	22
4.9.2	Steering unit . . . . .	23
4.9.3	Gear set . . . . .	24
4.9.4	Steering cylinder . . . . .	24
<b>5</b>	<b>Validation of the model</b>	<b>25</b>
5.1	Theoretical validation . . . . .	25
5.1.1	Neutral steering . . . . .	25
5.1.2	Rightward steering . . . . .	27
5.1.3	Leftward steering . . . . .	30
5.2	Finding the input . . . . .	31
<b>6</b>	<b>Linearization and State Space model</b>	<b>37</b>
6.1	Linearization . . . . .	37
6.1.1	Flow equation with fixed orifice . . . . .	37

6.1.2	Flow equation with variable orifice . . . . .	38
6.1.3	Flow from spool movement . . . . .	38
6.1.4	Pressure build-up in fixed volume chamber . . . . .	38
6.1.5	Pressure build-up in variable volume chamber . . . . .	38
6.1.6	Flow in gear set . . . . .	38
6.1.7	Newton's second law . . . . .	38
6.2	Summary of the linearized equations . . . . .	39
6.2.1	Priority valve . . . . .	39
6.2.2	Steering unit . . . . .	40
6.2.3	Gear Set . . . . .	40
6.2.4	Steering Cylinder . . . . .	41
6.3	State space Model . . . . .	41
<b>7</b>	<b>Sensitivity Analysis</b>	<b>43</b>
7.1	Specific state space model . . . . .	43
7.2	Analyzing the original linearized model . . . . .	44
7.3	Analyzing the effect of the discharge coefficients . . . . .	46
7.4	Analyzing the effect of the damping coefficient . . . . .	47
7.5	Analyzing the effect of Areas and Volumes . . . . .	49
7.5.1	Effect of the $V_{LS'}$ . . . . .	49
7.5.2	Effect of the $A_{LS'}$ . . . . .	51
7.5.3	Effect of $A_{2R}$ and $\dot{A}_{2R}$ . . . . .	52
7.6	Effect of $V_0$ . . . . .	56
<b>8</b>	<b>Improved Model</b>	<b>59</b>
8.1	Improved linear model . . . . .	59
8.2	Improved nonlinear model . . . . .	61
<b>9</b>	<b>Conclusions and future work</b>	<b>65</b>
	<b>Bibliography</b>	<b>67</b>
<b>A</b>	<b>Data Sheet OLS 40/80</b>	<b>69</b>
<b>B</b>	<b>Linearized parameters</b>	<b>73</b>
<b>C</b>	<b>More sensitivity analysis</b>	<b>75</b>

# 1 | Introduction

In this section, an introduction to the company *Danfoss* will be given, followed by a description of both the priority valve and steering unit used in the project and a brief presentation of the assignment.

## 1.1 Danfoss Group

Although the company was founded in 1931 (originally called *Dansk Køleautomatik og Apparatfabrik*), their intrusion in the hydraulic market was in 1961. Since then, *Danfoss* has become one of the largest manufacturers in the world of steering components for hydrostatic steering systems on off-road vehicles. *Danfoss* steering components are used in vehicles where the driver has to control high steering forces, reliably, comfortably and with maximum safety. The steering unit described in this project is the OSPB ON (due to its simplicity), and the priority valve is the OLS 40. Also, a complex steering system is presented (OSPF LS) as an example of how a symmetric steering system works and its differences with an asymmetric one. Finally, the asymmetric system that is going to be analyzed in the project, the OSPS LS speed steering system, is presented.

## 1.2 Steering Unit

Regardless of brand and model, all steering units are essentially designed with the same task in mind: metering oil from the supply to the steering cylinder in proportion to the angle of the steering wheel. The operation of *Danfoss* steering units OSP- is hydrostatic. That is to say, there is no mechanical connection between the steering column and the steered wheels. Instead there are hydraulic pipes and hoses between steering unit and steering cylinder. When the steering wheel is turned, the steering unit meters in an oil volume proportional to the rate of rotation of the steering wheel. This volume is directed to the appropriate side of the steering cylinder, while simultaneously the displaced oil is directed to tank, [Danfoss, 2017].

### 1.2.1 OSPB ON

OSP is how *Danfoss* name their steering units, and *OSPB* is specifically is for steering units with no valve functions. This steering unit will be described as it is the most simple one, and thus better for understanding the steering process.

The specification *ON* is an abbreviation for Open-center Non-reaction. Open-center steering units have open connections between pump and tank in the neutral position. With Non-reaction steering units, no external forces acting on the steered wheels will result in any corresponding movement of the steering wheel when the driver is not steering the vehicle, [Sauer-Danfoss, 2002].

Since in *ON* steering units the center spool is overlapping both output ports, thus creating a sort of dead-band, this creates good stability properties. However, it may cause the steering to

feel somewhat insensitive and delayed when the steering wheel is only slightly turned. If the steering unit was *OR* (Open center Reacting), this would be solved, since it introduces small gaps between the input and output ports, so the pressure is at all times regulated by continuous throttling. Unfortunately, this also causes stability issues due to the nature of the cross coupling between the chambers, and it decreases in the system efficiency due to continuous throttling. All these problems are attempted to be solved by implementing a priority valve (OLS 40) on the steering unit.

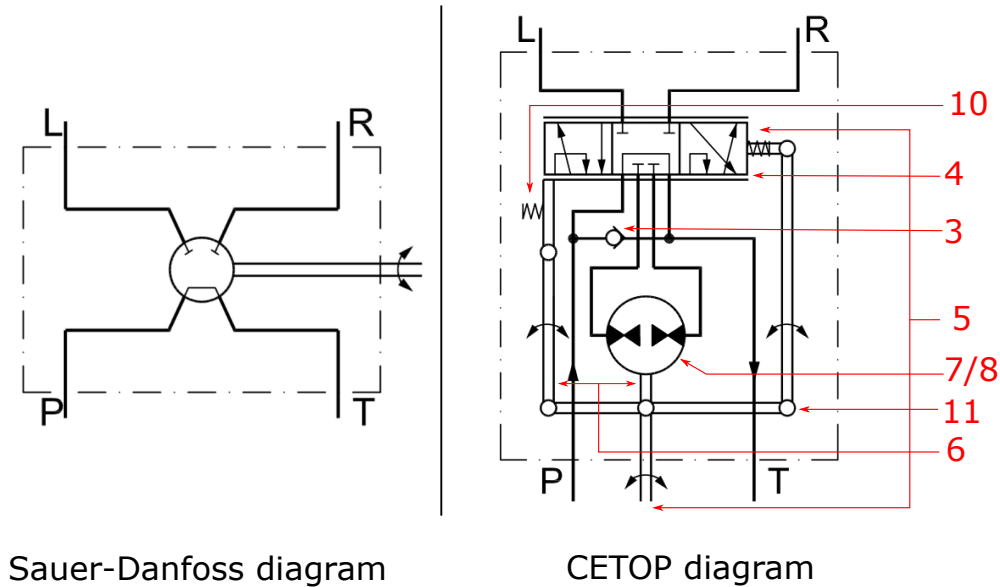


**Figure 1.1:** Diagram of the OSPB ON steering unit. On the left is the Sauer-Danfoss schematic representation and on the right the CETOP one [Sauer-Danfoss, 2002]. In the right diagram, numbers correlating the diagram to some of the pieces showed in Fig.1.2 can be seen.

The steering unit (Fig.1.1) works with the following principle: When the driver needs to steer the vehicle, the steering column is rotated by the steering wheel. The column rotates the spool and the neutral position spring package is deflected. The relative position, spool to sleeve changes. The maximum difference in angle between the spool and sleeve for the OSPB is  $15^\circ$ . Because of this, oil is lead from P-port across the spool/sleeve set to the gear set. Then, from the other side of the gear set, back across spool/sleeve set and the oil will be metered into the correct side of the steering cylinder so that the vehicle wheels move in the corresponding direction to which the steered wheel is rotated. In the same sequence, return oil from the opposite port of the steering cylinder is metered out across the spool/sleeve set to the tank. The gear wheel, cardan shaft, cross pin and sleeve rotates synchronously. The amount of oil metered into the cylinder per revolution is determined by the displacement of the gear set. The steering torque is determined by the force of the spring package, [Danfoss, 2015]. The gear wheel, which is part of the rotary meter, operates as a motor when steering normally, but can operate as a pump when in emergency steering. The emergency steering is activated when the oil flow from the steering system pump is too small or fails, although it requires a manual force of maximum 120 Nm to be able to turn the steering wheel, [Carsten Lund, 2002]. The actual look of all these pieces can be seen in Fig.1.2.

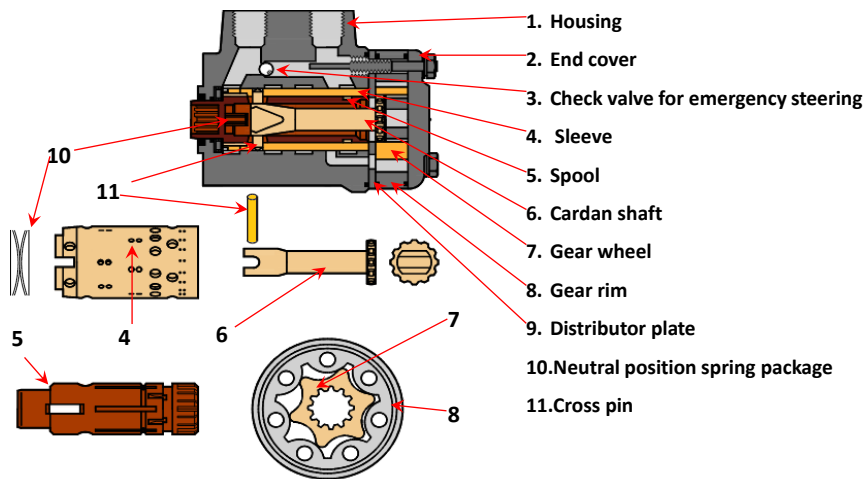


**Figure 1.2:** Drawing of the different parts of a typical steering unit, with the names of the different parts included.

### 1.2.2 OSPS

The steering unit used in this project is the Speed Steering Unit. An ISO/CETOP representation of this steering unit can be seen in Fig.1.3.

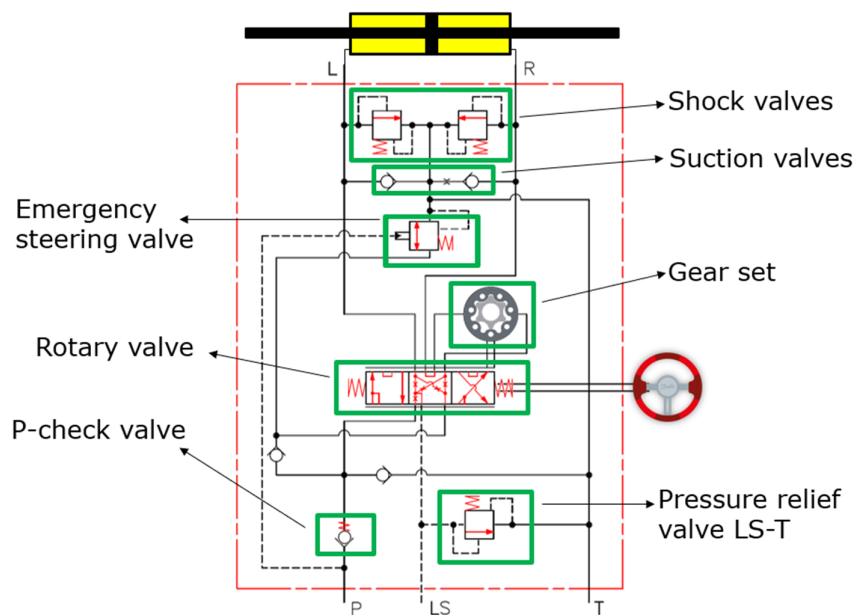


**Figure 1.3:** ISO/CETOP hydraulic design of the Speed steering unit used in this project with the different control valves that it contains.

The shock valves protect the steering unit, limit the maximum external forces on the steering cylinder and limit the maximum pressure drop from L/R to tank (T). The suction valves ensure oil suction to avoid cavitation (space without oil) in the steering cylinder. The check valve protects the driver against steering wheel jerks, by preventing oil from flowing backwards into the pump line when steering against a high pressure on the cylinder side. The check valve is built into the steering unit P connection. When steering against end stroke, the steering pressure will be limited by the pilot pressure relief valve: pressure in LS line will be limited and so the priority valve will lead the pump flow to EF port of the priority valve and on to tank. When

pump flow becomes insufficient, the emergency steering check valve will open and oil will be led to the gear set from the return side of cylinder, additional flow will be sucked from tank as needed, [Sauer-Danfoss, 2002].

The main difference between the OSPB steering unit and the OSPS is that the gear set is placed on the right output port on the OSPS, allowing it to serve as a flow separator between the two chambers when no steering is being done. The new structure permits all bleeds to be partially open under neutral steering conditions, thus transforming the system from ON to OR by definition. This will theoretically improve the transient steering response without sacrificing any straight line stability, if the gear set is considered to be ideal, [Nielsen, 2018]. A comparison between a symmetrical and an asymmetrical steering unit is done later in the chapter.

### 1.3 OLS 40

The OLS 40 is the name of the priority valve implemented in the steering unit. A priority valve ensures that steering always has first priority. When the steering wheel is turned, the oil flow is distributed in the priority valve in such a way that the oil flow necessary for steering is led to the steering unit through the CF (controlled flow) connection. The remaining oil flow is available for the working hydraulics through the EF (excess flow) connection. The distribution is controlled by the LS signal from the steering unit, so that the oil flow to the steering unit is always determined by the actual steering rate, [Danfoss, 2017].

The OLS 40 is a load sensing (LS) priority valve, which means that the flow going to the steering unit changes depending on the momentary demands. It can be either a static or a dynamic priority valve. Static means that there is no oil flow in the LS connection when the steering unit is in neutral position, while dynamic means that there is constant oil flow in the LS connection from the priority valve to the steering unit even when the steering unit is in neutral position. A CETOP diagram of both can be seen in Fig.1.4.

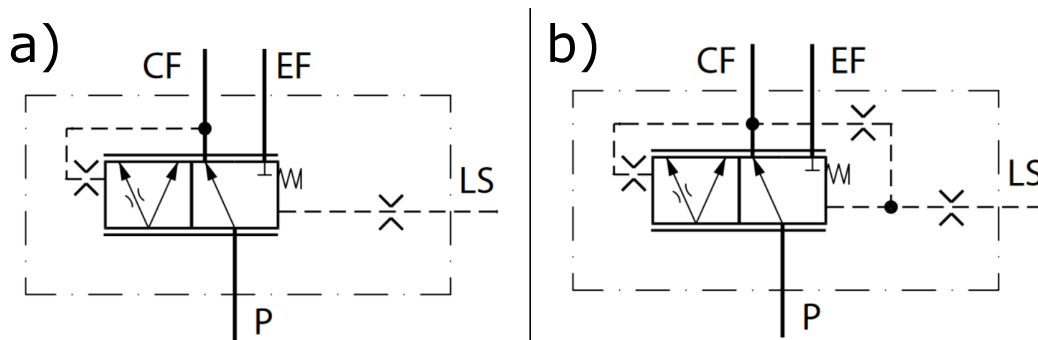


**Figure 1.4:** a) Static LS priority valve b) Dynamic LS priority valve [Danfoss, 2017]

The priority valve used in this project is the OLS 40 dynamic one (the 40 refers to the maximum flow capacity, which is 40l/min). It has been chosen to use the OLS as it is installed inline, and it is therefore easy to measure pressure and flow between the priority valve and the steering unit.

## 1.4 Example of symmetric steering system: OSPF

As an example of how the classical symmetric steering unit works, the OSPF LS steering unit is shown. This steering unit uses the priority valve OLS 80, which has the same internal mechanism than the OLS 40 but has larger dimensions (Appendix.A), since it supports an oil flow of 80 l/min. It is called symmetric due to the fact that the path the oil takes to go from the pump to the steering cylinder is the same one regardless if the input is a leftward or rightward steering. A schematic representation of the OSPF LS steering system and the steering cylinder can be seen in Fig.1.5, where the flow to tank is represented in blue and the flow from the pump is represented in pink. A black line means that there is no flow going through that route.

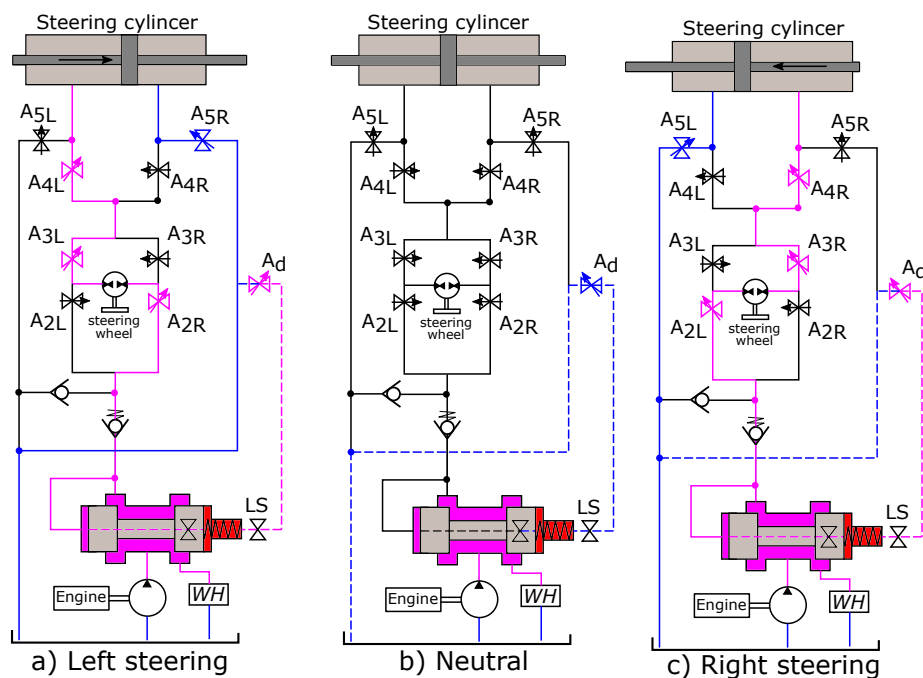


**Figure 1.5:** Representation of the directions of the flow for Leftward, Neutral and Rightward steering.

The inner workings of the OSPF steering system is explained as follows:

- **Neutral steering:** when the wheel is in neutral position, orifices 2, 3, 4, 5 are fully closed and orifice  $A_d$  is fully open. Since it is fully open the oil will flow freely through LS and its pressure will be low. Also since orifices 2-5 are closed, the flow from CF goes to the pilot pressure chamber, then through the dynamic orifice and finally to tank. The rest of the flow goes to the working hydraulics through the EF port.
- **Leftward or Rightward steering:** When the wheel is being steered, orifices 2 and 5 will open and orifice  $A_d$  will start to close (it will close more or less depending on the changes in velocity of the steering). Since  $A_d$  starts to close, the  $P_{LS}$  starts to rise which will lead to the displacement of the spool in order to provide more flow through the CF port ( $A_{CF}$  will increase).

As said before, one of the drawbacks and a reason of why an asymmetric steering unit is being studied, is that for the OSPF (and for all symmetric steering units) the areas of the orifices  $A_2, A_3, A_4, A_5$  do not remain partially open, and so they do not allow leakage. Also, the orifice area of  $A_d$  open and close inversely proportional to the angular lag between the spool and sleeve

of the steering unit. That is, when the steering unit is being turned,  $A_d$  will start closing, which will lead to an increase of the LS pressure. In summary, when the steering unit turns, flow will be supplied to the LS port, increasing the pressure; when the turning stops, the flow will stop and the pressure will decrease.

## 1.5 The assembled OSPS LS

A more complete representation of the OLS 40 priority valve can be seen in Fig.1.6, where the different areas and flows are also represented.

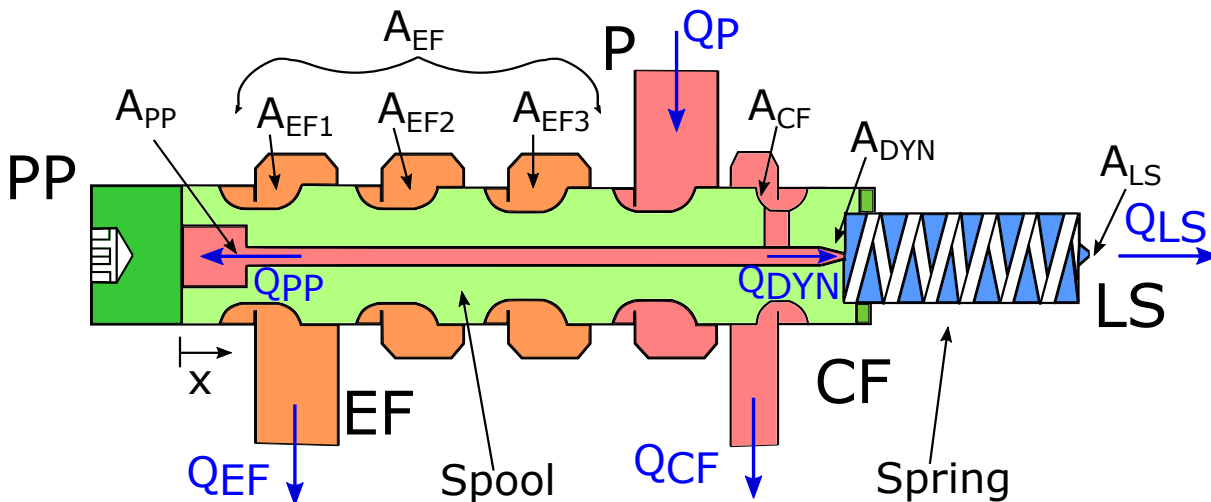


**Figure 1.6:** Representation of the OLS40 priority valve, where the areas and the directions of the different flows are indicated.

The priority valve consists of a pilot assisted spool-spring system, generating the flow sharing between the steering unit and the other working hydraulics. The *CF* (Control Flow) directs the flow to the steering unit, the *PP* is the Pilot Pressure port, the *P* (Pump) port connects to the pump, the *EF* (Excess Flow) directs the flow to the other working hydraulics and the *LS* (Load Sensing) port gives feedback pressure from the steering unit. The excess flow consists in three orifices in order to reduce noise in the OLS when flow is going to the working hydraulics.

The percentage of flow that goes to the *CF* or *EF* ports is generated by the position of the spool. This position depends on the pilot pressure, the spring and the pressure buildup in the spring chamber. So in the end, the quantity of flow that goes through *CF/EF* is controlled by the *CF* and *LS* pressures. When the steering unit is not being used, there will be flow going from the pump to the *EF* port, since the *LS* pressure will be low. When the steering wheel starts to turn, the *LS* pressure will increase and together with the spring move the spool inside the valve. Because of this, flow will start going through the *CF* port and then the flow going through the *EF* port will be reduced or even stopped. The spring in the *LS* line is used to make sure that there is always a standby pressure available for the steering unit, such that the steering process can start immediately instead of having a dead-band while the pump builds up pressure.

The *PP* is connected to the *CF* and serves to dampen the oscillations of the spool such that it does not move back and forth with the pressure pulsations.

Dynamic steering units require a dynamic flow  $Q_{DYN}$  which is normally provided from the priority valve. The amount of flow needed depends on the type of steering unit used, and is adjusted by using the correct dynamic orifice.

The complete system, including the OSPS LS and the steering cylinder can be seen in Fig.1.7, where the different steering directions are represented and where the flow from the pump is colored pink and the flow to the tank is colored blue.

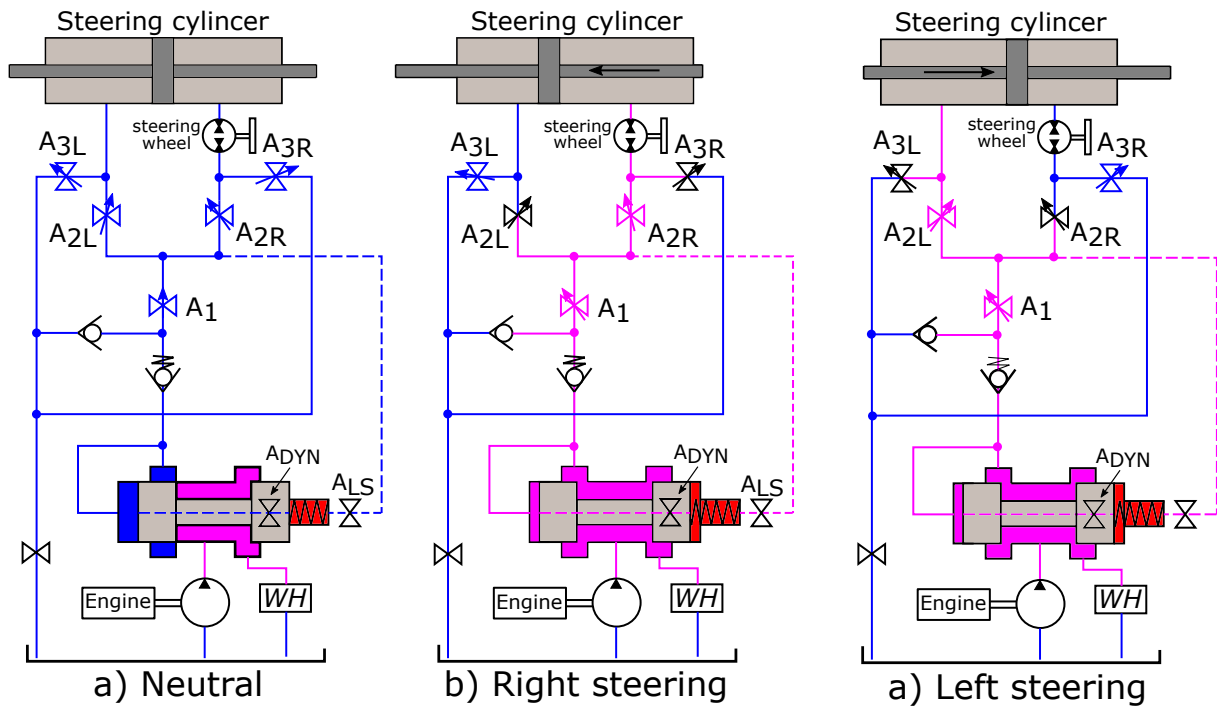


**Figure 1.7:** Representation of the directions of the flow for the two possible steering directions (Left/Right) and for when the wheel is not being steered (Neutral).

Now follows a description of what happens in each of the positions:

- **Neutral:** The priority valve is positioned so the main flow coming from the pump goes to the Working Hydraulics. The LS signal is taken out of the steering unit straight after  $A_1$ . The small quantity of flow in the steering unit gets separated; one part crosses  $A_{2L}$  and goes directly to the left side of the steering cylinder while the other part goes through  $A_{2R}$ , the steering wheel and to the right side. Finally, the standby flow coming from the pump across  $A_1$ ,  $A_2$  and  $A_3$  joins after  $A_{3R}/A_{3L}$  and goes to tank through the emergency steering valve.
- **Right steering:** When the steering wheel starts to rotate to the right  $A_{2R}$  and  $A_{3L}$  begin to enlarge, while  $A_{2L}$  and  $A_{3R}$  start to close. The LS pressure rises which makes the spool inside the priority valve move, widening the opening to the CF port and closing the one to the EF port. From the  $A_{2R}$  orifice the oil goes through the steering wheel (gear set) to the right chamber of the steering cylinder.
- **Left steering:** When the steering wheel rotates to the left, the flow goes through the  $A_{2L}$  orifice instead, and from there directly to the left side chamber of the steering cylinder. The oil in the right side of the SC is pushed through the gear set and dumped in tank.

## 1.6 The Problem

Although it is explained in more detail in the following chapter, the main problem with the steering unit, which this project tries to tackle, is the asymmetric behavior occurring when the steering wheel is turned left and right. It performs correctly when the wheel is in neutral position and when it is turned in the rightward direction, but produces vibrations when the wheel is turned in the leftward direction.

To define the problem to be solved in the project, it is presented in one sentence, the initiating problem:

*Can the reason for the unsatisfactory response described by Danfoss be found and is it possible to change the designed parameters of the model to improve this response?*

## 2 | Problem Description

In this chapter the assignment, set by *Danfoss*, is described. In short terms, the assignment is an analysis of the unsatisfactory response, which appears under some working conditions.

As the OSPS steering unit is still in development, *Danfoss* is investigating the actual system behavior in an experimental setup. The results obtained in this setup show promising results, although some stability issues have arisen, which are believed to come from the asymmetrical configuration of the system (due to the steering wheel being placed on the right side of the system instead of the center). The OSPS LS system performs correctly in the neutral position and when it is being steered to the right, but some instability vibrations appear when it is steered to the left, as it can be seen in Fig.2.1. This behavior may produce discomfort while driving the vehicle and may even compromise the safety of the driver.

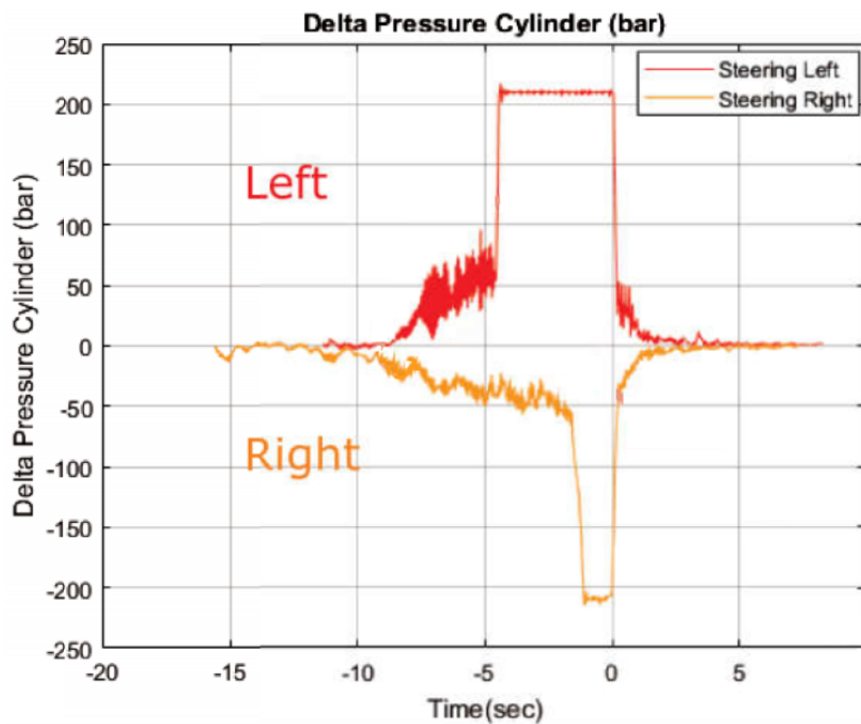


**Figure 2.1:** Pressure oscillations across the steering cylinder both with leftward and rightward steering.

The goals for this project, aimed to solve this issue, are defined from conversations with *Danfoss*:

- Can a mathematical model of the components (priority valve and steering unit) be made to be used for an analysis of the real system?
- Can a sensitivity analysis of the system give the reason and thereby lead to the solution of the instability problem?
- Can stability be obtained by changing the design parameters of the steering system?

In the following chapter, a description of the procedure followed to reach each of the goals is described.



# 3 | Methodology

This chapter presents a short description of the procedure followed throughout the report, and a brief description of what each chapter comprises. Each of the chapters contain a part of the process to find the solution for the problem presented in Chapter 2 (Problem description). This is done to justify each of the chapters and their order in the report, which is the same one followed in reality. In Fig.3.1 a flow chart of the project, with the different paths taken to solve the problem, is presented.

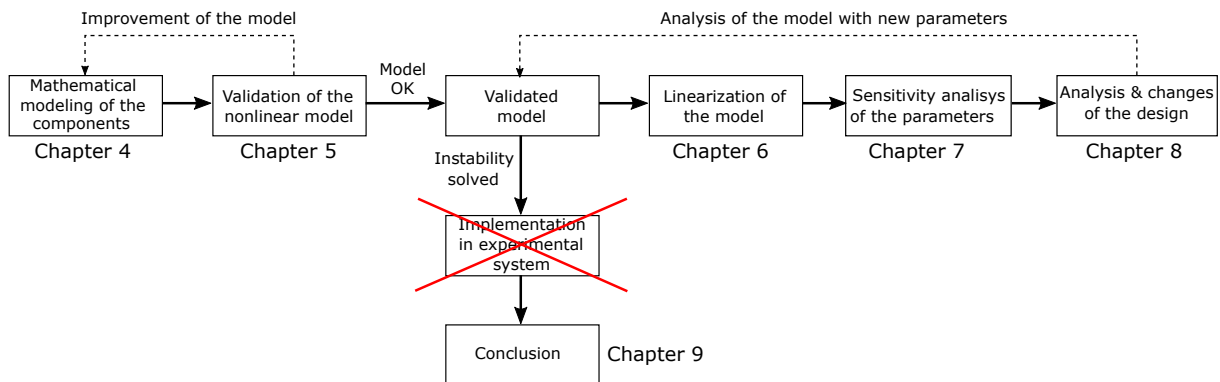


**Figure 3.1:** Flow chart representing the working procedure.

The composition of the remaining report is shown below:

- Chapter 4: Mathematical description of each of the components which, once assembled, gives the complete simulation model.
- Chapter 5: Verification of the model by analyzing its behavior and comparing it to theoretical and experience knowledge.
- Chapter 6: Simplification and linearization of the simulated model.
- Chapter 7: Sensitivity analysis of the different soft parameters.
- Chapter 8: Creation of improved model by changes on the design.
- Chapter 9: Conclusion of the experiment

## Chapter 4: Mathematical Model

The mathematical model is based in a previous Simulink model provided by *Danfoss*. The components described are the OLS 40 priority valve, OSPS steering unit, the gear set and the safety pressure valves.

The types of components modeled are considered to be mechanical translational, mechanical rotational or hydraulic. The procedure for modeling the system is to set up the mathematical equations taken from the laws of physics (Newton's 2nd law, orifice equation, pressure equation,...) and the necessary constants for the components, which are provided by *Danfoss*.

Once all the equations for the different components are obtained, a full mathematical model of the system can be set. To simplify, the steering cylinder that would turn the wheels have been simplified with an orifice which will be slowly draining the flow back to the tank.

The aim of this full mathematical model is to obtain a system that behaves exactly as the real one does when the same input is applied. This verification is done in the following chapter.

## **Chapter 5: Validation of the nonlinear model**

The validation with the real system was not possible, so a theoretical validation is done instead. The flow and pressure responses for different inputs have been recorded and analyzed to verify that the system responds correctly when compared to the responses obtained theoretically. Also, an analysis of the influence on the output by the input is done, in order to find the necessary input for the desired outputs used in the linearization.

## **Chapter 6: Linearization of the model**

A linearized model of the nonlinear system is obtained for three key points of the model. From the linear model, a State Space model is created. This model will be used in the next chapters for the sensitivity analysis and will be the basis for the improved model.

## **Chapter 7: Sensitivity analysis**

Since the validation with the real system was not possible to conduct, a sensitivity analysis of the soft parameters (discharge coefficient, damping coefficient) has been conducted instead. Also, the influence of changing the different areas and volumes of the steering unit on the position of poles and zeros, and thus in the stability and response of the system, have been analyzed.

This analysis has been performed on a linearization point placed on the range of pressures where the unwanted vibrations have been found, that is, at 50 bar.

## **Chapter 8: Creation of improved model**

An improved model has been created, choosing new parameters that would improve the stability and response curve of the system. The new model has been designed following the premise that the parameters can only be adjusted and not completely changed, since radical changes could work in the simulation but have no sense physically. For example, theoretically an orifice area could be increased by 100 times, but that area would not physically fit in the volume to which it is attached, and thus the simulation would not be able to know.

Also, the new values of the discharge coefficients and damping coefficient have been chosen by researching its value in other similar models.

Both a linear and a nonlinear version of the improved model are created.

# 4 | Mathematical model

In this chapter, the mathematical model of the system is extracted from the Simulink model. Throughout the chapter, there are drawings representing how the different equations look like in Simulink blocks form, and how these equations are being calculated by Simulink. The steering cylinder has been simplified to look like an orifice, and the flow going through the Excess Flow orifices, instead of going to the Working Hydraulics (other parts of the vehicle that also use oil, like an hydraulic crane) is bleeding directly to tank. In order to simplify the model even further, it is assumed that the hydraulic flow is supplied by a fixed displacement pump rotating at a constant speed, since this allows the pump flow to be used as the model's input.

The mathematical model uses two basic hydraulic equations:

## Pressure equation

The pressure equation is used to calculate the pressure build-up in a volume. In a lumped volume the flow rate is integrated with respect to time to calculate the pressure. The describing differential equation is

$$\dot{P} = \frac{\beta}{V} \cdot (Q_{in} - Q_{out}) \quad (4.1)$$

where  $\beta$  is the bulk modulus,  $Q_{in}$  is the flow coming into the volume,  $Q_{out}$  is the flow coming out of the volume and  $V$  is the volume. The bulk modulus accounts for the stiffness of the fluid-air mixture, as this parameter influences the compressibility of the oil.

## Orifice equation

Control valves rely on variable orifices to regulate certain parameters within a hydraulic system. As the orifice has a flow area smaller than the rest of the pipe/tube, the flow velocity will, due to continuity, increase and be higher in the orifice. This change in flow velocity will induce a pressure drop. Taking into account Bernoulli's equation for incompressible fluids the following equation is obtained:

$$Q = C_d \cdot A \cdot \sqrt{\frac{2}{\rho}} \cdot \text{sign}(P_{in} - P_{out}) \cdot \sqrt{|P_{in} - P_{out}|} \quad (4.2)$$

Where  $Q$  is the flow going through the orifice,  $C_d$  is the discharge coefficient of the orifice,  $A$  is the area of the orifice,  $\rho$  is the atmospheric mass density, and  $P_{in}/P_{out}$  are the pressures at both sides of the orifice. This version of the orifice equation accounts for the flow direction; that is why a sign convention has to be established beforehand. For a variable orifice, the area will be dependent of time or position.

For the mechanical translational and rotational parts (so the forces acting in the different spool/sleeves):

## Newton's Second Law

The second law states that the acceleration of an object is dependent upon two variables: the net force acting upon the object and the mass of the object.

$$\sum F = M\ddot{x}_p \quad (4.3)$$

Where  $\ddot{x}$  is the acceleration of the piston (or  $\ddot{\alpha}$  when talking about the the rotational acceleration of the steering unit) and  $M$  is the mass of the piston.

## 4.1 Pump

The pump is modeled as a constant flow pump, with a flow of  $Q_P = 40\text{l/min}$ . The pump chamber has a volume of  $V_P = 1\text{l}$ , where the pressure  $P_P$  is built up.

$$\dot{P}_P = \frac{\beta}{V_P} \cdot (Q_P - Q_{CF} - Q_{EF}) \quad (4.4)$$

## 4.2 OSP 40 Flow Equations

The flow/pressure equations for the priority valve have to be obtained. To do this, the Simulink model given by *Danfoss* is analyzed. An explanatory drawing of how the different flows behave and where the different pressures are located is given in Fig.4.1. Also, a miniature of Fig.1.6 is shown in the top left corner, as a reminder of how it looks in real life.

$$Q_{EF} = \frac{P_P - P_{EF}}{((P_P - P_{EF})^2 + P_{trans}^2)^{1/4}} \cdot C_{d1} A_{EF}(x) \cdot \sqrt{\frac{2}{\rho_{local}}} \quad (4.5)$$

$$Q_{CF} = \frac{P_P - P_{CF}}{((P_P - P_{CF})^2 + P_{trans}^2)^{1/4}} \cdot C_{d1} A_{CF}(x) \cdot \sqrt{\frac{2}{\rho_{local}}} \quad (4.6)$$

$$Q_{PP} = \frac{P_{CF} - P_{PP}}{((P_{CF} - P_{PP})^2 + P_{trans}^2)^{1/4}} \cdot C_{d2} A_{PP} \cdot \sqrt{\frac{2}{\rho_{local}}} \quad (4.7)$$

$$Q_{DYN} = \frac{P_{CF} - P_{SpC}}{((P_{CF} - P_{SpC})^2 + P_{trans}^2)^{1/4}} \cdot C_{d2} A_{DYN} \cdot \sqrt{\frac{2}{\rho_{local}}} \quad (4.8)$$

$$Q_{LS} = \frac{P_{SpC} - P_{LS}}{((P_{SpC} - P_{LS})^2 + P_{trans}^2)^{1/4}} \cdot C_{d2} A_{LS} \cdot \sqrt{\frac{2}{\rho_{local}}} \quad (4.9)$$

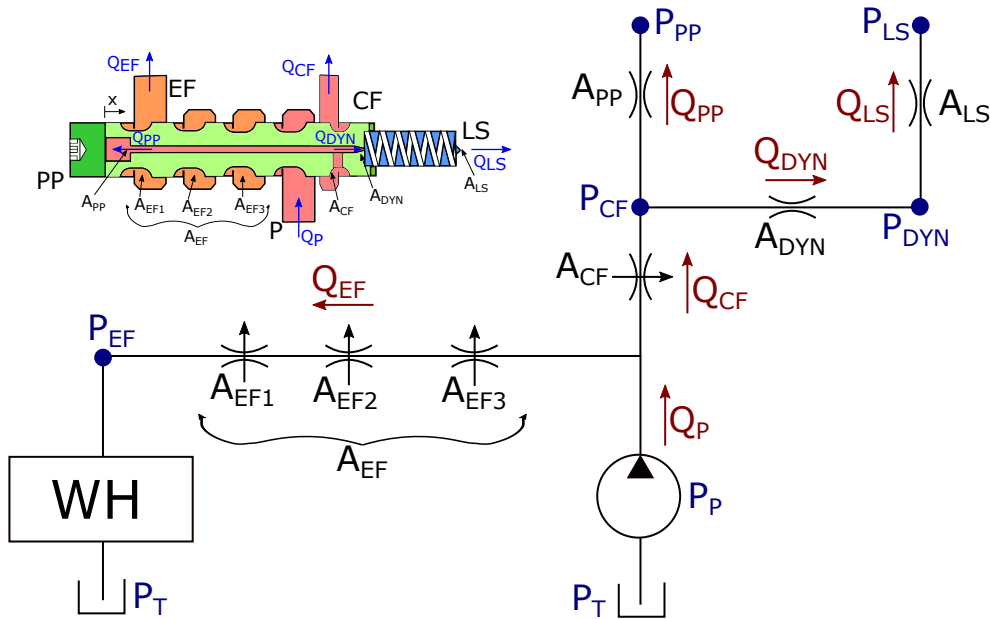


**Figure 4.1:** Schematic representation of the OPS 40 priority valve with the different orifices modeled (whose areas are named  $A_n$ ). The *WH* represents the working hydraulics, and the direction of the different flows are represented by the  $Q$ . The pressures are  $P_n$ . In the top left there is a reminder of how the OLS 40 looks taken from Fig.1.6.

The look up tables for the Excess Flow and Control Flow orifice areas are obtained experimentally from the setup in *Danfoss* and look like Fig.4.2.

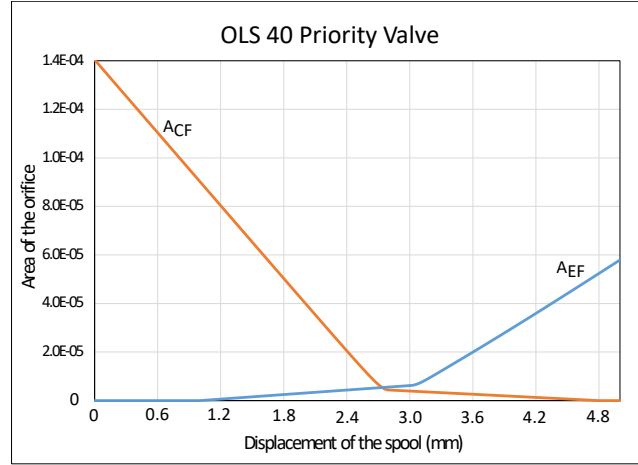


**Figure 4.2:** Graph representation of the opening of the EF and CF orifices depending on the position of the spool

The pressure buildup for both the Control Flow and Load Sensing chambers are obtained through the equations (4.10) and (4.11), respectively.

$$\dot{P}_{CF} = \frac{\beta}{V_{CF}} \cdot (Q_{CF} - Q_{Dyn} - Q_{PP} - Q_{A1}) \quad (4.10)$$

$$\dot{P}_{LS} = \frac{\beta}{V_{LS}} \cdot (Q_{LS} - Q_{LS'}) \quad (4.11)$$

Where the volumes are given in Table 4.1.

The pressure in the Spool Chamber ( $P_{SpC}$ ) and the Pilot Pressure ( $P_{PP}$ ) are obtained with the pressure buildup equation for chambers with variable volumes in equations. (4.12) and (4.13), respectively.

$$\dot{P}_{SpC} = \frac{V_{SpCi}}{\beta} \cdot \Delta Q_{SpC} \quad (4.12)$$

$$\dot{P}_{PP} = \frac{V_{PPi}}{\beta} \cdot \Delta Q_{pp} \quad (4.13)$$

Where  $V_{SpCi}$  and  $V_{PPi}$  are the initial volumes of the chamber and are defined in Table 4.1,  $\beta$  is the bulk modulus and  $\Delta Q_{SpC}$  and  $\Delta Q_{PP}$  are the change in flow in the respective chambers.

This change in flow depends both of the flow that comes from the orifices and the one created by the movement of the spool (Eq.4.14 and Eq.4.15).

$$\Delta Q_{SpC} = A_{sp} \cdot \dot{x} + Q_{Dyn} + Q_{LS} \quad (4.14)$$

$$\Delta Q_{PP} = A_{sp} \cdot \dot{x} + Q_{PP} \quad (4.15)$$

Where the Spool Area  $A_{sp}$  of the Priority Valve is defined in Table 4.3.

Symbol	Description	Value	Unit
$V_{CF}$	Volume of Control Flow chamber	0.005	l
$V_{LS}$	Volume Load Sensing chamber	0.001	l
$V_{PPi}$	Initial volume Pilot Pressure chamber	0.005	l
$V_{SpCi}$	Initial volume Spool chamber	0.00712	l

**Table 4.1:** The table defines the constant values for the different volumes of the OLS 40.

These Pilot Pressure and Spool Chamber pressure are used later to obtain the displacement  $x$  of the spool.

### 4.3 Steering unit Flow Equations

The same procedure used for the priority valve is again followed for obtaining the OSPS flow equations. An explanatory drawing of the flow system on the steering unit can be seen in Fig.4.3. In this figure the different orifices are represented in black, the flow directions in red and pressures in blue.

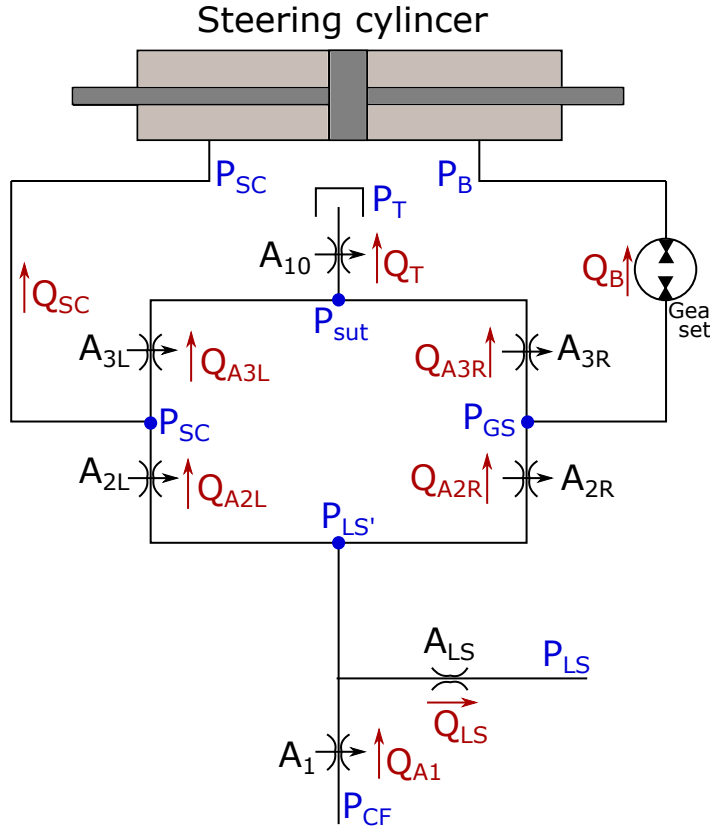


**Figure 4.3:** Schematic representation of the flows and pressures on the OSPS steering unit.

$$Q_{LS'} = \frac{P_{LS} - P_{LS'}}{((P_{LS} - P_{LS'})^2 + P_{trans}^2)^{1/4}} \cdot C_{d2} A_{LS} \cdot \sqrt{\frac{2}{\rho_{local}}} \quad (4.16)$$

$$Q_{A1} = \frac{P_{CF} - P_{LS'}}{((P_{CF} - P_{LS'})^2 + P_{trans}^2)^{1/4}} \cdot C_{d2} A_1(\alpha) \cdot \sqrt{\frac{2}{\rho_{local}}} \quad (4.17)$$

$$Q_{A2R} = \frac{P_{LS'} - P_{GS}}{((P_{LS'} - P_{GS})^2 + P_{trans}^2)^{1/4}} \cdot C_{d2} A_{2R}(\alpha) \cdot \sqrt{\frac{2}{\rho_{local}}} \quad (4.18)$$

$$Q_{A2L} = \frac{P_{LS'} - P_{SC}}{((P_{LS'} - P_{SC})^2 + P_{trans}^2)^{1/4}} \cdot C_{d2} A_{2L}(\alpha) \cdot \sqrt{\frac{2}{\rho_{local}}} \quad (4.19)$$

$$Q_{A3L} = \frac{P_{SC} - P_{sut}}{((P_{SC} - P_{sut})^2 + P_{trans}^2)^{1/4}} \cdot C_{d2} A_{3L}(\alpha) \cdot \sqrt{\frac{2}{\rho_{local}}} \quad (4.20)$$

$$Q_{A3R} = \frac{P_{GS} - P_{sut}}{((P_{GS} - P_{sut})^2 + P_{trans}^2)^{1/4}} \cdot C_{d2} A_{3R}(\alpha) \cdot \sqrt{\frac{2}{\rho_{local}}} \quad (4.21)$$

$$Q_T = \frac{P_{sut} - P_T}{((P_{sut} - P_T)^2 + P_{trans}^2)^{1/4}} \cdot C_{d2} A_{10}(\alpha) \cdot \sqrt{\frac{2}{\rho_{local}}} \quad (4.22)$$

As for the priority valve, for the different orifices areas, a look-up table obtained through *Danfoss* experiments is used (Fig.4.4). As it has already been mentioned, for a neutral position of the spool (so in the center of the graph), all the valves are partially open.

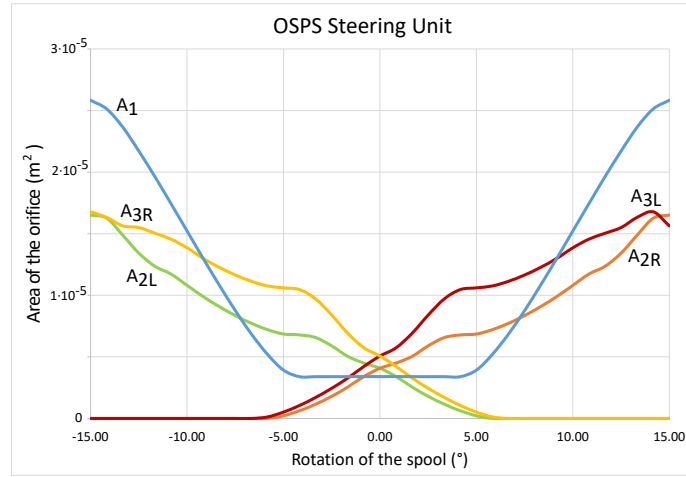


**Figure 4.4:** Graphical representation of the OSPS orifice opening areas in relation of the rotation of the spool.

Symbol	Description	Value	Unit
$P_{trans}$	Transition Pressure	12	Pa
$C_{d2}$	Orifice constant	0.7	—
$\phi_{LS}$	Diameter of the Load Sensor Orifice	2.5	mm

**Table 4.2:** The table defines the hydraulic constant values for the OLS 40.

The pressure buildup for the  $LS'$  and steering unit to tank ( $sut$ ) chambers are obtained with (4.23) and (4.24) respectively.

$$\dot{P}_{LS'} = \frac{\beta}{V_{LS'}} \cdot (Q_{A1} - Q_{LS'} - Q_{A2R} - Q_{A2L}) \quad (4.23)$$

$$\dot{P}_{sut} = \frac{\beta}{V_{sut}} \cdot (Q_{A3L} + Q_{A3R} - Q_T) \quad (4.24)$$

Where the volumes are  $V_{LS'} = 0.0011$  and  $V_{sut} = 0.0051$ . Also, the pressure  $P_{SC}$  which is the pressure in the left side of the steering cylinder is obtained with (4.25).

$$\dot{P}_{SC} = \frac{\beta}{V_L} \cdot (Q_{SC} - Q_B) \quad (4.25)$$

Where  $V_L = 0.0051$  is the volume on the left side of the steering cylinder and  $Q_{SC} = Q_{A2L} + Q_{A3L}$ .

#### 4.4 Displacement of the spool in the priority valve

To obtain the displacement of the spool, Newton's 2<sup>nd</sup> Law is used. This displacement is used to extrapolate from a look-up table the opening areas of the  $EF$  and  $CF$  variable orifice valves (Fig.4.2). The equation obtained is:

$$m_{sp}\ddot{x} = P_{PP} A_{SP} - P_{SpC} A_{SP} + (F_{CF} - F_{EF}) - b_{ols}\dot{x} - k_{spring} x \quad (4.26)$$

As it can be seen in Fig.4.5 to obtain the displacement of the spool the following steps are done:

- In (1) the difference  $(F_{CF} - F_{EF})$  obtained in the linear endstop and  $F_{PP}$  (which is  $P_{PP} \cdot A_{sp}$ ) are added.
- In (2) the spring constant is multiplied by the displacement of the spool  $(-k_{spring} \cdot \Delta x)$
- In (3) the damping force, which takes into account both Coulomb and Stribeck frictions, is obtained  $(-b_{ols} \cdot \dot{x})$
- (4) adds both (2) and (3)
- (5) adds (4) with the negative force from the Spool Chamber,  $-F_{SpC}$  (negative since the Pilot Pressure one is positive,  $P_{SpC} \cdot A_{sp}$ )
- In (6) both  $F_1$  and  $F_2$  are added and divided by the mass of the spool ( $m_{sp}$ ), and this  $\ddot{x}$  obtained is internally integrated to get the velocity ( $\dot{x}$ ). This velocity is integrated again outside to get the displacement of the spool.

The friction coefficient ( $b_{ols}$ ) used in (3) is obtained with the following equation:

$$b_{ols} \cdot \dot{x} = \sqrt{2}e(F_{brk} - F_C) \cdot e^{-\left(\frac{\dot{x}}{v_{st}}\right)^2} \cdot \frac{\dot{x}}{v_{st}} + F_C \cdot \tanh \frac{\dot{x}}{v_C} + b \cdot \dot{x} \quad (4.27)$$

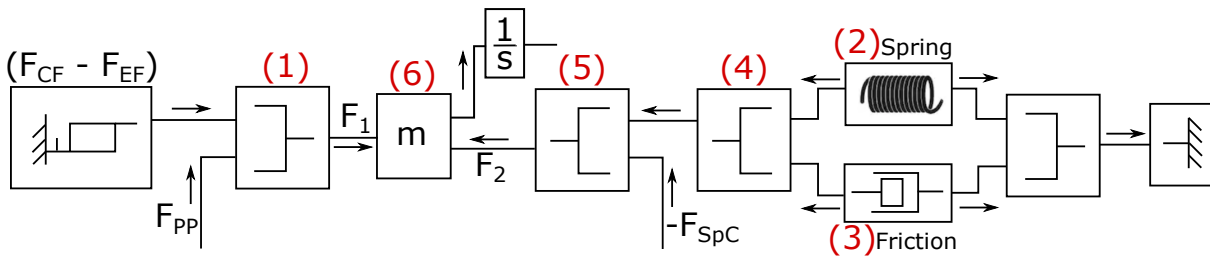


**Figure 4.5:** Simulink model to obtain the displacement of the spool on the priority valve.

Symbol	Description	Value	Unit
$C_{d1}$	Orifice constant	0.645	--
$C_{d2}$	Orifice constant	0.700	--
$\phi_{PP}$	Diameter of Pilot Pressure Orifice	0.8	mm
$\phi_{DYN}$	Diameter of Dynamic Orifice	0.9	mm
$\phi_{LS}$	Diameter of Load Sensor Orifice	1.2	mm
$P_{trans}$	Transition pressure	12	Pa
$T_{fl}$	Global Fluid temperature	70	°C
$m_{sp}$	Priority Valve Spool mass	0.06	kg
$A_{sp}$	Priority Valve Spool area	200.8609	mm <sup>2</sup>
$k_{spring}$	Priority Valve Spring stiffness	16,700	N/m
$s_{init}$	Spring pre-compression	10.1	mm
$F_{pre}$	Priority Valve Spring precharge	170	N
$b$	Viscous friction coefficient	20	N/(m/s)
$F_C$	Coulomb friction	0.5	N
$F_{brk}$	Breakaway friction	1.0	N
$v_{brk}$	Breakaway velocity	0.001	m/s
$v_{st}$	Stribeck velocity threshold	$v_{brk} \cdot \sqrt{2}$	m/s
$v_C$	Coulomb velocity threshold	$v_{brk}/10$	m/s

**Table 4.3:** The table defines the constant values for hydraulic part of the OSPS and the mechanical part of the OLS 40.

## 4.5 Angular displacement of the steering unit

The  $\alpha$  (the lag) that is used in the different variable orifice valves is obtained by subtracting the rotation of the Gear Set from the one of the Steering Wheel ( $\omega_{SW} - \omega_{GS}$ ). This difference in velocities is integrated to obtain the lag in displacement. The angular velocity of the steering wheel, which is the one that moves the spool, is produced manually by turning the steering wheel. The angular velocity of the gear set moves the sleeve, and is calculated using the Newton's second law in the Gear Set, expressed by equation (4.28).

$$J_{sl} \cdot \ddot{\alpha} = M_{nps} + T_{sss} + \omega_{GS} \cdot b_{GS} + (P_R - P_{GS}) \cdot \frac{V_0 \cdot 10^{-6}}{2\pi} \quad (4.28)$$

Where  $J_{sl}$  is the moment of inertia of the sleeve, gear wheel and cardan shaft,  $M_{nps}$  is the moment of forces obtained from the neutral position spring (which depends on the lag between angles, as seen in Fig.4.6),  $T_{sss}$  is torque obtained in the spool sleeve set,  $P_R$  and  $P_{GS}$  are the pressures in the right side of the steering cylinder and Gear set respectively,  $V_0$  is the displacement per revolution and  $b_{GS}$  is the damping coefficient in the Gear set.

This  $T_{sss}$  takes different forms depending on whether the lag ( $\Delta\alpha$ ) is inside the limits  $[-15^\circ, +15^\circ]$  or outside (4.29)

$$T_{sss} = \begin{cases} 0 & \text{if } -15^\circ < \Delta\alpha < +15^\circ \\ 2 \cdot \Delta\alpha \cdot k_{sp} + \dot{\alpha} D, & \text{if } -15^\circ \leq \Delta\alpha \text{ or } 15^\circ \geq \Delta\alpha \end{cases} \quad (4.29)$$

Where  $k_{sp}$  is the stiffness spring constant and  $D$  is a damping coefficient (as seen in Table 4.4).

$P_{GS}$  is the pressure buildup between the spool-sleeve set and the gear set, and is obtained through Eq.(4.30)

$$\dot{P}_{GS} = \frac{\beta}{V_{SS-GS}} \cdot (Q_{GS-R} - Q_{GS'}) \quad (4.30)$$

Where  $V_{SS-GS} = 0.0051$ ,  $Q_{GS-R} = Q_{A2R} + Q_{A3R}$  and  $Q_{GS'}$  is described in the next section.

Symbol	Description	Value	Unit
$b_{GS}$	Damping coefficient	0.1	Nm s/rad
$J_{sl}$	Inertia of sleeve	$6.17 \cdot 10^{-5}$	kg · m <sup>2</sup>
$k_{sp}$	Spring constant	$10^5$	N · m/ deg
$D$	Damping coefficient	1000	N · m · s/ deg
$V_0$	Displacement per revolution	135	ccm/rev

**Table 4.4:** The table defines the stiffness and damping constants for the spool-sleeve set torque.

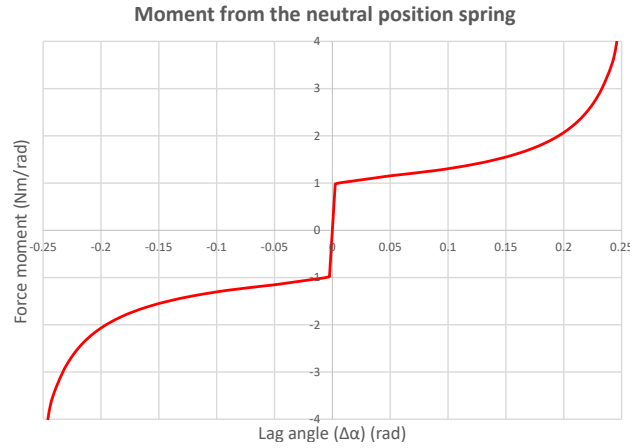


**Figure 4.6:** Look-up table of the constants for the spool-sleeve set.

## 4.6 Flows in the Gear Set

In the Gear set, the pressure from the right side of the of the Steering cylinder ( $P_R$ ) and the pressure in the gear set chamber ( $P_{GS}$ ) are used together with  $\omega_{GS}$  and the leakage coefficient ( $k_{leak}$ ) to obtain both  $Q_{GS'}$  (which is the flow going to the steering unit)(4.31) and  $Q_{GS-R}$  which is the flow going from the gear set towards the right side of the steering cylinder(4.32)

$$Q_{GS'} = -P_{GS} \cdot \frac{k_{leak}}{60 \cdot 10^3 \cdot 10^5} - \frac{V_0 \cdot 10^{-6}}{2\pi} \cdot \omega_{GS} \quad (4.31)$$

$$Q_{GS-R} = -P_R \cdot \frac{k_{leak}}{60 \cdot 10^3 \cdot 10^5} + \frac{V_0 \cdot 10^{-6}}{2\pi} \cdot \omega_{GS} \quad (4.32)$$

Where  $k_{leak}$  has a value of  $10^{-4}$  lpm/bar

The pressure on the right side of the steering cylinder is obtained through Eq.(4.33)

$$\dot{P}_R = \frac{\beta}{V_R} \cdot (Q_B - Q_{GS-R}) \quad (4.33)$$

Where the volume on the right chamber is  $V_R = 0.0051$

## 4.7 Steering Cylinder

To simplify the model, the steering cylinder allowing the wheels to turn is instead modeled by an orifice with  $P_{SC}$  as the input pressure, described in the Steering unit section, and as output the  $P_R$  pressure described in the Gear set section. The flow going through this orifice is:

$$Q_B = \frac{P_{SC} - P_R}{((P_{SC} - P_R)^2 + P_{trans}^2)^{1/4}} \cdot C_{d3} \cdot A_{L/R} \cdot \sqrt{\frac{2}{\rho_{local}}} \quad (4.34)$$

Symbol	Description	Value	Unit
$P_{trans}$	Transition Pressure	12	Pa
$C_{d3}$	Orifice Constant	0.72	--
$\phi_{L/R}$	Diameter of the orifice	1.5	mm

**Table 4.5:** The table defines the constant values for the Steering Cylinder.

## 4.8 Bulk modulus

The formula used to obtain the bulk modulus used in this system is shown in Eq.4.35:

$$\beta_{eff} = \frac{1 + V_{fr} \cdot \left(\frac{P_a}{P_a + P}\right)^{1/\kappa}}{1 + \frac{\left(\frac{P_a}{P_a + P}\right)^{1/\kappa} \cdot V_{fr} \cdot \frac{E_L}{\kappa}}{P_a + P}} \cdot E_L \quad (4.35)$$

Where,  $E_L$  is the pure liquid bulk modulus,  $V_{fr}$  is the relative gas content at atmospheric pressure ( $V_G/V_L$ ),  $P_a$  is the atmospheric pressure,  $P$  is the gauge pressure of the fluid in the chamber and  $\kappa$  is a gas-specific heat ratio.

Symbol	Description	Value	Unit
$V_{fr}$	Content of free air	0.01	--
$\kappa$	Polytropic exponent	1	--
$P_a$	Atmospheric pressure	$10^5$	Pa

**Table 4.6:** The table defines the constant values for Bulk modulus.

The look-up table for the pure liquid bulk modulus depending on the gauge pressure (which is the input pressure) can be seen in Fig.4.7.

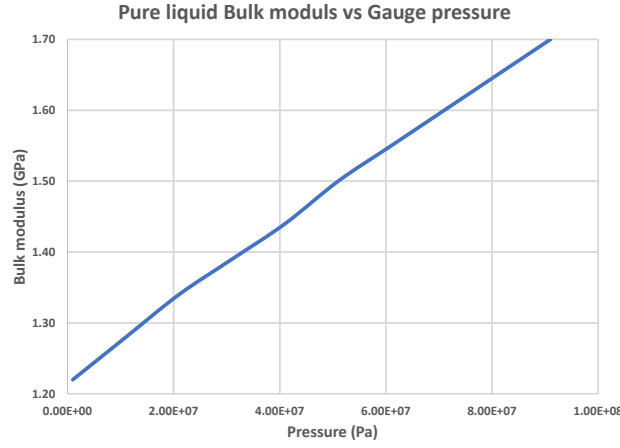


Figure 4.7: Look-up table relating the input pressure with the bulk modulus of the liquid.

## 4.9 Equation Summary

The compilation of the equations that are subsequently linearized are the following.

### 4.9.1 Priority valve

First, the hydraulic part of the priority valve can be separated in three different types of equations. The flow equations in the priority valve are:

$$Q_{EF} = \frac{P_P - P_{EF}}{((P_P - P_{EF})^2 + P_{trans}^2)^{1/4}} \cdot C_{d1} A_{EF}(x) \cdot \sqrt{\frac{2}{\rho_{local}}} \quad (4.36)$$

$$Q_{CF} = \frac{P_P - P_{CF}}{((P_P - P_{CF})^2 + P_{trans}^2)^{1/4}} \cdot C_{d1} A_{CF}(x) \cdot \sqrt{\frac{2}{\rho_{local}}} \quad (4.37)$$

$$Q_{PP} = \frac{P_{CF} - P_{PP}}{((P_{CF} - P_{PP})^2 + P_{trans}^2)^{1/4}} \cdot C_{d2} A_{PP} \cdot \sqrt{\frac{2}{\rho_{local}}} \quad (4.38)$$

$$Q_{DYN} = \frac{P_{CF} - P_{SpC}}{((P_{CF} - P_{SpC})^2 + P_{trans}^2)^{1/4}} \cdot C_{d2} A_{DYN} \cdot \sqrt{\frac{2}{\rho_{local}}} \quad (4.39)$$

$$Q_{LS} = \frac{P_{SpC} - P_{LS}}{((P_{SpC} - P_{LS})^2 + P_{trans}^2)^{1/4}} \cdot C_{d2} A_{LS} \cdot \sqrt{\frac{2}{\rho_{local}}} \quad (4.40)$$

The flow created by the movement of the spool is modeled with the equations:

$$\Delta Q_{SpC} = A_{sp} \cdot \dot{x} + Q_{Dyn} + Q_{LS} \quad (4.41)$$

$$\Delta Q_{PP'} = A_{sp} \cdot \dot{x} + Q_{PP} \quad (4.42)$$

The pressure build-up equations for fixed volume chambers in the pump and priority valve are:

$$\dot{P}_P = \frac{\beta}{V_P} \cdot (Q_P - Q_{EF} - Q_{CF}) \quad (4.43)$$

$$\dot{P}_{CF} = \frac{\beta}{V_{CF}} \cdot (Q_{CF} - Q_{Dyn} - Q_{PP} - Q_{A1}) \quad (4.44)$$

$$\dot{P}_{LS} = \frac{\beta}{V_{LS}} \cdot (Q_{LS} - Q_{LS'}) \quad (4.45)$$

Finally, the pressure build-up equations for variable volume chambers are:

$$\dot{P}_{SpC} = \frac{V_{SpCi}}{\beta} \cdot \Delta Q_{SpC} \quad (4.46)$$

$$\dot{P}_{PP} = \frac{V_{PPi}}{\beta} \cdot \Delta Q_{PP'} \quad (4.47)$$

Second, the movement equations are obtained through Newton's second law:

$$\ddot{x} = \frac{P_{PP} A_{SP} - P_{SpC} A_{SP} + (F_{CF} - F_{EF}) - b_{ols}\dot{x} - k_{spring} x}{m_{sp}} \quad (4.48)$$

### 4.9.2 Steering unit

Following the same framework as for the priority valve, the flow equations in the steering unit are:

$$Q_{LS'} = \frac{P_{LS} - P_{LS'}}{((P_{LS} - P_{LS'})^2 + P_{trans}^2)^{1/4}} \cdot C_{d2} A_{LS} \cdot \sqrt{\frac{2}{\rho_{local}}} \quad (4.49)$$

$$Q_{A1} = \frac{P_{CF} - P_{LS'}}{((P_{CF} - P_{LS'})^2 + P_{trans}^2)^{1/4}} \cdot C_{d2} A_1(\alpha) \cdot \sqrt{\frac{2}{\rho_{local}}} \quad (4.50)$$

$$Q_{A2R} = \frac{P_{LS'} - P_{GS}}{((P_{LS'} - P_{GS})^2 + P_{trans}^2)^{1/4}} \cdot C_{d2} A_{2R}(\alpha) \cdot \sqrt{\frac{2}{\rho_{local}}} \quad (4.51)$$

$$Q_{A2L} = \frac{P_{LS'} - P_{SC}}{((P_{LS'} - P_{SC})^2 + P_{trans}^2)^{1/4}} \cdot C_{d2} A_{2L}(\alpha) \cdot \sqrt{\frac{2}{\rho_{local}}} \quad (4.52)$$

$$Q_{A3L} = \frac{P_{SC} - P_{sut}}{((P_{SC} - P_{sut})^2 + P_{trans}^2)^{1/4}} \cdot C_{d2} A_{3L}(\alpha) \cdot \sqrt{\frac{2}{\rho_{local}}} \quad (4.53)$$

$$Q_{A3R} = \frac{P_{GS} - P_{sut}}{((P_{GS} - P_{sut})^2 + P_{trans}^2)^{1/4}} \cdot C_{d2} A_{3R}(\alpha) \cdot \sqrt{\frac{2}{\rho_{local}}} \quad (4.54)$$

$$Q_T = \frac{P_{sut} - P_T}{((P_{sut} - P_T)^2 + P_{trans}^2)^{1/4}} \cdot C_{d2} A_{10}(\alpha) \cdot \sqrt{\frac{2}{\rho_{local}}} \quad (4.55)$$

The pressure build-up equations for fixed volumes in the steering unit are:

$$\dot{P}_{LS'} = \frac{\beta}{V_{LS'}} \cdot (Q_{A1} - Q_{LS'} - Q_{A2R} - Q_{A2L}) \quad (4.56)$$

$$\dot{P}_{sut} = \frac{\beta}{V_{sut}} \cdot (Q_{A3L} + Q_{A3R} - Q_T) \quad (4.57)$$

$$\dot{P}_{SC} = \frac{\beta}{V_L} \cdot (Q_{SC} - Q_B) \quad (4.58)$$

The pressure buildup for the spool displacement is modelled with:

$$\dot{P}_{GS} = \frac{\beta}{V_{SS-GS}} \cdot (Q_{GS-R} - Q_{GS'}) \quad (4.59)$$

The movement equation for the steering unit also follows Newton's second law:

$$\ddot{\alpha} = \frac{M_{nps} + T_{sss} + \omega_{GS} \cdot b_{GS} + (P_R - P_{GS}) \cdot \frac{V_0 \cdot 10^{-6}}{2\pi}}{J_{st}} \quad (4.60)$$

### 4.9.3 Gear set

The flow equations through the gear set are:

$$Q_{GS'} = -P_{GS} \cdot \frac{k_{leak}}{60 \cdot 10^3 \cdot 10^5} - \frac{V_0 \cdot 10^{-6}}{2\pi} \cdot \omega_{GS} \quad (4.61)$$

$$Q_{GS-R} = -P_R \cdot \frac{k_{leak}}{60 \cdot 10^3 \cdot 10^5} + \frac{V_0 \cdot 10^{-6}}{2\pi} \cdot \omega_{GS} \quad (4.62)$$

### 4.9.4 Steering cylinder

The pressure on the right side of the cylinder (on the left one is  $P_{SC}$ ) is:

$$\dot{P}_R = \frac{\beta}{V_R} \cdot (Q_B - Q_{GS-R}) \quad (4.63)$$

The flow through the steering cylinder orifice is:

$$Q_B = \frac{P_{SC} - P_R}{((P_{SC} - P_R)^2 + P_{trans}^2)^{1/4}} \cdot C_{d3} \cdot A_{L/R} \cdot \sqrt{\frac{2}{\rho_{local}}} \quad (4.64)$$

# 5 | Validation of the model

Once the model of the system is complete, it is time to validate it. Due to unforeseen events it was not possible to validate the model with the real setup located in the company, so instead a theoretical validation is going to be performed. Also, several tests are executed in order to find some missing or provisional parameters.

To do so, three test are going to be carried out, one with neutral steering, one with leftward steering and one with rightward, and all the pressures and flows found in the previous chapter are going to be measured for each of them. These pressures and flows are going to be analyzed theoretically to prove that they behave in the predicted way.

Afterwards, since the actual steering input used to obtain the unwanted vibrations is unknown, an analysis of how the output ( $\Delta P$ ) changes when the input is changed is performed. Since the input, output and displacement per revolution of the gear set are all linked, a third analysis of how the output changes by leaving the input untouched but varying the displacement per revolution is also carried out.

With this analysis, a provisional displacement per revolution is obtained. Also, three inputs used to obtain the required pressure differences in three key parts of the output, are acquired.

A final analysis comparing the unwanted oscillations obtained with a step and a ramp input is performed in order to see the effect of abrupt or progressive changes of the input in the output.

## 5.1 Theoretical validation

### 5.1.1 Neutral steering

For the neutral steering, a velocity of 0 rad/s and a  $Q_P = 40\text{l/min}$  are used as input. Next, four graphs showing the pressure and flow in both the priority valve and the steering unit are shown.

In Fig.5.1, the pressures in the priority valve are shown. Since there is no steering, there is no pressure build-up either. The pressure in the Excess Port remains constantly at zero since it is directly attached to the tank. Since there is no change in flow, the pressure in both the Pilot Pressure and the Control Flow chambers is the same.

In Fig.5.2, the flows through the priority valve are shown. As said before, the flow from the Pump can be seen as 40l/min. Since there is no steering the pressure in the load sensing will be low and thus the priority valve directs most of the flow towards the Excess Port, and since it is a dynamic orifice there is some throttle towards the control port ( $Q_P = Q_{EF} + Q_{CF}$ ). Also, since there is no steering the the flow through the Pressure Port is zero ( $Q_{PP} = Q_{Dym} + Q_{LS}$ ).

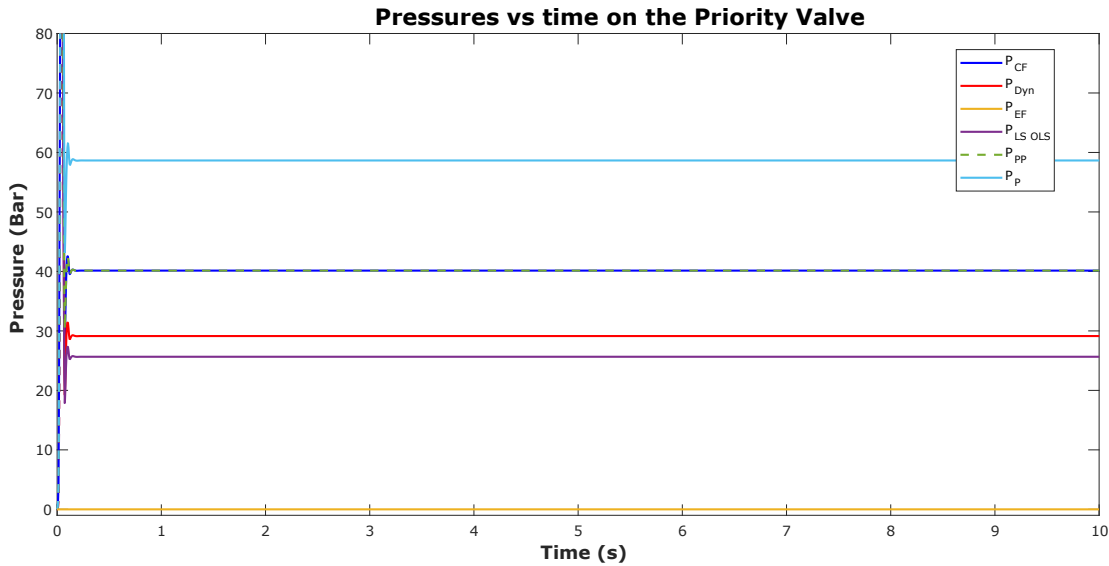


Figure 5.1: Graph showing the main pressures in the priority valve when performing neutral steering.

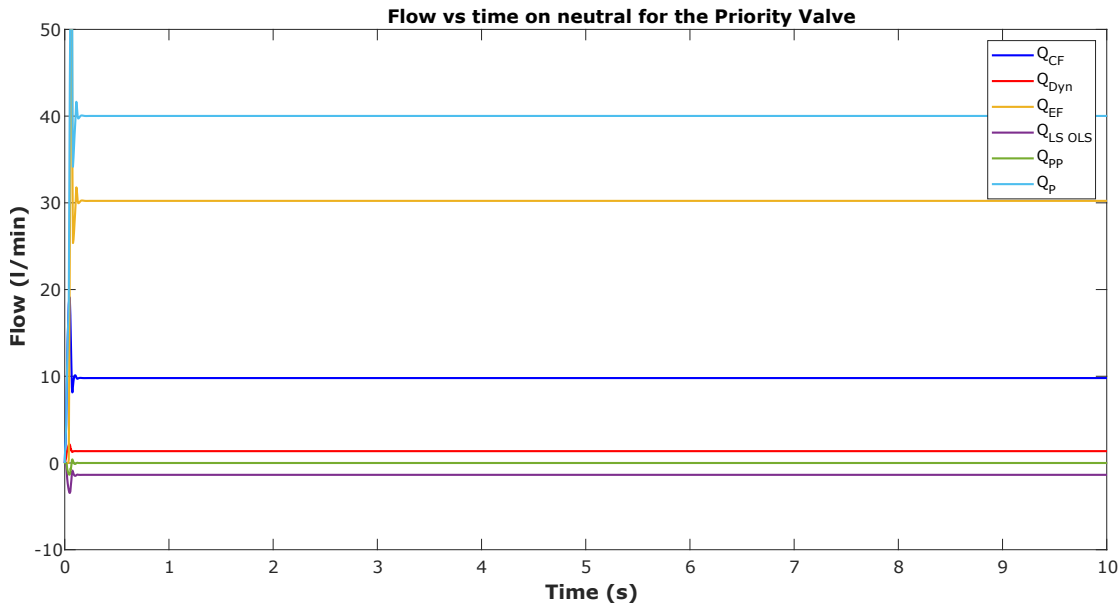


Figure 5.2: Graph showing the main flows in the priority valve when performing neutral steering.

In Fig.5.3 the pressures on the different chambers of the steering unit are shown. As for the priority valve, since there is no steering there is no change in flow and thus no difference in pressure. The highest pressures are located after the  $A_1$  and  $A_{LS'}$  orifices, which makes sense since they are the ones directly joined to the the priority valve and therefore receiving the most flow. The middle pressures are  $P_{2L}$ ,  $P_{2R}$ ,  $P_{GS}$ ,  $P_{SC}$ , which are all interconnected through the steering cylinder, and since it is not moving, the pressures don't change. The lowest pressures are the ones in  $A_{3R}$  and  $A_{3L}$ .

In Fig.5.4 the flows going through the steering unit are shown. Both  $Q_{GS}$  and  $Q_{SC}$  are zero because both depend on the movement of the steering cylinder.  $Q_{LS'}$  is greater than zero since there is always some standby flow to not have a lag between the steering of the wheel and the response. The flows through  $A_{2L}$ ,  $A_{2R}$ ,  $A_{3L}$  and  $A_{3R}$  are equal because since there is no flow going towards the steering cylinder, all the flow that goes through the  $A_2$ s goes directly through

the  $A_3s$  and from there to tank.

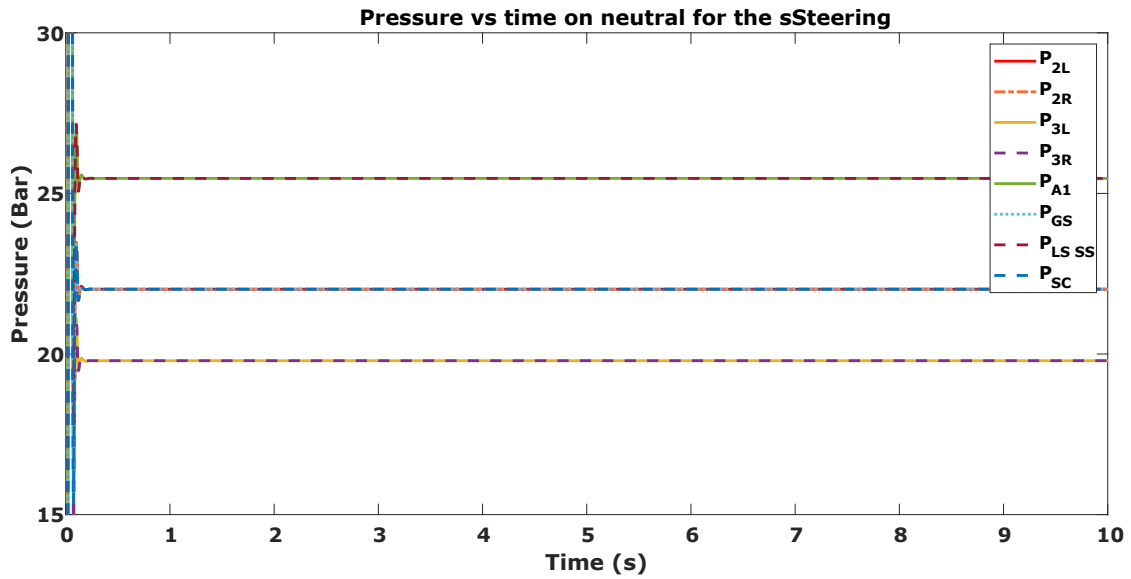


Figure 5.3: Plot showing the pressures at different points of the steering unit when the steering wheel is in neutral.

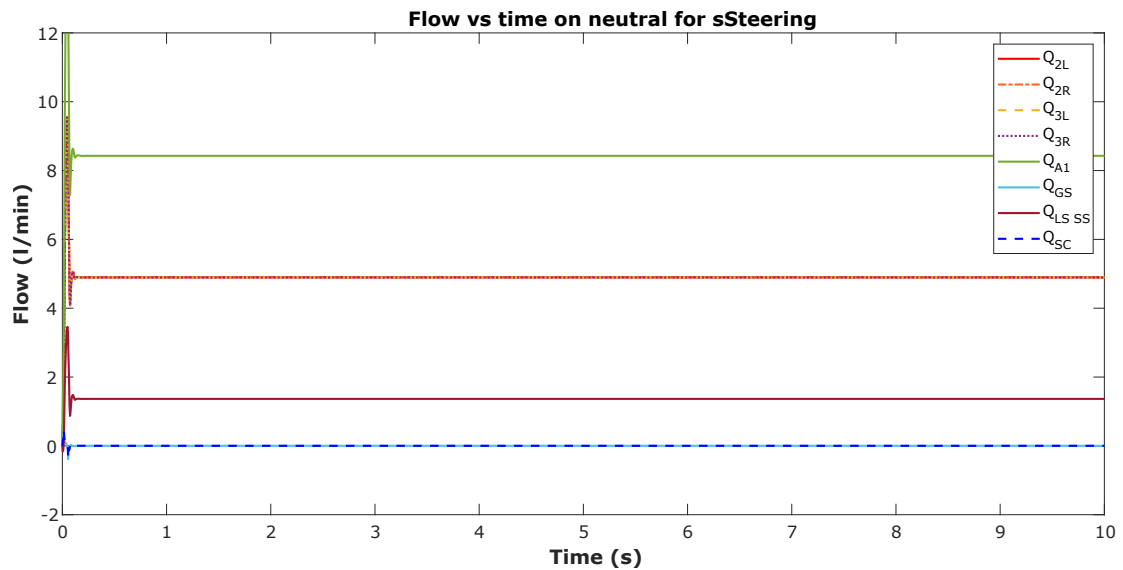


Figure 5.4: Graph showing the different flows going through the steering unit when the steering wheel is in neutral.

### 5.1.2 Rightward steering

For the rightward steering, a step input is used. This step input will increase the velocity from 1 rad/s to 1.5 rad/s, 5 seconds into the simulation. The graphs for the changes in pressure and flow for the priority valve and steering unit are shown below. In all the graphics some unwanted vibrations can be observed after the step, until the new flow is stabilized, due to the sudden increase in velocity. This behavior will be analyzed in subsequent sections.

In Fig.5.5, the  $P_{EF}$  is not represented in order to show with more clarity the remaining pressures, but it remains constant at 0 Bar. All the pressures increase in value with the increase in velocity,

and since the increase in velocity is translated into more flow into the steering unit, the build-up pressure for  $P_{CF}$ ,  $P_{Dyn}$ ,  $P_{LS}$  and  $P_{PP}$  is greater than the pressure build-up for the pump chamber.

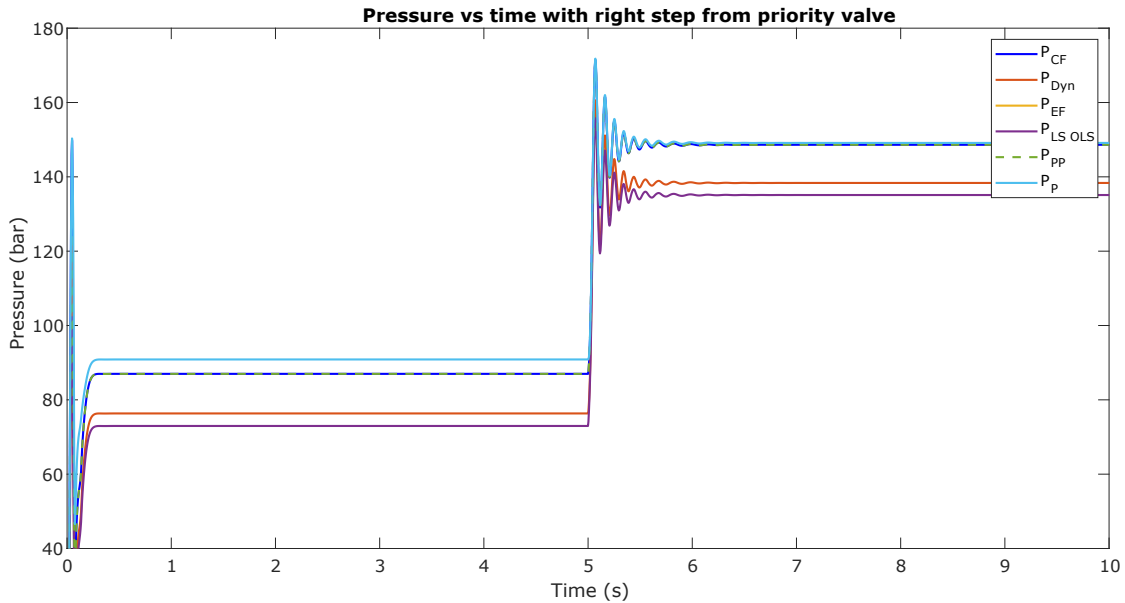


**Figure 5.5:** Graph showing the pressures in the priority valve when performing a rightward step steering.

In Fig.5.6 it can be seen that, when the velocity increases, the priority valve conducts more flow towards the Control Flow and the flow in the Excess Port decreases. As said in the introduction, the pilot pressure is used to dampen the oscillations, and so the  $Q_{CF}$  is less oscillatory than  $Q_P$  or  $Q_{EF}$ .

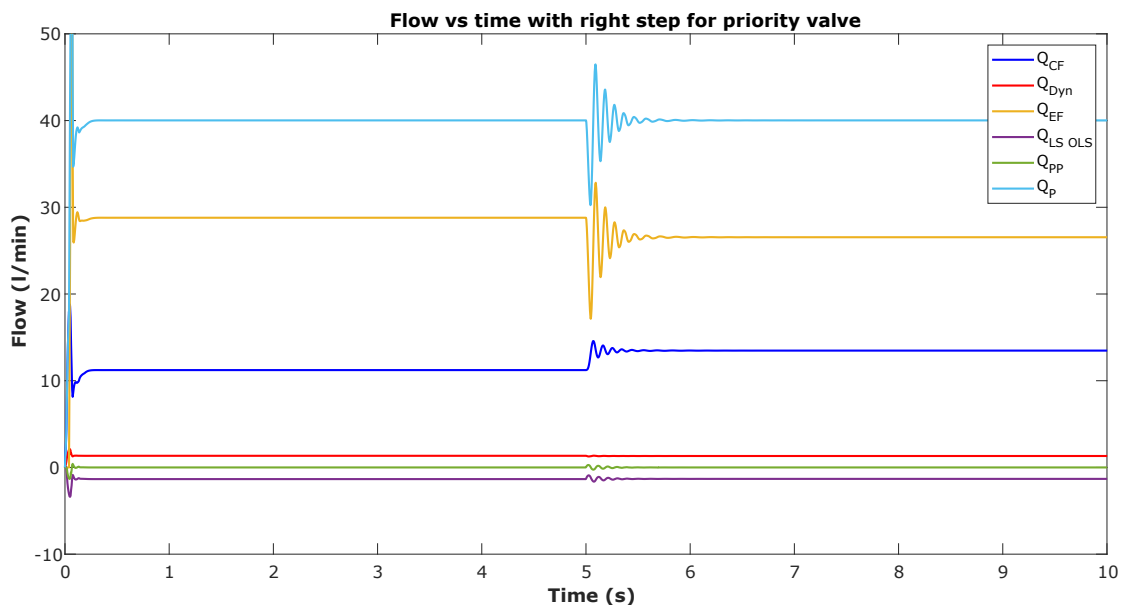


**Figure 5.6:** Graph showing the main flows in the priority valve when performing a rightward step steering.

For the steering unit, the pressures and the flows are measured as shown in Fig.5.7. That means that  $P_{2L}$  and  $P_{SC}$  are the same pressure; the same happens with  $P_{3L}$  and  $P_{3R}$ ,  $P_{2R}$  and  $P_{GS}$  and with  $P_{A1}$  and  $P_{LS}$ . Although somewhat redundant information, it is chosen to present it like



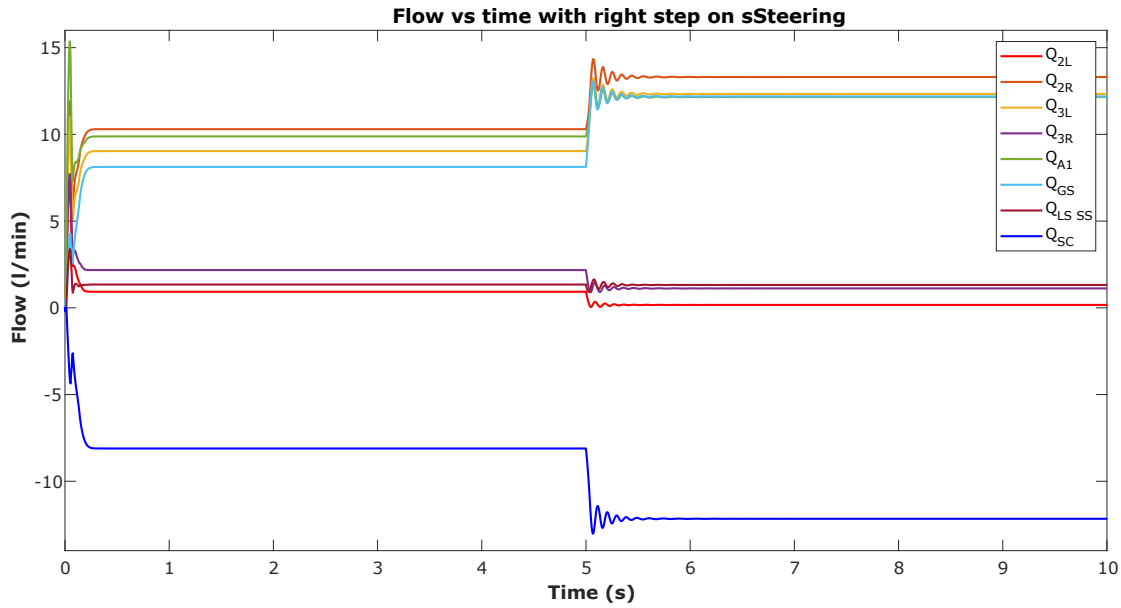


**Figure 5.9:** Graph showing the main flows in the steering unit when performing a rightward step steering.

### 5.1.3 Leftward steering

For the leftward steering a step input is used. The step goes from  $-1$  rad/s to  $-1.5$  rad/s, 5 seconds into the simulation. The flow from the pump is assumed as constant with a value of 40 l/min as before. The pressures and flows through the priority valve remain the same as the ones obtained with a right step (Fig.5.5 and Fig.5.6 respectively). This is because the priority valve only intervenes in the amount of flow that goes to the steering unit, which depends on the amount of movement in the steering unit, not the direction of the movement.

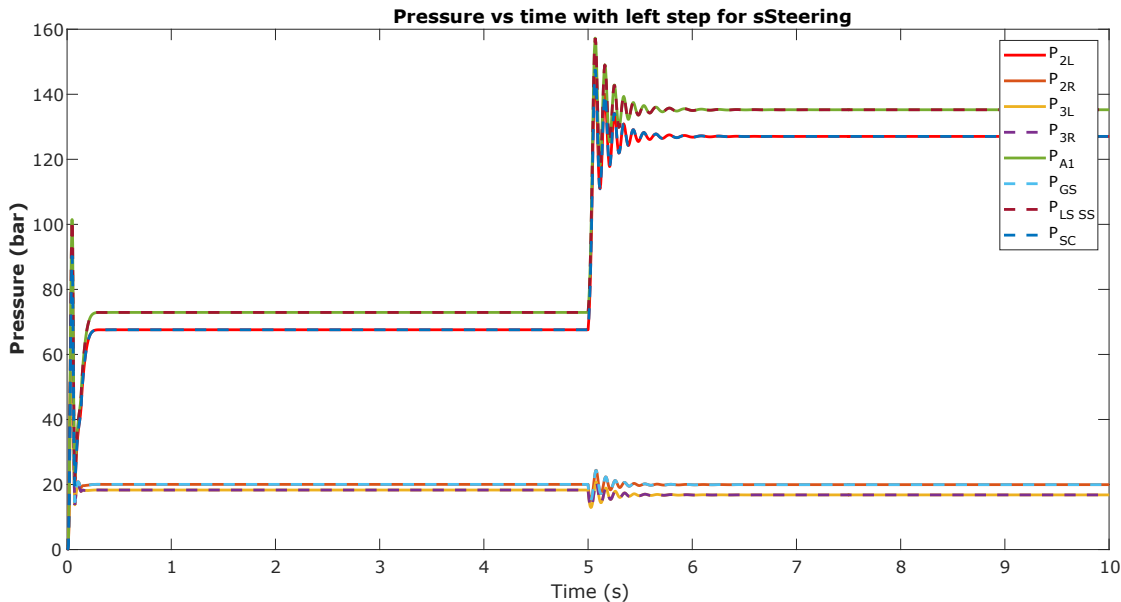


**Figure 5.10:** Graph showing the different pressures in the steering unit when performing a leftward step steering.

In Fig.5.10 the pressures in the different chambers of the steering unit can be seen. Similar to

the rightward steering pressures (Fig.5.8), the  $P_{A1}$  increases due to the increment in flow going to the steering unit. But unlike it, for the leftward steering the  $P_{2L}$  is the one that increase, while  $P_{3L}$  decreases.

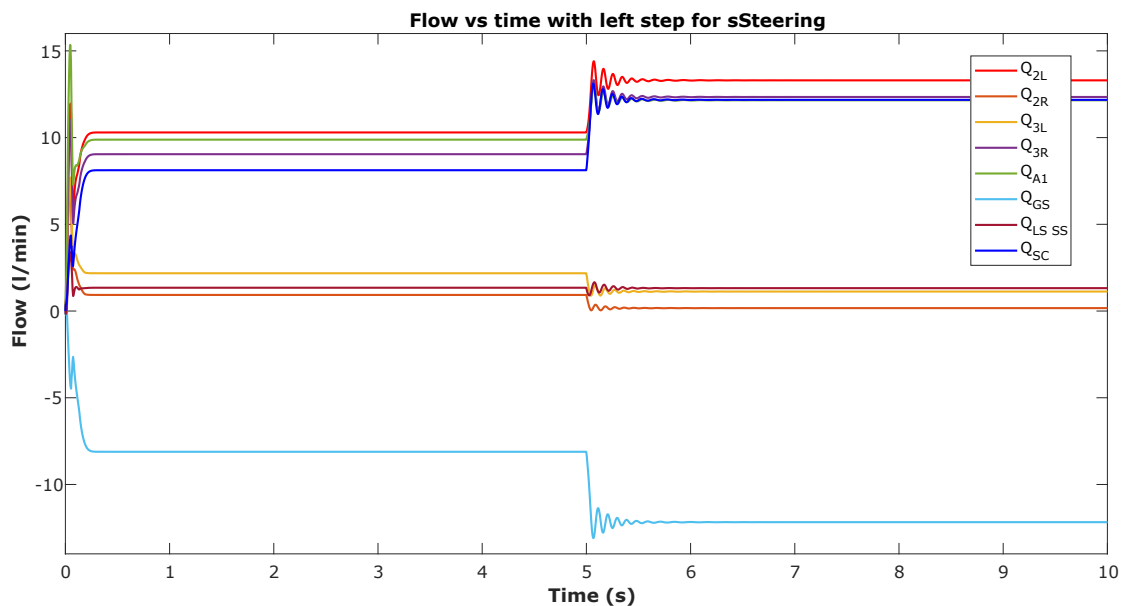


**Figure 5.11:** Graph showing the main flows in the steering unit when performing a leftward step steering.

In Fig.5.11 the flows going through the steering unit are shown. This figure opposes Fig.5.9, since the flow now goes through  $Q_{A1}$ , then  $Q_{2L}$  and finally  $Q_{SC}$ , thus increasing these. As happened before with  $Q_{SC}$ , now the absolute value of  $Q_{GS}$  also increases, with the flow going from the right chamber, through  $Q_{3R}$  and from there to tank.  $Q_{3L}$  decreases since most of the flow goes now towards  $Q_{SC}$ .  $Q_{LS}$  does not change, since it only changes while there is an increment in velocity, not when the steady state has been reached (It can be seen changing when the input is a ramp and not a step).

## 5.2 Finding the input

In this section, an analysis is going to be performed in order to find the input used by the company when the unwanted vibrations were found. Looking at Fig.5.12 it can be extrapolated that the steering wheel input, assuming that the flow from the pump is constant, is an step input, with the initial velocity being 0 for the first 10s and then a step increment that makes the pressure on the steering cylinder increase until around 210 bar.

Manually in the test facility it is difficult to obtain a real step. This can be seen in the figure, where the pressure increases gradually for some seconds before following the step. To solve this, a ramp is going to be modeled to mimic the input created physically.

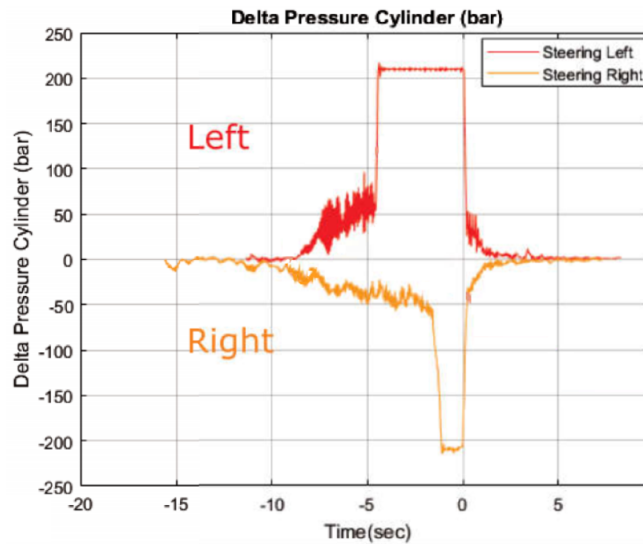


**Figure 5.12:** Reminder of how the output pressure in the steering cylinder looks like in the real system, when the steering wheel turns leftward (red) and rightward (orange).

The input flow on the steering unit is proportional to the velocity of the steering wheel multiplied by the displacement of the gear set. Since the model has the priority valve in between the steering unit and the pump, it is not possible to know exactly what percentage of the flow provided by the pump ends up going to the steering unit, rather than to the excess port. Also, the amount of flow going into the steering unit depends on the pressure created by the load sensing, making it more difficult to predict the quantity of flow going into the steering unit. Due to these inconveniences, a trial and error test has been conducted to find the most accurate input.

With the original model provided by *Danfoss*, it was not possible to reach the maximum  $\Delta P$  obtained in the graph (210 bar), before instability vibrations appeared, as seen in Fig.5.13. Due to this, some trials have been performed in order to find the correct value of  $V_0$  (displacement per revolution) and of velocity so as to achieve said pressure.

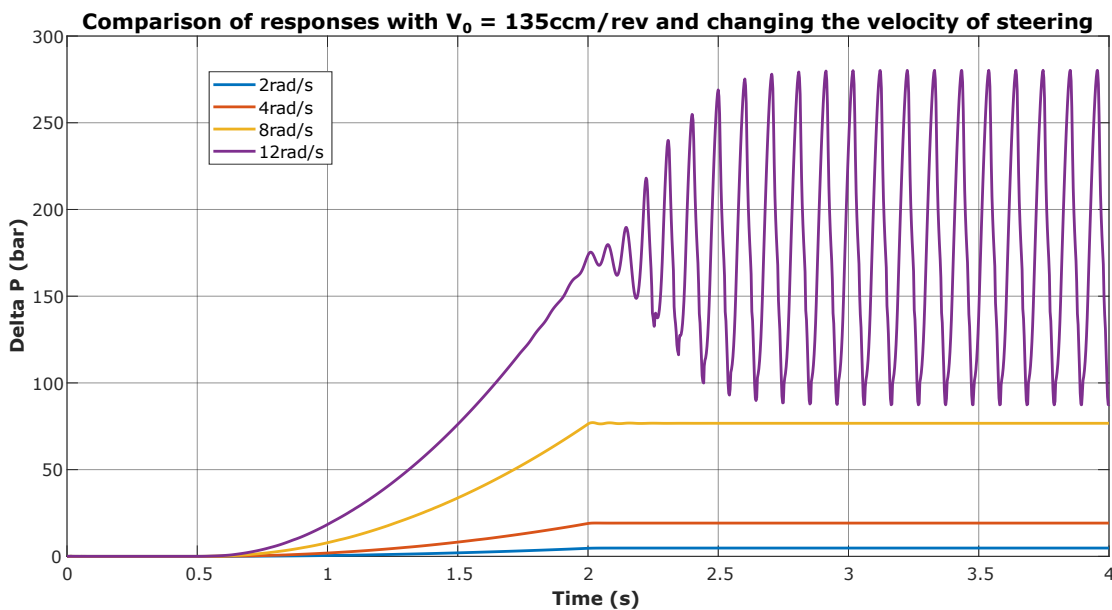


**Figure 5.13:** Graph showing the increase in pressure with the original  $V_0$  when the velocity of the steering wheel is increased.

For the first trial, the same input for all the runs is used, which is a ramp input that starts at 5 s and grows linearly until it reaches 2.5 rad/s at 10 s and remains constant there until 12 s where the velocity drops again to zero. This is done to try and mimic the response obtained in the experimental setup. Seven tests are done, each one with a different value of displacement per revolution of the gear set. The difference in pressure between the chambers ( $\Delta P = P_L - P_R$ ) is measured, and the results of the trial can be seen in Fig.5.14.

As seen in the figure, when the displacement per revolution of the gear set increases, the absolute pressure build-up of the steering cylinder also increases. This is proved by the theory, since with a bigger displacement per revolution more oil will be displaced, so more flow created, when the wheel is turned.

In the trial, first the pressure build-up of the system with the current displacement per revolution ( $V_0$ ) is measured. As it can be seen, it is too low, since the goal is to obtain a pressure build-up of around 210 bar. But if the  $V_0$  is increased too much in order to obtain the desired pressure (as in the case of  $V_0 = 700$  ccm/rev) unwanted vibrations appear (which are different to the vibrations causing problems in the real system). It can also be seen that the response is completely symmetrical when turning both to the left and to the right side. Since that is the case, the following test is done only in one direction.

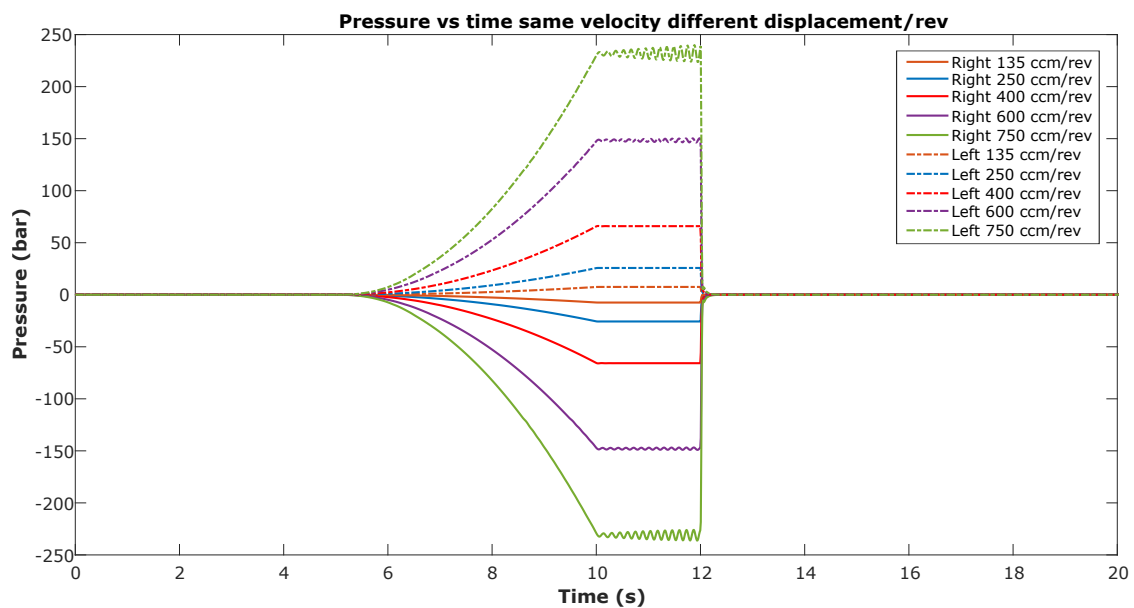


**Figure 5.14:** Graph showing the differences in the measured pressure for the leftward (top) and rightward (bottom) displacement per revolution of the gear set is changed.

Taking this into account, the next step is using a  $V_0$  of 400 - 500 ccm/rev. This number is chosen as it is fairly large, but not too much so as to create vibrations. It is then attempted to increase the velocity until a pressure of 210 bar is obtained. The  $V_0$  used is 450 ccm/rev. The results of this step can be seen in Fig.5.15, where the velocities used are 2.5 rad/s (the one used in the previous step), 3 rad/s, 3.5 rad/s and 3.7 rad/s.

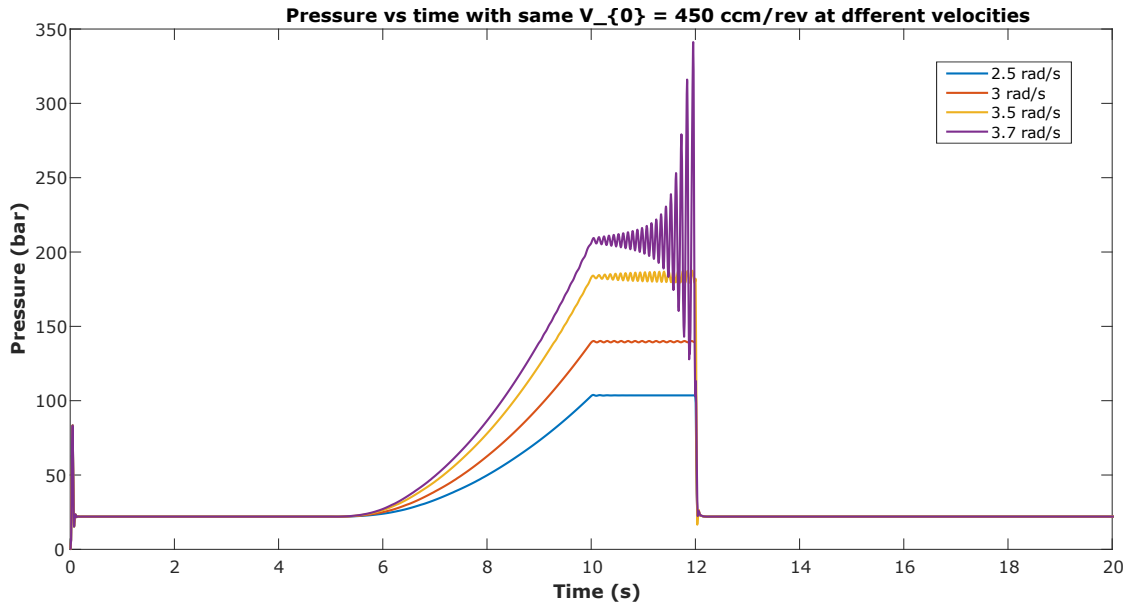


**Figure 5.15:** Graph showing the differences in the measured pressure in the rightward direction when the displacement per revolution of the gear set remains constant but the velocity changes.

Looking at Fig.5.15 it can be seen that increasing the velocity also creates the unwanted vibrations, and so when the velocity needed to reach a pressure of 210 bar is used (3.7 rad/s) the vibrations appear.

Analyzing both trials it can be concluded that the pressure vibrations are more sensitive to changes in the velocity. With this in mind, a third analysis is done where the desired pressure is tried to be obtained with the lower value of  $V_0$ .

A summary of this analysis can be observed in Table 5.1 where the velocity needed to obtain 210 bar and its corresponding  $V_0$  are recorded. For smaller values of  $V_0$  or larger velocities than the ones shown in the table the pressure either became unstable or larger than 210 bar.

Velocity(rad/s)	Displacement(ccm/rev)	Stability at 210 bar
1.7	1000	Stable
1.88	900	Stable
2	850	Stable
2.15	800	Stable
2.3	750	Stable
2.45	700	Stable
2.6	650	Stable
2.82	600	Increased vibrations
3.1	550	Increased vibrations
3.44	500	Unstable

**Table 5.1:** Contains the velocity and its corresponding displacement necessary to obtain pressure of 210 bar. The stability of the pressure is also noted.

Taking this information into account, three step inputs are going to be used to obtain three  $\Delta P$  corresponding to three key points in Fig. 5.12: The first one is for pressures around the beginning of the slope (more exactly for a pressure of 12 bar), which is obtained with an input of 0.5 rad/s. The second one is for pressures in the middle of the slope, where the unwanted

vibrations are located ( $\Delta P = 50$  bar), which is obtained with an input of 1.02 rad/s. Lastly, the third one is to obtain a pressure of 210 bar, which is achieved with a velocity of 2.06 rad/s. All these inputs are paired with a displacement per revolution of 850 ccm/rev, since it gives some instabilities but only at the beginning of the top part of the step, similar to the small peak at Fig.5.12.

Before moving to the next chapter, an extra comparison is going to be performed. This comparison is going to be of the response obtained between a ramp input and a step input. For this past analysis a ramp input was used, since the real input was trying to be replicated, but for the sensitivity analysis performed in Chapter 7 a step input is used. Thus, it is important to see how the output differs for each of the two.

In the analysis the step input is done 2s into the analysis and the ramp input starts increasing at 0.5s and arrives to the desired velocity at 2s. Six different end velocities have been used for the input: 1.02 rad/s, 1.1 rad/s, 1.2 rad/s, 1.3 rad/s, 1.4 rad/s and 1.5 rad/s. The outputs are paired in colors, and for each color the dashed line represents the ramp input and the solid line the step input. The result of the analysis can be seen in Fig.5.16.

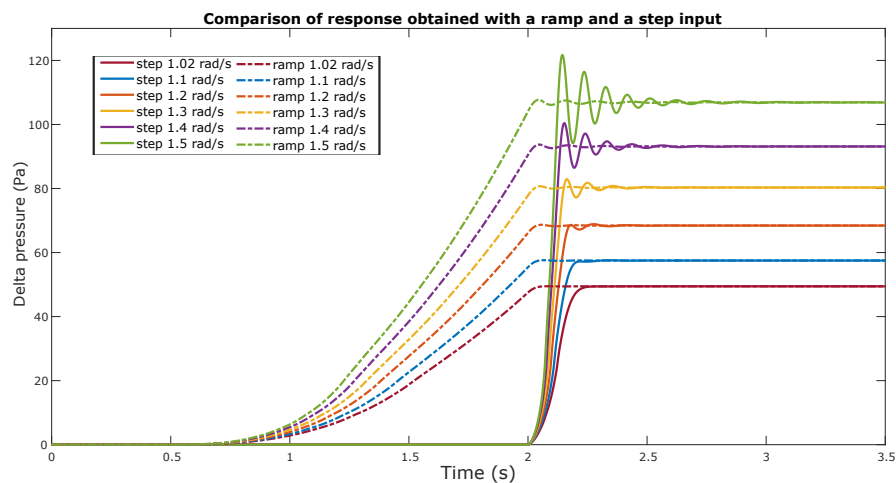


**Figure 5.16:** Comparison of the responses obtained with a ramp and a step input.

It can be seen how, since with a ramp input the change in velocity is less abrupt, the system becomes less unstable, being able to reach larger outputs before starting to show any vibrations.

Having looked at this graph, the option of choosing 850 ccm/rev is corroborated, since there are not vibrations neither with the step nor with the ramp inputs.



# 6 | Linearization and State Space model

Once the mathematical model has been created and validated it is time to linearize it. The linearization is done to analyze the stability of the system and to find new parameters that, when applied in the stable system, remove the unwanted vibrations. Linearization is the process of taking the gradient of a nonlinear function with respect to its variable(s) and creating a linear representation at that point.

Once the model is linearized, a state space model of the whole system can be constructed.

## 6.1 Linearization

The seven main equations in the steering unit model are:

- Flow equation with fixed orifice
- Flow equation with variable orifice
- Flow from spool movement
- Pressure build-up with fixed volume
- Pressure build-up with variable volume
- Flow in the gear set
- Newton's second law

A formulaic linearization of each of them will be performed, in where the actual constant parameters can be substituted later.

### 6.1.1 Flow equation with fixed orifice

Since the area of the orifice does not change over time, the only variable is the pressure change ( $\Delta P = P_{in} - P_{out}$ ). Using the orifice equation (6.1):

$$Q = C_d A \sqrt{\frac{2 \cdot \Delta P}{\rho}} \quad (6.1)$$

and differentiating it with respect to pressure (6.2):

$$q = \left. \frac{\partial Q}{\partial \Delta P} \right|_i \cdot \Delta p \Leftrightarrow q(s) = k_{qp} \cdot \Delta p(s) \quad (6.2)$$

where the sub-index  $i$  refers to the different equations with fixed orifices.  $k_{qp}$  is the linearization constant (6.3), which will change for every equation:

$$k_{qp} = \frac{C_d \cdot A \cdot \sqrt{\frac{2}{\rho}}}{2 \cdot \sqrt{\Delta P_i}} \quad (6.3)$$

### 6.1.2 Flow equation with variable orifice

The linearized equation for the flow with variable orifice is similar to the one with fixed orifice but with a second variable, the area of the orifice  $A(x)$ . The flow equation used now is then (6.4):

$$Q = C_d A(x) \sqrt{\frac{2 \cdot \Delta P}{\rho}} \quad (6.4)$$

and the differentiation of the equation looks like (6.5):

$$q = \left. \frac{\partial Q}{\partial X} \right|_i \cdot x + \left. \frac{\partial Q}{\partial \Delta P} \right|_i \cdot \Delta p \Rightarrow q(s) = k_{qx} \cdot x(s) + k_{qp} \cdot \Delta p(s) \quad (6.5)$$

where  $k_{qx}$  and  $k_{qp}$  are (6.6):

$$k_{qx} = C_d \cdot \sqrt{\frac{2}{\rho} \cdot \Delta P_i} \cdot \frac{\partial A(X_i)}{\partial X}, \quad k_{qp} = \frac{C_d \cdot A(X_i) \cdot \sqrt{\frac{2}{\rho}}}{2 \cdot \sqrt{\Delta P_i}} \quad (6.6)$$

### 6.1.3 Flow from spool movement

The linearized form for the flow created by the spool movement follows the structure of (6.7):

$$q(s) = A \cdot x(s) \cdot s + \Delta q(s) \quad (6.7)$$

### 6.1.4 Pressure build-up in fixed volume chamber

The pressure build-up equation is already linear, and looks like (6.8):

$$p(s) = \frac{\beta}{V \cdot s} \cdot (q_{in}(s) - q_{out}(s)) \quad (6.8)$$

### 6.1.5 Pressure build-up in variable volume chamber

This pressure build-up equation is also already linearized, and follows the form of (6.9):

$$p(s) = \frac{V_{initial}}{\beta \cdot s} \cdot (q_{in}(s) - q_{out}(s) - v(s) \cdot s) \quad (6.9)$$

### 6.1.6 Flow in gear set

The general linearized equation for the flow going through the gear set has the form of (6.10):

$$q(s) = \frac{-k_{leak}}{60 \cdot 10^8} \cdot p(s) + \frac{-V_0 \cdot 10^{-6}}{2\pi} \cdot \alpha(s) \cdot s \quad (6.10)$$

### 6.1.7 Newton's second law

The standard Newton's second law used looks like (6.11):

$$m \cdot \ddot{X} = (P_1 - P_2) \cdot A - b \cdot \dot{X} - k \cdot X \quad (6.11)$$

This equation is already linear, and can be solved for  $x$ , as shown in (6.12):

$$x(s) = \frac{(P_1(s) - P_2(s)) \cdot A}{m \cdot s^2 + b \cdot s + k} \quad (6.12)$$

## 6.2 Summary of the linearized equations

Once the structure of the different types of linear equations needed have been obtained, a summary of all the equations used in the model (mirroring the previous summary with the nonlinear equations) is shown below. The  $k_{qp}$  and  $k_{qx}$  are not solved and are left in this index form since their actual value depends on the chosen linearization point.

### 6.2.1 Priority valve

First, the flow equations (variable orifice, fixed orifice, and created by the spool) are presented. Then it is turn for the pressures for both fixed volume chambers and variable volume chambers and finally the Newton Second Law.

The flow equations are:

$$q_{EF}(s) = k_{qxEF} \cdot x(s) + k_{qpEF} \cdot \Delta p_{P-EF}(s) \quad (6.13)$$

$$q_{CF}(s) = k_{qxCf} \cdot x(s) + k_{qpCF} \cdot \Delta p_{P-CF}(s) \quad (6.14)$$

$$q_{PP}(s) = k_{qpPP} \cdot \Delta p_{CF-PP}(s) \quad (6.15)$$

$$q_{DYN}(s) = k_{qpDYN} \cdot \Delta p_{CF-SpC}(s) \quad (6.16)$$

$$q_{LS}(s) = k_{qpLS} \cdot \Delta p_{SpC-LS}(s) \quad (6.17)$$

$$q_{SpC}(s) = A_{sp} \cdot x(s) \cdot s + q_{DYN}(s) + q_{LS}(s) \quad (6.18)$$

$$q_{PP'}(s) = A_{sp} \cdot x(s) \cdot s + q_{PP}(s) \quad (6.19)$$

The linearized pressure equations in the priority valve and pump chambers are:

$$p_P(s) = \frac{\beta}{V_P \cdot s} \cdot (q_P(s) - q_{CF}(s) - q_{EF}(s)) \quad (6.20)$$

$$p_{CF}(s) = \frac{\beta}{V_{CF} \cdot s} \cdot (q_{CF}(s) - q_{DYN}(s) - q_{PP}(s) - q_{A1}(s)) \quad (6.21)$$

$$p_{LS}(s) = \frac{\beta}{V_{LS} \cdot s} \cdot (q_{LS}(s) - q_{LS'}(s)) \quad (6.22)$$

$$p_{SpC}(s) = \frac{V_{SpCi}}{\beta \cdot s} \cdot q_{SpC}(s) \quad (6.23)$$

$$p_{PP'}(s) = \frac{V_{PPi}}{\beta \cdot s} \cdot q_{PP'}(s) \quad (6.24)$$

Finally, the movement of the spool is modelled with equation:

$$x(s) = \frac{(P_{PP}(s) - P_{SpC}(s)) \cdot A_{SP}}{m_{sp} \cdot s^2 + b_{ols} \cdot s + k_{spring}} \quad (6.25)$$

### 6.2.2 Steering unit

Imitating the order in which the equations were written in the previous summary, for the linearized equations it is also going to be first the flow equations, then the pressure equations and finally Newtons Second Law.

The linearized flow equations for the steering unit are:

$$q_{LS'}(s) = k_{qpLS'} \cdot \Delta p_{LS-LS'}(s) \quad (6.26)$$

$$q_{A1}(s) = k_{qx A1} \cdot x(s) + k_{qp A1} \cdot \Delta p_{CF-LS'}(s) \quad (6.27)$$

$$q_{A2R}(s) = k_{qx A2R} \cdot x(s) + k_{qp A2R} \cdot \Delta p_{LS'-GS}(s) \quad (6.28)$$

$$q_{A2L}(s) = k_{qx A2L} \cdot x(s) + k_{qp A2L} \cdot \Delta p_{LS'-SC}(s) \quad (6.29)$$

$$q_{A3L}(s) = k_{qx A3L} \cdot x(s) + k_{qp A3L} \cdot \Delta p_{SC-sut}(s) \quad (6.30)$$

$$q_{A3R}(s) = k_{qx A3R} \cdot x(s) + k_{qp A3R} \cdot \Delta p_{GS-sut}(s) \quad (6.31)$$

$$q_T(s) = k_{qx T} \cdot x(s) + k_{qp T} \cdot \Delta p_{sut-T}(s) \quad (6.32)$$

The linearized pressure build-up equations for fixed volumes are:

$$p_{LS'}(s) = \frac{\beta}{V_{LS'} \cdot s} \cdot (q_{A1}(s) + q_{LS'}(s) - q_{A2R}(s) - q_{A2L}(s)) \quad (6.33)$$

$$p_{sut}(s) = \frac{\beta}{V_{sut} \cdot s} \cdot (q_{A3L}(s) + q_{A3R}(s) - q_T(s)) \quad (6.34)$$

$$p_{SC}(s) = \frac{\beta}{V_{SC} \cdot s} \cdot (q_{SC}(s) - q_B(s)) \quad (6.35)$$

$$p_{GS}(s) = \frac{\beta}{V_{SS-GS} \cdot s} \cdot (q_{A2R}(s) - q_{A3R}(s) - q_{GS}(s)) \quad (6.36)$$

Where  $q_{SC}(s) = q_{A2L}(s) - q_{A3L}(s)$ . Finally the displacement of the spool-sleeve in the steering unit looks similar to the one in the priority valve but with angular displacement instead of linear:

$$\alpha_{sl}(s) = \frac{(P_R(s) - P_{GS}(s)) \cdot \frac{V_0 \cdot 10^{-6}}{2\pi} + b_{GS} \cdot \alpha \cdot s + \delta T_{sss}(\alpha_i) \cdot \alpha}{J_{sl} \cdot s^2} \quad (6.37)$$

Where  $\alpha_{sl}$  is the angular displacement of the sleeve and  $\alpha$  is the angular lag between the spool and the sleeve.

### 6.2.3 Gear Set

In the Gear Set, the flows are modelled, which linearized look like:

$$q_{GS}(s) = \frac{-k_{leak}}{60 \cdot 10^8} \cdot p_{GS}(s) + \frac{-V_0 \cdot 10^{-6}}{2\pi} \cdot \alpha(s) \cdot s \quad (6.38)$$

$$q_{GS-R}(s) = \frac{-k_{leak}}{60 \cdot 10^8} \cdot p_R(s) + \frac{V_0 \cdot 10^{-6}}{2\pi} \cdot \alpha(s) \cdot s \quad (6.39)$$

### 6.2.4 Steering Cylinder

Finally, the flow through the orifice that does the part of the steering cylinder and the pressure-buildup in the right chamber (the pressure in the left chamber is  $p_{SC}(s)$ ) are:

$$q_B(s) = k_{qpB} \cdot \Delta p_{R-SC}(s) \quad (6.40)$$

$$p_R(s) = \frac{\beta}{V_R \cdot s} \cdot (q_{GS-R}(s) - q_B(s)) \quad (6.41)$$

## 6.3 State space Model

Once the parametric linear equations are obtained they can be used to set up a state space model of the whole system (priority valve, steering unit and steering cylinder). For the state space model, both the pressure, the velocities and the positions ( $x$  and  $\alpha$ ) are used as states, which creates a 14x14 state matrix. The inputs are the pump flow (which is considered constant and with a value of 40l/min), the tank pressure (which is considered to be 0 bar) and the speed of steering with the steering wheel (which is going to be modeled as a step input). The output is  $\Delta P = P_{SC} - P_R$ , which is the difference in pressure between both sides of the steering cylinder.

The state space matrices and vectors can be seen in Pag. 42. Here,  $x$  are the state vector (and  $\dot{x}$  the derivative over time of the state vector),  $A$  is the state matrix,  $B$  is the input matrix,  $C$  is the output matrix and  $u$  and  $y$  the input and output vectors, respectively.

The fully developed linearization parameters  $k_{qx}$  and  $k_{qp}$  can be seen in Appendix B.



# 7 | Sensitivity Analysis

With the state space model obtained in Chapter 6 and the three inputs decided at the end of Chapter 5, a sensitivity analysis can be performed.

The sensitivity analysis is carried out as follows: while leaving the rest of the soft parameters constant, each of them will be analyzed with an array of values. Then, the outputs for the pressure in the steering cylinder will be compared to each other, to see for which value the output is the most similar to the one obtained in the real system. Besides that, the root locus plot will be analyzed where the changing position of the poles and zeros will be studied. This is done in order to find the value in which the stability of the system is optimum.

The parameters that are going to be analyzed are thus the discharge coefficient of the orifices, the damping coefficient of the different mechanical parts, the dimensions of the different volumes and areas of the steering unit and the displacement per revolution of the gear set. The bulk modulus, although another soft parameter, is going to remain unchanged, since in the mathematical model it has already been modeled taking into account the changes caused by temperature, pressure and content of air in the oil.

Before all this, the specific value of the linearization parameters for each of the inputs has to be found. To simplify things, the input chosen to analyze, is the one with  $\omega_{sp} = 1.02$  rad/s, since it is the one that gives the pressure with the unwanted vibrations.

## 7.1 Specific state space model

To obtain the state space model specific to the desired input, the values for the linearization parameters have to be found. This means that the initial pressures for all the states and the initial position for both the priority valve spool and the steering unit sleeve need to be obtained.

This is done by using the input on the nonlinear model and, once the system has reached a steady state, the values of the pressures and positions can be extracted.

The last thing needed is the  $\frac{\delta A}{\delta x/\alpha}$  and  $\frac{\delta M_{nps}}{\delta \alpha}$ , which are modeled as the slope created by the different area openings/spring stiffness between two positions around the linearization position. An example of the Simulink model used to obtain the linearization areas and slopes for the priority valve can be seen in Fig.7.1.

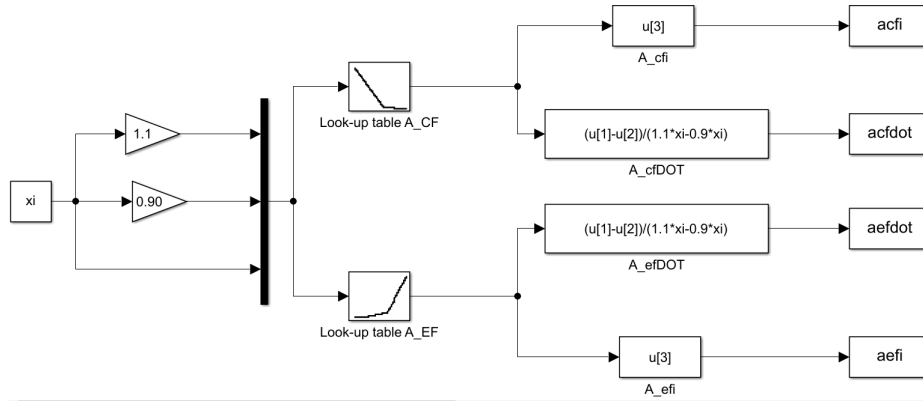


Figure 7.1: Simulink model for the obtaining of the areas and slopes for the priority valve.

## 7.2 Analyzing the original linearized model

Once the state space model is obtained, it can be used to obtain a transfer function model of the system. A transfer function representation is useful since it shows the value of the different poles and zeros of the system. The transfer function of the linearized model for the input of 1.02 rad/s given in the form of gain-zero-pole is:

$$Tf = \frac{N}{D} \begin{cases} N = -3.30e10 s^2 (s + 2.44e14) (s + 1.70e6) (s + 2.16e5) (s + 1.71e5) (s + 2.44e4) \cdots \\ \quad \cdots (s + 6373) (s + 381.2) (s^2 + 333.3 s + 2.81e5) (s^2 - 1.06e4 s + 2.46e8) \\ D = s^2 (s + 2.44e14) (s + 1.70e6) (s + 2.15e5) (s + 1.59e5) (s + 7641) (s + 5840) \cdots \\ \quad \cdots (s + 381.2) (s + 22.03) (s^2 + 333.3 s + 2.81e5) (s^2 + 2.01e4 s + 1.43e11) \end{cases} \quad (7.1)$$

In a transfer function, poles refer to the values of  $s$  for which the denominator ( $D$ ) is equal to zero; Zeros refer to the values of  $s$  for which the nominator ( $N$ ) is equal to zero. As it can be seen in Eq.7.1 the system is comprised of 14 poles and 13 zeros. It can also be seen that some poles and zeros have a really negative value ( $s = -2.44 \times 10^{14} \text{ s}^{-1}$ ) which, if represented in a root locus plot, would be placed on the far left of the plane. These zeros and poles are non-dominant and so they will have almost no influence in the control and stability of the system.

To reduce the order of the transfer function and thus simplify the analysis, a comparison of the responses obtained while poles and zeros from the far left are neglected have been done. This comparison can be seen in Fig.7.2. The order of the transfer function has been reduced but only neglecting poles and zeros that are purely real, since the elimination of complex poles/zeros translated into largely different responses. The transfer function obtained is the purple one (11th order), since the green one (10th order) already gives noticeable differences in the position of the steady state response.

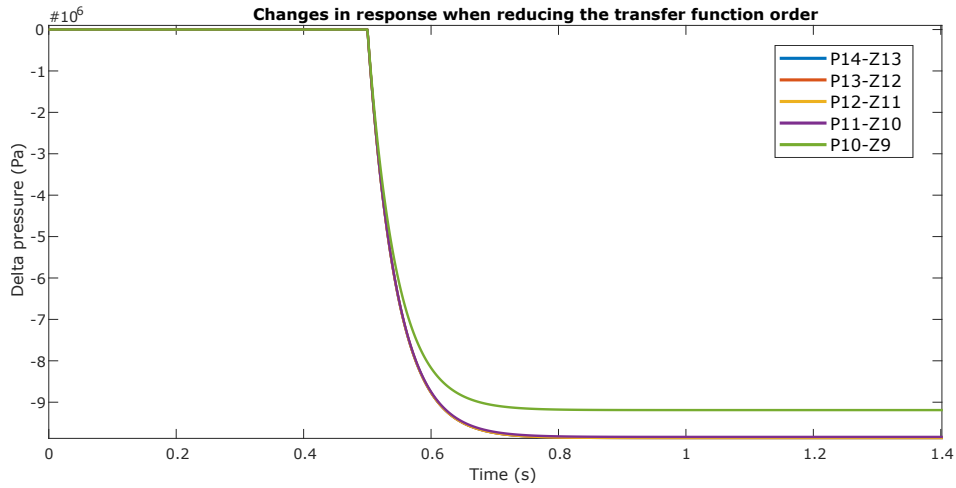


**Figure 7.2:** Plot showing how the response changes when the number of poles and zeros are reduced. The blue, orange, yellow and purple lines are overlapping.

$$Tf_{red} = \frac{N_{red}}{D_{red}} \begin{cases} N_{red} = -3.30e10 s^2 (s + 1.71e5) (s + 2.44e4) (s + 6373) (s + 381.2) \cdots \\ \quad \cdots (s^2 + 333.3 s + 2.81e5) (s^2 - 1.06e4 s + 2.46e8) \\ D_{red} = s^2 (s + 1.59e5) (s + 7641) (s + 5840) (s + 381.2) (s + 22.03) \cdots \\ \quad \cdots (s^2 + 333.3 s + 2.81e5) (s^2 + 2.01e4 s + 1.43e11) \end{cases} \quad (7.2)$$

Thus, the  $Tf_{red}$  (7.2) is the transfer function used for the sensitivity analysis. A close-up of the root locus plot for this transfer function can be seen in Fig.7.3.

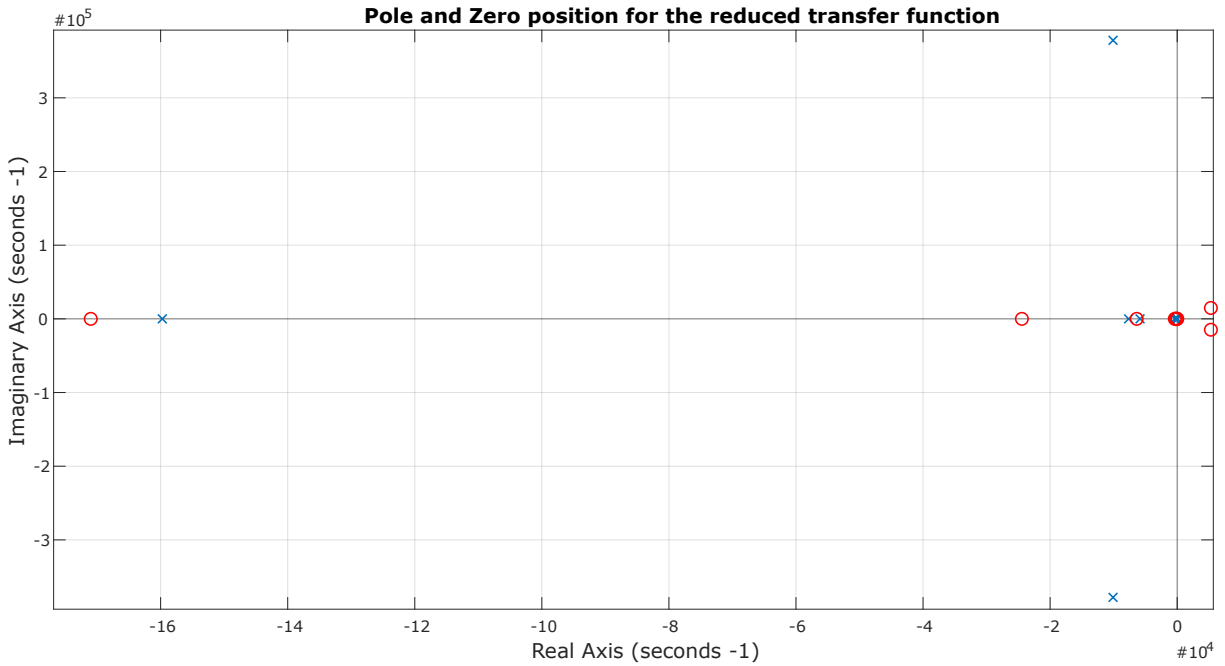


**Figure 7.3:** Plot showing the poles and zeros for the reduced transfer function. The poles are represented by blue X and the zeros as red circles.

In Fig.7.3 the dominant poles and zeros of the system are shown. Ideally all the poles and zeros

should be on the left side of the plot and with a large margin between them and the origin, so the system would remain stable for a wider range of inputs. It can be seen that all the poles (blue Xs) are on the negative side of the real axis, which is the stable part, but there are two complex zeros (red circles) on the right side of the plot, which may increase the instability of the system and affect the response. Besides that, there are several poles and zeros at the origin, which are marginally stable now but can become unstable at some inputs.

The change of position of the marginally stable poles and zeros and the position of the RHS (right hand side) zeros is what is going to be analyzed and optimized by adjusting the soft parameters.

### 7.3 Analyzing the effect of the discharge coefficients

As it was said in the introduction of the chapter, the analysis is performed by creating an array with different values of the  $C_d$  and obtaining the transfer function for each of systems with the different discharge coefficients. Afterwards, a comparison of the root locus plots for all the transfer functions is performed, in order to see the trend of how the position of the poles and zeros change.

The discharge coefficient is an indicator of the energy loss on an orifice due to the constriction of the fluid and the resistance that the orifice pieces imposes upon the flow. The discharge coefficient thus varies from 0 (which would indicate complete loss) to 1 (no loss). It cannot have a value greater than 1 because that would violate the conservation of energy laws. So in the analysis the value of  $Cd_2$  is going to vary from 0.1 to 1 with an increment of 0.1 each time.

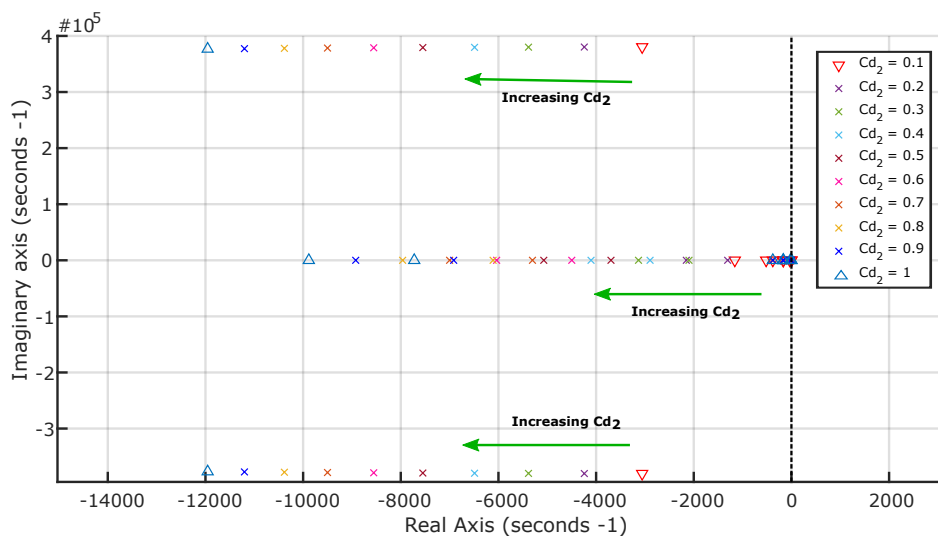


**Figure 7.4:** Root locus plot showing the movement tendency of the poles while increasing the  $Cd_2$ .

In Fig.7.4 the change in position of the dominant poles is shown and in Fig.7.5 the change in the zeros is shown. As it can be seen in both figures, for the poles and zeros on the left side plane an increment in the value of  $Cd_2$  translate into an increment in stability, while an increment of  $Cd_2$  for the zeros on the right hand side it translates into an increment in magnitude both in its real and complex values.

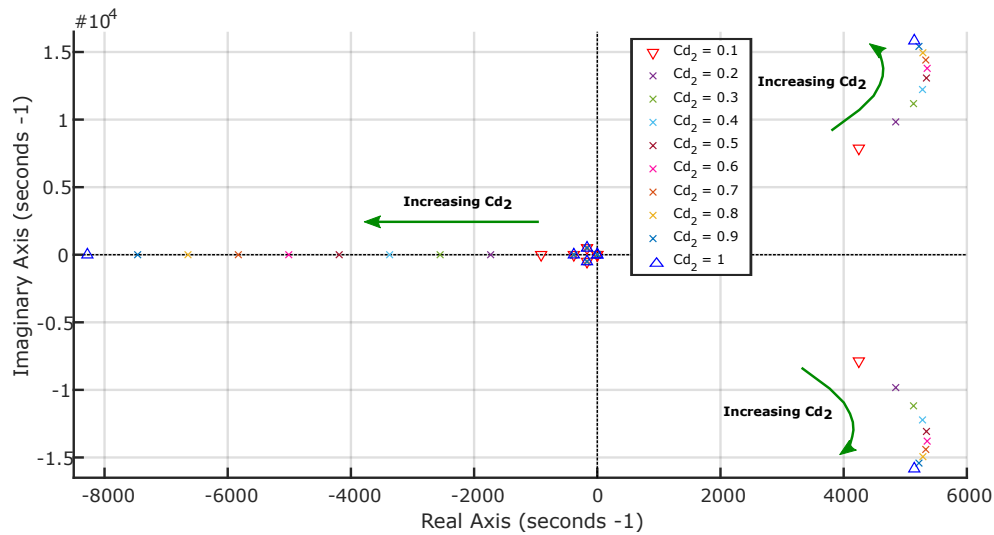


Figure 7.5: Root locus plot showing the movement tendency of the zeros while increasing the  $Cd_2$ .

### 7.4 Analyzing the effect of the damping coefficient

Next, the effect on the stability for changes in the damping coefficient of the gear set ( $b_{GS}$ ) and the priority valve ( $b_{ols}$ ) are going to be analyzed. The damping coefficient can have a wide range of values, so the analysis for the  $b_{ols}$  is done from 1 to 50,000 Ns/m and the  $b_{GS}$  from 0.01 to 150 Ns/rad.

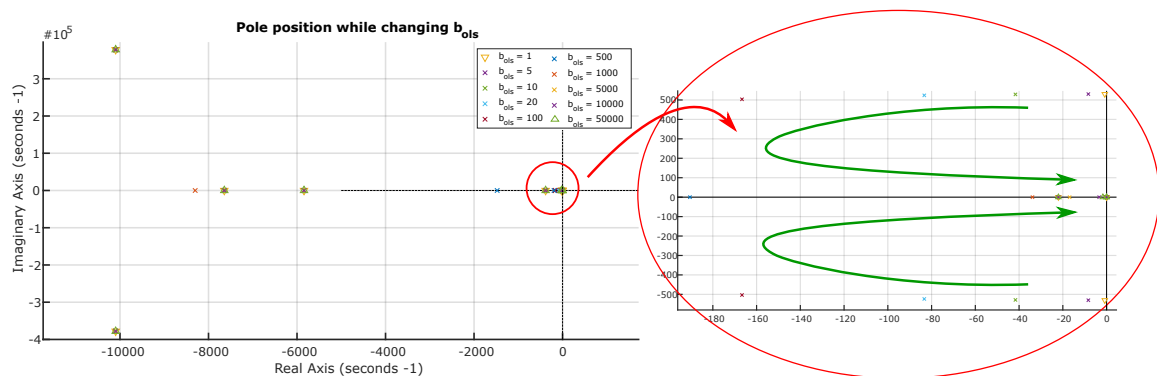


Figure 7.6: Plot of the changing position of the poles of the system when the  $b_{ols}$  is increased

In Fig.7.6 the changing positions of the poles while increasing the the  $b_{ols}$  are shown. It can be seen that the poles follow a tendency of stability until reaching 100 Ns/m. At 500 Ns/m the complexity of the poles disappear and from then on their stability start to decrease. This means than an increment of the damping will, at first, dampen the oscillatory behavior of the poles (which is a good thing), but too much damping will start to affect negatively the stability. Although in the figure only a closeup of some of the poles is shown, all the ones affected follow this same path.

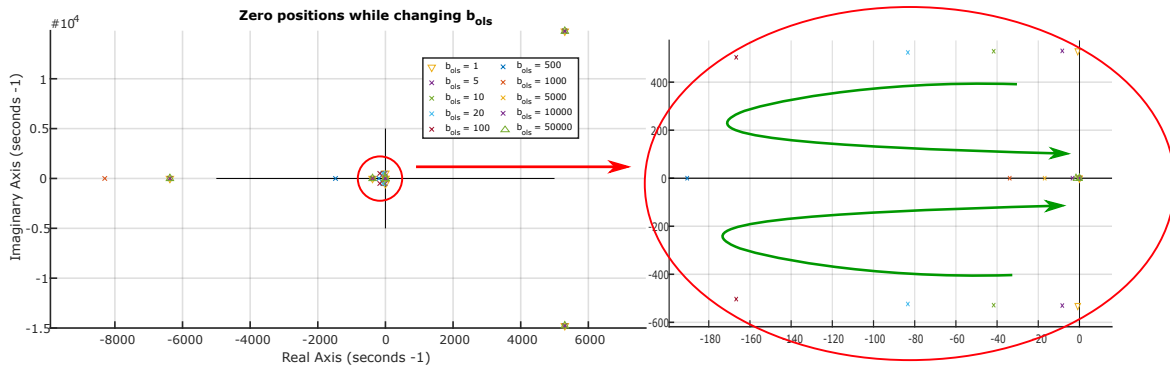


Figure 7.7: Plot of the changing position of the zeros of the system when the  $b_{ols}$  is increased.

As seen in Fig.7.7 the left hand side of the zeros follow the same trajectory as the poles, but the RHS zeros do not change positions noticeably.

Now the effect of  $b_{GS}$  is going to be analyzed. In Fig.7.8 it is seen again that there is a point where the complex poles become purely real and then start to lose stability, while the poles next to the origin become complex.

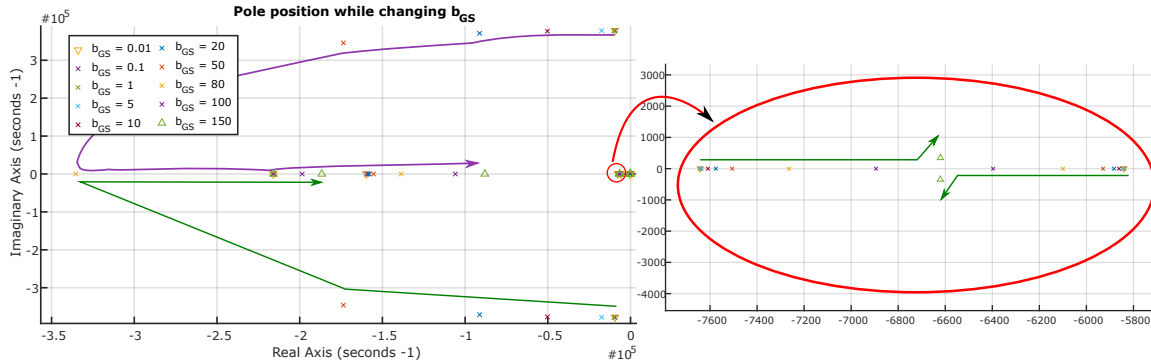


Figure 7.8: Plot of the changing position of the poles of the system when the  $b_{GS}$  is increased.

In Fig.7.9 it can be seen that, both the less dominant zeros on the LHS (left hand side) and the complex zeros on the RHS move towards the origin when the damping coefficient increases. The zeros closer to the origin are not affected by changes in the  $b_{GS}$ .

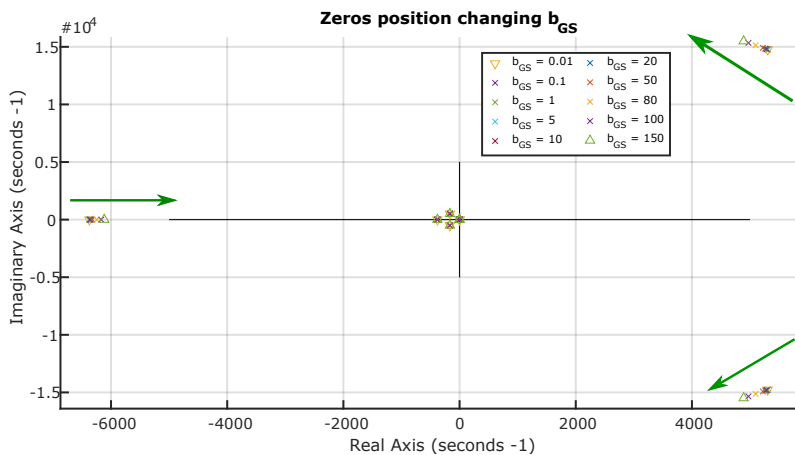


Figure 7.9: Plot of the changing position of the zeros of the system when the  $b_{GS}$  is increased.

## 7.5 Analyzing the effect of Areas and Volumes

Another cause of the instabilities can be the dimensions of the volumes and areas. Although the unwanted vibrations could be caused by the priority valve, in this project it is going to be assumed that the priority valve works correctly, and only the volumes and the areas in the steering unit (SU) are going to be changed. This is also due to the believe that it would be easier for the company to fix their new steering unit rather than to create a brand new priority valve just to fit the new SU design.

In the SU there are three volumes ( $V_{LS'}$ ,  $V_{sut}$  and  $V_{GS}$ ) and seven areas ( $A_1$ ,  $A_{LS'}$ ,  $A_{2R}$ ,  $A_{2L}$ ,  $A_{3R}$ ,  $A_{3L}$  and  $A_{sut}$ ). These areas can be either static, like the one from the orifice connecting the load sensing channel from the priority valve to the SU,  $A_{LS'}$ , or dynamic like  $A_1$ . If the area belongs to a static orifice, a change in its dimension is what is going to be analyzed. However if it belongs to a dynamic orifice, both the dimension of the orifice and the slope of the area's opening curve are going to be analyzed.

Two different analyses are going to be performed in order to demonstrate the influence of the different parameters on the stability and the response of the system. For the stability the position of the zeros and poles is going to be plotted, and for the response the different responses when the parameters are changed are going to be compared.

Now, an example of each of these types is going to be shown, with a final table summarizing the effect of all the parameters at the end of the chapter.

### 7.5.1 Effect of the $V_{LS'}$

As example of the effect of changing the volumetric capacity of the chambers, the  $V_{LS'}$  analysis is shown now. The analysis have been done by reducing and increasing the value of the volume. The decrease reaches up to 50% less of volume and the increment is of at most 100% of the original (so twice the volume). This is done since it is assumed that the goal is to tweak the parameters in order to gain stability, not completely change them. By altering the parameters in a unrealistic manner, they would start affecting each other, and thus a more in deep analysis should be done, maybe adding or subtracting elements.

In Fig.7.10 the position of the poles when the value of the volume is changed, is shown. The red square represent the original value of the volume, which is  $10^{-6} \text{ m}^3$ . When the volume is increased the complex poles lose complexity and gain stability, but the purely real poles become more unstable (although all of them remain in the left hand plane). When the volume is decreased the opposite is true. The poles that are closer to the origin, hence the most dominant poles, are not affected by the changing volumes.

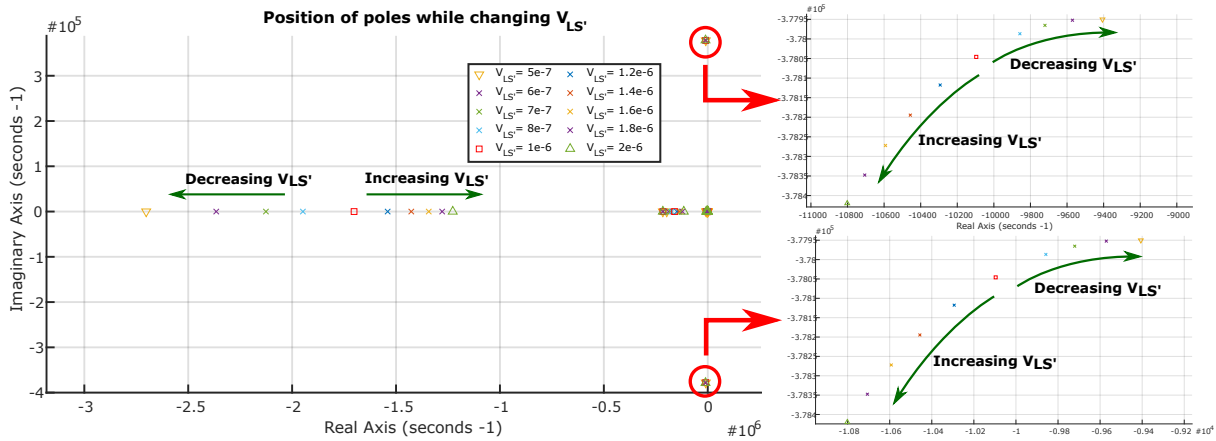


Figure 7.10: Pole location when changing the value of  $V_{LS'}$ .

The position of the zeros can be seen in Fig.7.11. It is seen that the LHS zeros increase in magnitude when the volume is decreased, and the RHS zeros, although they do not cross the 0 axis, they move towards the origin, albeit increasing in complexity. On the other hand, when the volume is increased the zeros on the LHS move towards the origin and the zeros on the RHS decrease in complexity but increase their real magnitude.

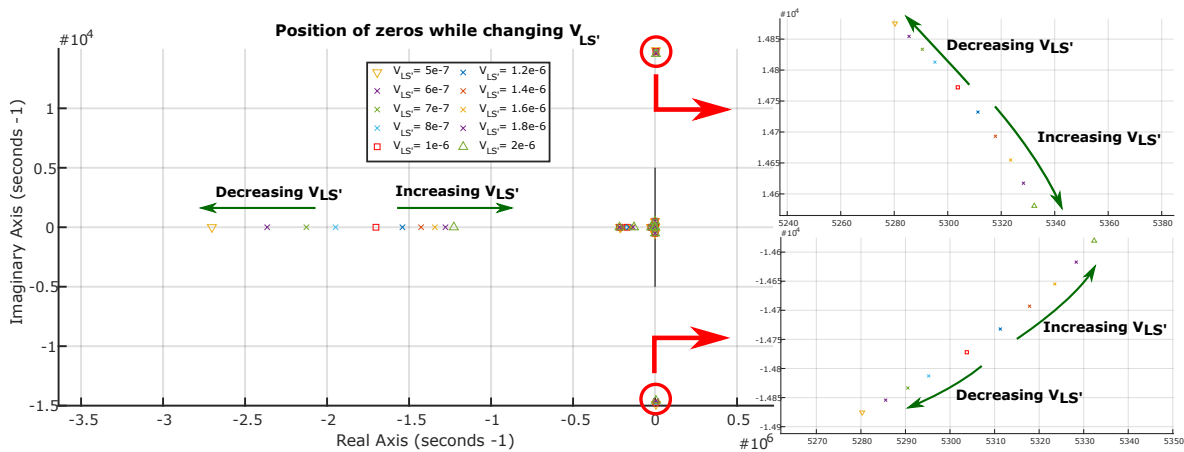
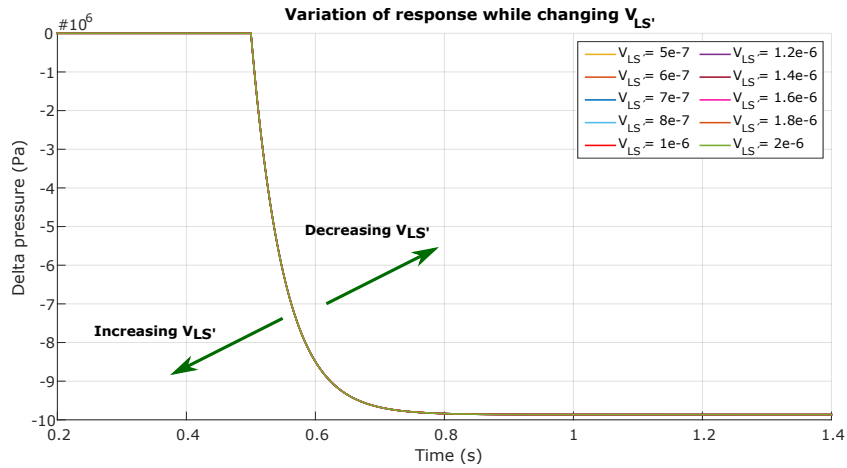


Figure 7.11: Zero location when changing the value of  $V_{LS'}$ .

In Fig.7.12 the effect on the response for the different values of  $V_{LS'}$  can be seen. Although in the figure the different paths cannot be discerned, the scale has been picked to be of these dimensions in order to be consistent for all the plots, hence making them more easily comparable visually. To counter the poor visibility, arrows showing the trends when the parameter is increased or decreased are added. Although it is marked that the system becomes faster when the volume is increased and slower when it is decreased, it can be seen that changes in the dimensions of this volume have minimal effect on the response.



**Figure 7.12:** Changes and trends of change of the response when the value of  $V_{LS'}$  is changed. The original value is represented with a red line.

The plots for the position of zeros and poles for the other two volumes ( $V_{GS}$  and  $V_{sut}$ ) and the change in the response can be seen in Appendix.C.

### 7.5.2 Effect of the $A_{LS'}$

Following the same premise as in the previous subsection, the dimensions of the  $A_{LS'}$  are also going to be varied in a scope of  $[0.5 \cdot A_{LS'} - 2 \cdot A_{LS'}]$ , with the original value being  $A_{LS'} = 4.91 \times 10^{-6} \text{ m}^2$ .

In Fig.7.13 the changing positions of the poles are shown. Over all, the system becomes more stable when the dimensions of  $A_{LS'}$  are increased.

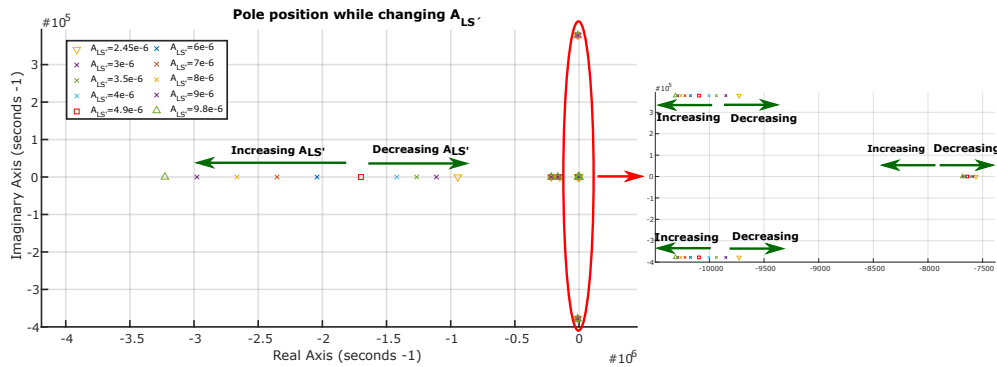


**Figure 7.13:** Position of the poles for different values of  $A_{LS'}$ . The original position is marked with a red square.

In Fig.7.14 the changing positions of the zeros can be seen. The zeros on the RHS increase in magnitude but their complexity remains unchanged, and the zeros that are affected on the LHS overall move towards the origin when the area is decreased.

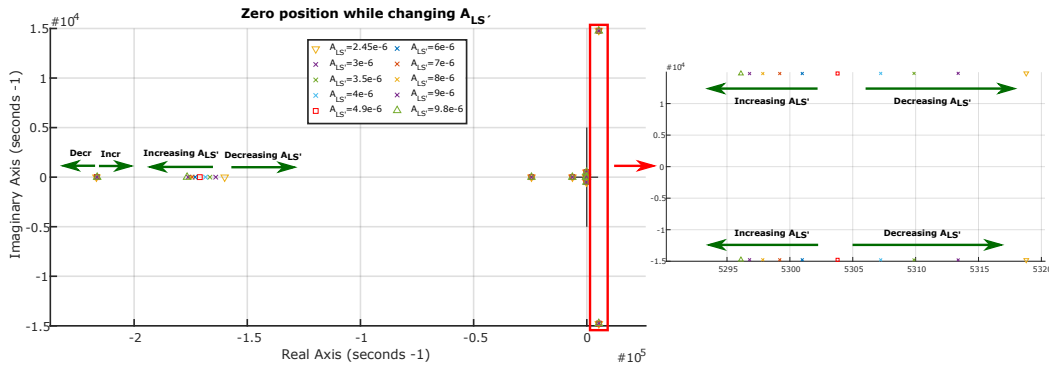


**Figure 7.14:** Position of the zeros for different values of  $A_{LS'}$ . The original position is marked with a red square.

Finally, the differences in the response when the parameter is varied is shown in Fig.7.15. When compared to the response of the  $V_{LS'}$ , it can be seen that they are inversely proportional, with the response becoming faster when the dimensions of  $A_{LS'}$  are reduced. But, similarly to the response in  $V_{LS'}$ , the changes on the volume have omittable effect in the response.

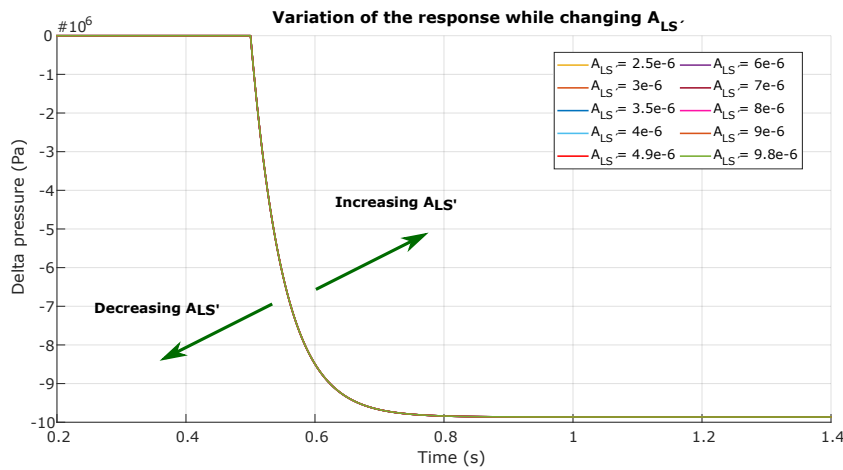


**Figure 7.15:** Changes and trends of change of the response when the value of  $A_{LS'}$  is changed. The original value is represented with a red line.

### 7.5.3 Effect of $A_{2R}$ and $\dot{A}_{2R}$

As an example of the dynamic orifice, the area and the slope of the 2R orifice are analyzed. The analyses are done separately: first an analysis similar to the one shown above is done, where the area is varied from half its original size to twice its size. The second analysis is done by changing the value of the slope, from a less steep slope to a sharper slope.

The initial value of  $A_{2R}$  is  $6.897 \times 10^{-6} \text{ m}^2$ . With this in mind, the area is going to be varied in a scope ranging from  $3.45 \times 10^{-6} \text{ m}^2$  to  $1.38 \times 10^{-5} \text{ m}^2$ . The change in the position of the poles when the area is altered can be seen in Fig.7.16, where the poles become more stable as the area increases and more unstable when it decreases.

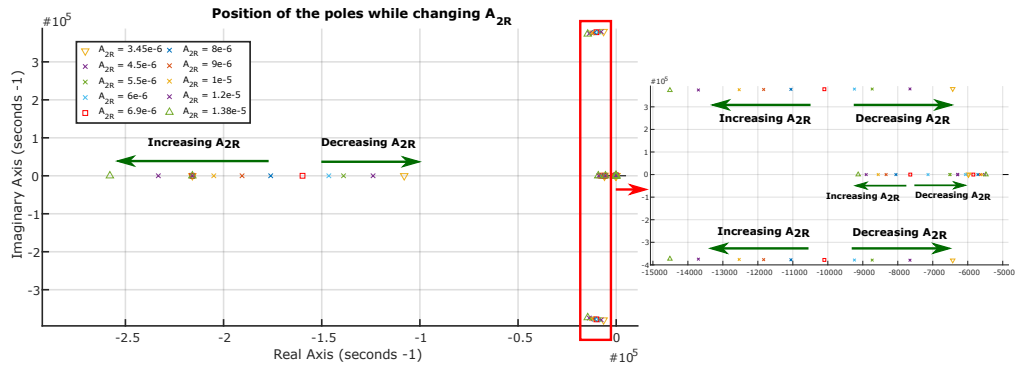


**Figure 7.16:** Position of the poles for a range of values of  $A_{2R}$ . The original value is represented with a red square.

In Fig.7.17 the zeros for the different areas are represented. As it happened with  $A_{LS'}$ , the zeros on the LHS move further towards the left when the area is increased, while the zeros on the RHS increase in magnitude, thus moving further towards the right. The opposite also occurs. It can also be seen that the changes in  $A_{2R}$  influence visibly more the position of the zeros than the changes in  $A_{LS'}$ .

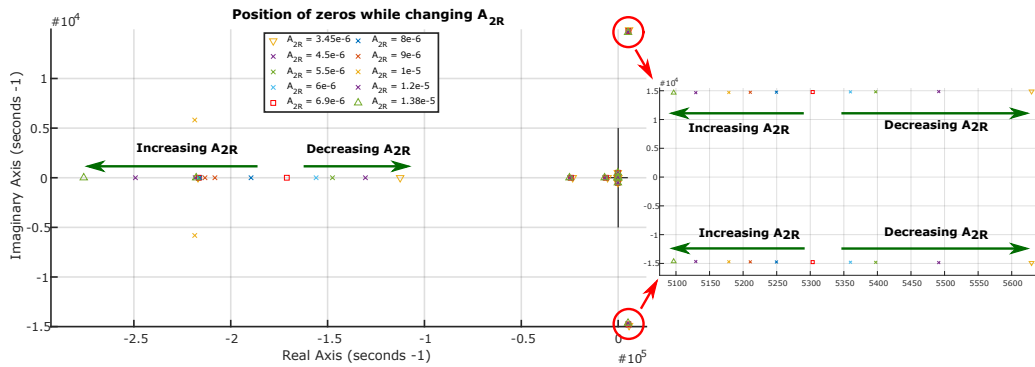


**Figure 7.17:** Position of the zeros for a range of values of  $A_{2R}$ . The original value is represented with a red square.

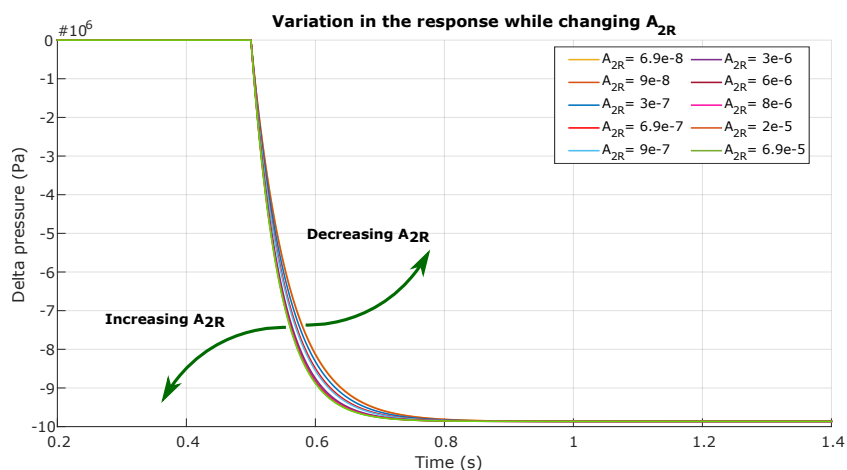


**Figure 7.18:** Changes and trends of change of the response when the value of  $A_{2R}$  is changed. The original value is represented with a red line.

Lastly, the variations in the response are plotted in Fig.7.18. As it can be seen, the system becomes faster when the dimensions of  $A_{2R}$  are increased, and slower when decreased. Although

the velocity of the response changes, they all follow the same path. When compared to the changes in the response obtained with  $V_{LS'}$  and  $A_{LS'}$ , it can be seen that the response is affected more visible when  $A_{2R}$  is changed.

While studying the influence of the slope in the position of both poles and zeros it is seen that it influences considerably less than the areas. Taking this into account, the analysis is done with a larger scope: from  $0.1 \cdot \dot{A}_{2R}$  to  $100 \cdot \dot{A}_{2R}$ . This is probably due to the fact that for an input of 1.02 rad/s, a lag ( $\Delta\alpha$ ) of around  $5^\circ$  is created. When looking at Fig.4.4, it shows that the slope is almost flat, and so it would need great increase to become noticeable.

In Fig.7.19 the pole position change is shown. As it can be seen, for a zoom similar to the one done in the other plots, no visible change in position is seen. No close-up plot of any region has been done for this poles, since the changes were so small that they have been neglected.

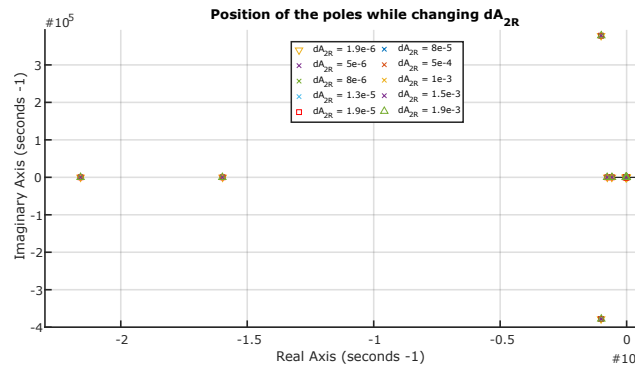


**Figure 7.19:** Position of the poles when the value of  $\dot{A}_{2R}$  is changed.

On the other hand, as seen in Fig.7.20, the position of the zeros is visibly affected by the change of slope. Although as said before, since the original slope is so flat, a reduction of it does not affect the position, only the increment of slope does. When the slope increases, the zeros on the right hand side increase both in magnitude and complexity; the zeros further away from the origin but on the left become more stable and the zeros closer to the origin become slightly more unstable.

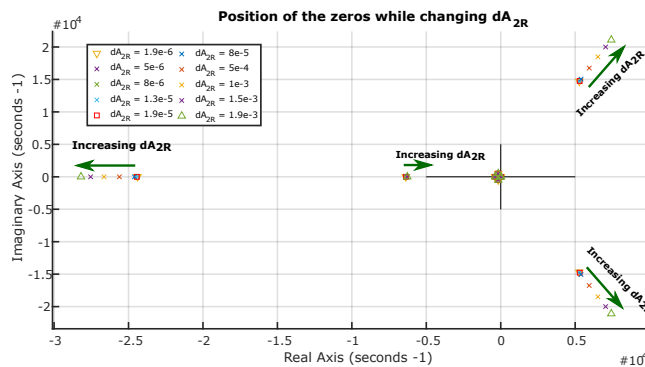


**Figure 7.20:** Position of the zeros when the value of  $\dot{A}_{2R}$  is changed. The zeros for the original value are represented with a red square.

For the analysis of the response, the plot in Fig.7.21 is shown. It is seen that when the slope of aperture of  $A_{2R}$  flattens, the system slows down, but when it becomes more of a steep curve the system shifts to an almost ideally fast response. As said before, the difference in the magnitude

of increment and decrease in the response is due to the fact that the slope is already considerably flat, so flattening it more will not affect the result significantly.

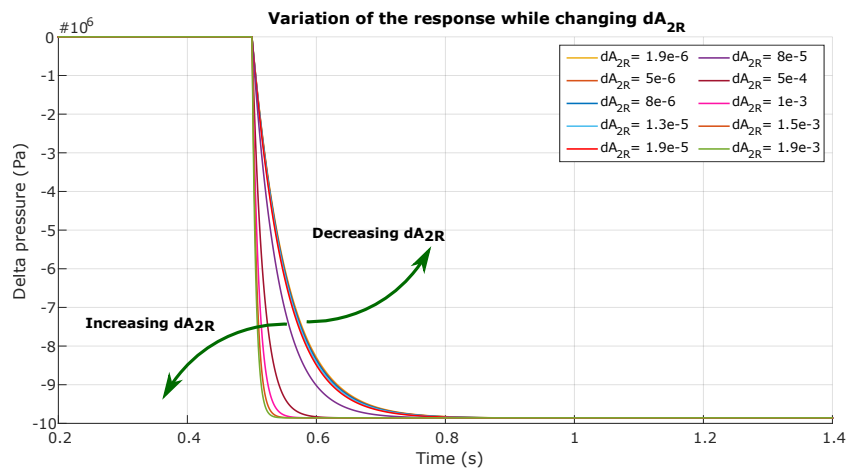


**Figure 7.21:** Changes and trends of change of the response when the value of  $\dot{A}_{2R}$  is changed. The original value is represented with a red line.

The same procedure followed in this subsection is followed for the analysis of the rest of the dynamic orifices. The plots for their poles and zero positions and for their responses can be seen in Appendix.C.

With this analysis it has been seen that  $A_1$  and  $A_{3R}$  have a great influence in the position of the pole whose initial position is  $p = 22.03s^{-1}$  (which is the most dominant pole before the marginally stable ones), which in turn have a big influence in the response. This is in accordance with the fact that  $A_1$  is the gateway for the flow, so its increase in dimension translates into more flow going through the SU. Furthermore, the  $A_{3R}$  dimensions are inversely proportional to the flow going through the steering cylinder, and thus to the  $\Delta P$  of the cylinder, since if the dimensions of  $A_{3R}$  increase more flow will go through it, hence less through  $A_{2R}$ . All of this is backed up with Fig.7.22 and Fig.7.23 respectively.

In Fig.7.22 it can be seen that, when the dimensions of  $A_1$  are reduced drastically, the pole becomes complex, and thus an oscillatory behavior is introduced to the response, which creates the overshoot in the yellow line.

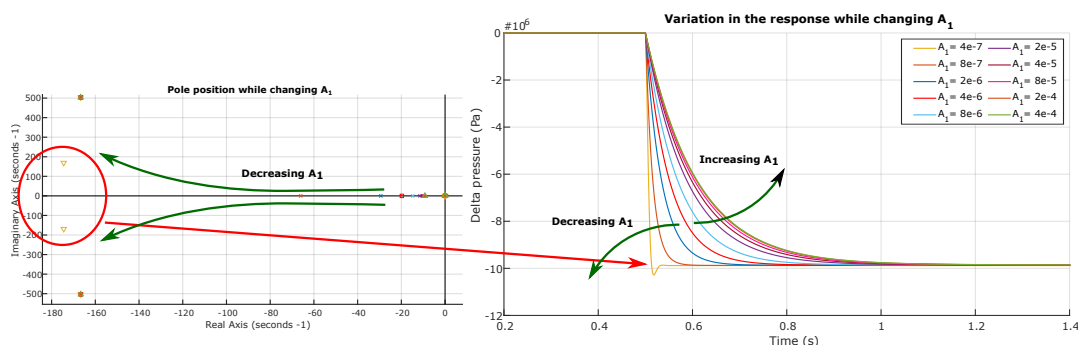


**Figure 7.22:** Relation between the position of the poles and the behavior of the response when  $A_1$  is changed. The original pole and response are represented with a red square and a red line respectively.

In Fig.7.23 it is shown how when  $A_{3R}$  is increased, the position of said pole changes visibly until it almost reaches zero. This is translated into a much slower system response, since less flow will

go to the steering cylinder. It can also be seen that, since the original dimensions of  $A_{3R}$  are considerably small, decreasing them more will just slightly affect the response.

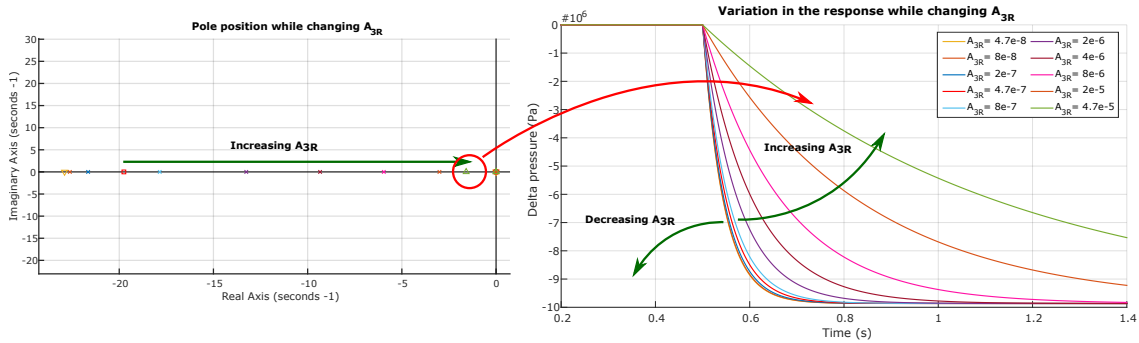


**Figure 7.23:** Relation between the position of the poles and the behavior of the response when  $A_{3R}$  is changed. The original pole and response are represented with a red square and a red line respectively.

This is also reflected in the change of the slopes  $\dot{A}_1$  and  $\dot{A}_{3R}$  where the sudden change in the response when the slope is increased also translates to a visible change in the pole from  $p = 22.03 \text{ s}^{-1}$  to  $p = 38.03 \text{ s}^{-1}$  when  $\dot{A}_1$  is increased and in a similar way when  $\dot{A}_{3R}$  is increased.

### 7.6 Effect of $V_0$

Finally, an analysis of the effect of the displacement per revolution of the gear set ( $V_0$ ) is performed. Although in Chapter 5 an analysis regarding the relation between the velocity of the gear wheel, the displacement per revolution and the  $\Delta P$  response has been done, in this new analysis the differences in value of the steady state are not going to be looked into. Instead, the influence of  $V_0$  in the stability of the system and in the velocity of the response is going to be analyzed.

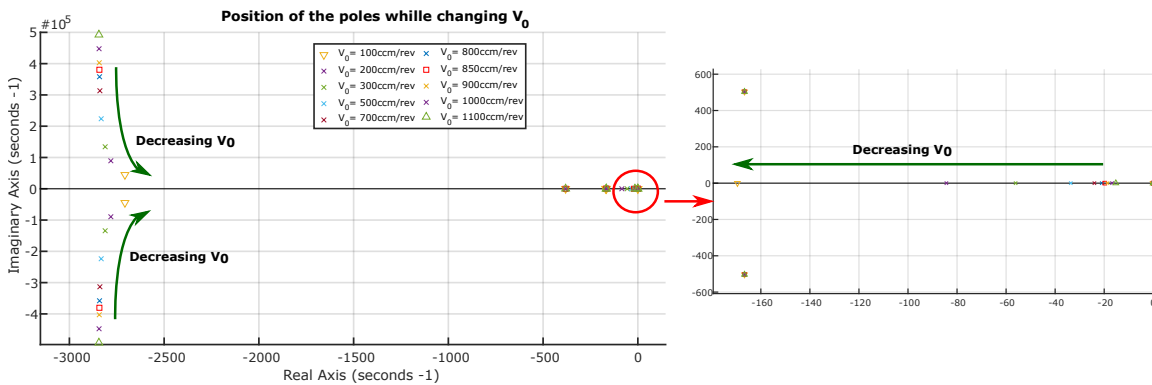


**Figure 7.24:** Variation of the positions of the poles when the value of  $V_0$  is changed. A close up of the smaller poles is shown on the right. The original position is marked with a red square.

As seen in Fig.7.24 the system becomes more stable when the value of  $V_0$  is reduced, both by increasing the magnitude of the poles closer to the origin and by reducing the complexity of the complex poles.

In Fig.7.25 the position of the zeros is represented. When the value of the displacement is reduced, the position of the zeros on the right hand plane is moved more towards the origin, and the zeros further away on the left hand plane also move towards the origin.

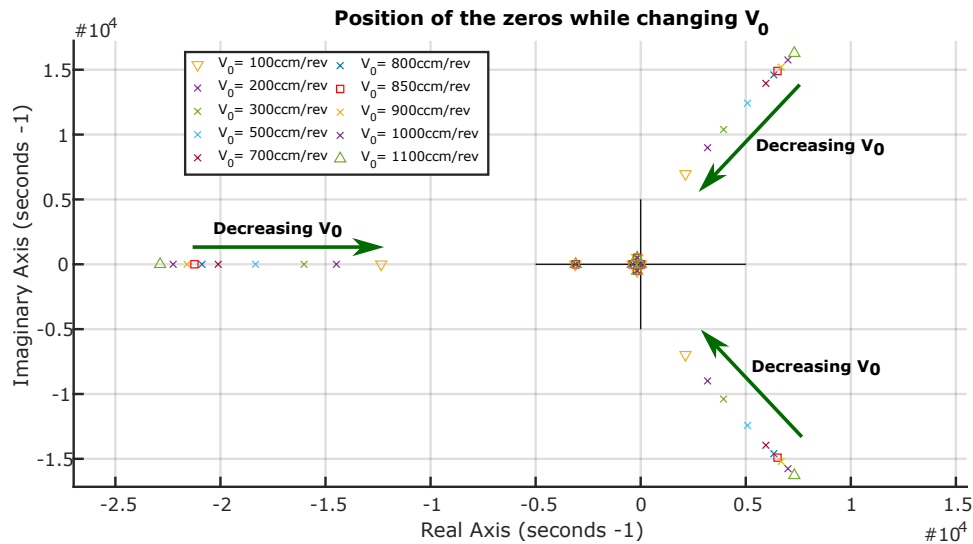


**Figure 7.25:** Variation of the positions of the zeros when the value of  $V_0$  is changed. A close up of the smaller poles is shown on the right. The original position is marked with a red square.

In Fig.7.26 the changes in the responses are shown. Looking past the differences in the steady state value, it can be seen that the system gets faster as the value of  $V_0$  decreases. This correlates with the change in position toward the far left of one of dominant pole shown in Fig.7.24.

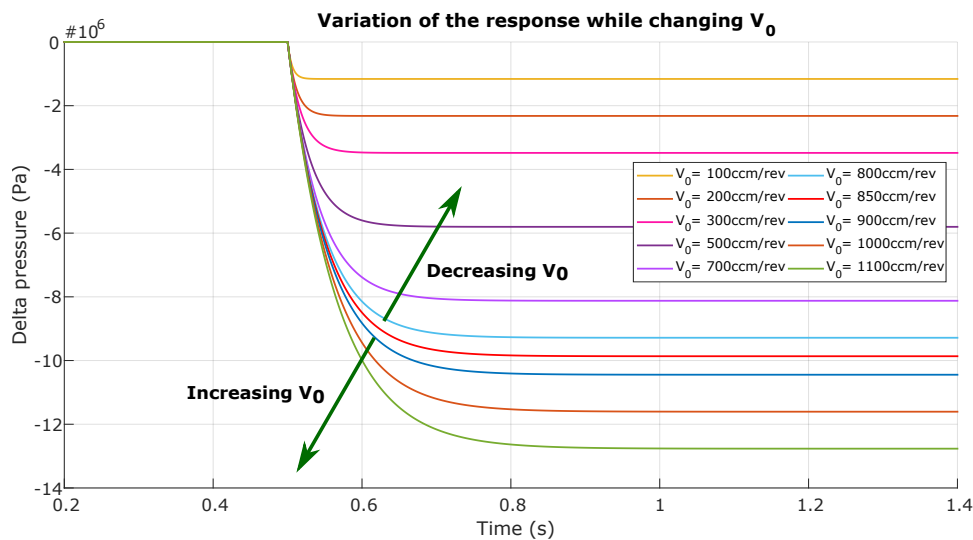


**Figure 7.26:** Changes and trends of change of the response when the value of  $V_0$  is changed. The original value is represented with a red line.

With the analysis done, but before finding the new parameters that would enhance the stability and response, some guidelines for these parameters are chosen. First, the minimum value of the areas is chosen to be  $A_{min} = 0.3 \text{ mm}^2$ , since due to the density of the oil, a smaller area would prevent the oil to pass through. Second, the maximum value an area can take is chosen to be  $A_{max} = 7 \text{ mm}^2$  since a bigger orifice would stop working properly since all the oil would be able to pass freely. Finally, by looking at other SU models from the company, it has been confirmed that the steering unit could have a reduced value of  $V_0$ .

As a summary of all the analyses, Table 7.1 has been created where each parameter is analyzed on how to change it in order to increase the overall stability and the response. Although the

scope of the new parameters will not have much of an impact in the response, it has been decided to increase the time it takes to reach the steady state slightly, since it is more in accordance with the real response. An *I* has been written as short for *Increase* if the parameter has to be increased, and a *D* short for *Decrease* if the parameters has to be decreased. If the parameter's value is marked with -- it means that it does not affect the result noticeably and thus it has been neglected.

In the table, parameters such as discharge coefficient or damping coefficient have not been written, since their values are much more fluid and will be used only for last retouches.

	Stability	Response		Stability	Response
$V_{LS'}$	I	-	$A_{3R}$	D	I
$V_{GS}$	D	-	$A_{3L}$	I	I
$V_{sut}$	D	-	$\dot{A}_1$	I	D
$A_{LS'}$	I	-	$\dot{A}_{2R}$	-	D
$A_1$	I	I	$\dot{A}_{2L}$	I	D
$A_{2R}$	I	D	$\dot{A}_{3R}$	I	D
$A_{2L}$	I	I	$\dot{A}_{3L}$	-	D
$V_0$	D	D			

**Table 7.1:** Summary of the action needed to do to the dimensions of each parameter in order to increase the stability or improve the response.

# 8 | Improved Model

## 8.1 Improved linear model

The first parameters that are going to be changed for the improved model are the ones that lie outside the maximum and minimum dimensions. That is,  $A_{2L}$  which is going to be increased from  $0.19\text{ mm}^2$  to  $0.3\text{ mm}^2$  and  $A_{3L}$  which is going to be decreased from  $10\text{ mm}^2$  to  $7\text{ mm}^2$ , to mach the limiting dimensions previously described. In reality, the increase in  $A_{2L}$  will reduce the amount of flow going through  $A_{2R}$  and thus to the gear set. However, it will increase the stability since, by increasing the area, the flow will be less irregular. In Fig.8.1 the new position for the poles and zeros when these two parameters are changed can be seen. Although the less dominant poles and zeros become more unstable, the pole in position  $p = -22\text{ s}^{-1}$  which, as seen in the previous chapter, was the one with most influence in the stability and response, doubles its value, thus increasing the stability.

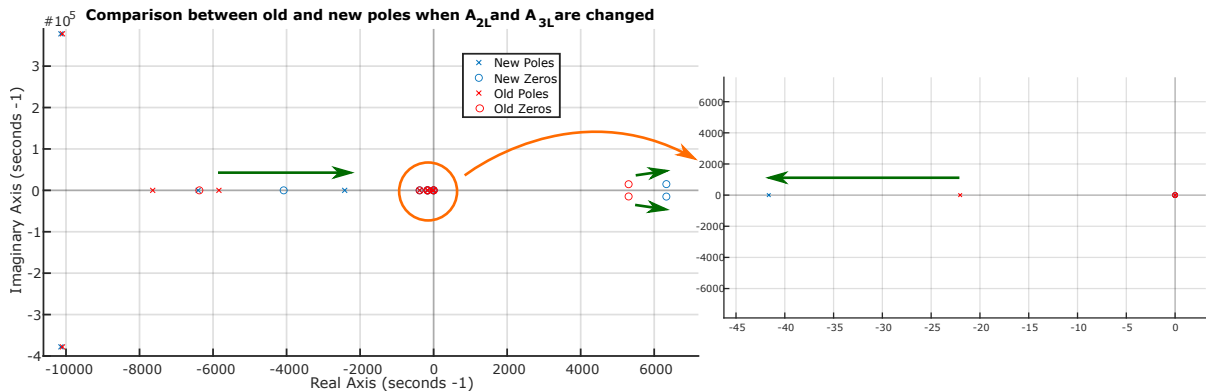


**Figure 8.1:** Comparison between the positions of the old and new poles and zeros. On the right a close up of the poles closer to the origin. The green arrows mark the trend of change between old and new models.

On the other hand, the steady state response does not change, even though the system becomes faster (due to said pole), as seen in Fig.8.2.

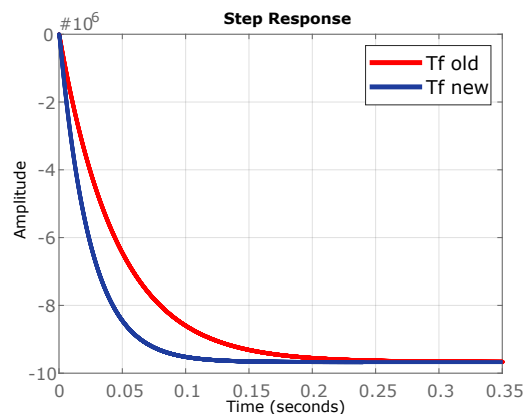


**Figure 8.2:** Comparison between the step response obtained with the original transfer function (red) and the new one with the  $A_{2L}$  and  $A_{3L}$  parameters changed (blue).

The next parameters that are going to be changed are: The area  $A_1$ , which is going to be decreased from  $4.9 \text{ mm}^2$  to  $4 \text{ mm}^2$  since, as seen in the previous chapter it shifts the poles closer to zero on the left. The area  $A_{3R}$  from  $0.47 \text{ mm}^2$  to the minimum, that is  $0.3 \text{ mm}^2$ , since it both improves the stability and also in the real model it would permit more flow to go through the gear set, since less flow would go through it and thus to tank. The last parameter is the displacement per revolution, which is going to be decreased from  $850 \text{ ccm/rev}$  to  $500 \text{ ccm/rev}$ . This is done to increase the stability, and also, it will make the gear wheel turns less powerful and thus make the changes in flux less abrupt in the real model.

A plot comparing the original model, the previous model (with only  $A_{2L}$  and  $A_{3L}$  changed) and this new model can be seen in Fig.8.3. In this plot it can be seen that with this new model the pole in  $p = -22 \text{ s}^{-1}$  becomes even more stable, moving from around  $44 \text{ s}^{-1}$  to around  $78 \text{ s}^{-1}$ , and the zeros on the right hand side move slightly closer to the origin.

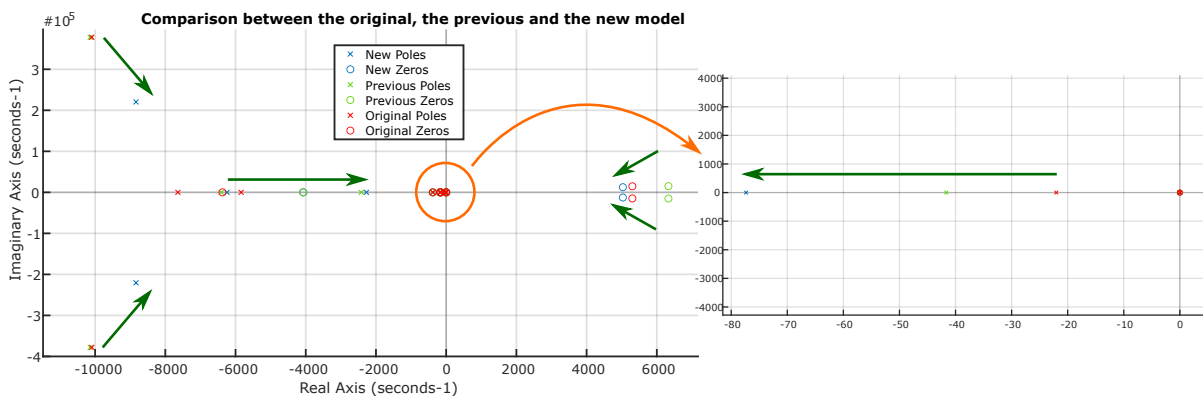


**Figure 8.3:** Comparison of the pole and zero position between the original model (red), the previous model (green) and the new model (blue). The green lines mark the direction of change between old and new positions.

The presence of zeros on the RHS usually creates "undershoot" in the system response. That is, for this system the response would have an initial positive slope before going negative, which would be dangerous in real life, since the vehicle would start turning to the wrong side before turning to the correct side. That is why it would be ideal to be able to move it to the origin or left hand side. Since that undershoot was not visible in any of the responses and the zeros were too far into the RHS to be able to move them to the left just by tweaking parameters, it has been decided to not try to improve their position any more.

The discharge coefficients of the system are not going to be changed either, since the original ones are acceptable enough when compared to other discharge coefficients from systems that have been tested experimentally. Ideally their value would be as close as possible to 1, limiting the energy lost from the system, but this is however difficult to obtain experimentally.

The damping coefficient for the gear set has been increased, in order to increase the time response of the system, to the same value as the damping coefficient from the priority valve. That is,  $b_{OLS} = 20 \text{ Ns/m}$ .

When choosing the changes in slope, it has been decided to only change  $\dot{A}_1$  by increasing it, since the other two slopes that affect the stability are  $\dot{A}_{2L}$  and  $\dot{A}_{3R}$ .  $\dot{A}_{2L}$  and  $\dot{A}_{3R}$  could improve the stability by being less steep, but those are the slopes corresponding to the areas that are already at its minimum value, and it would not be reasonable to reduce it more.

Finally, although the volumes do change the position of the poles, the poles that get changed are non-dominant poles, or at least poles whose change in position do not affect noticeably the response. Taking this into account it has been decided not to change the value of non of the three volumes.

Applying all these changes, the final position of the poles and zeros for the improved model looks like Fig.8.4.

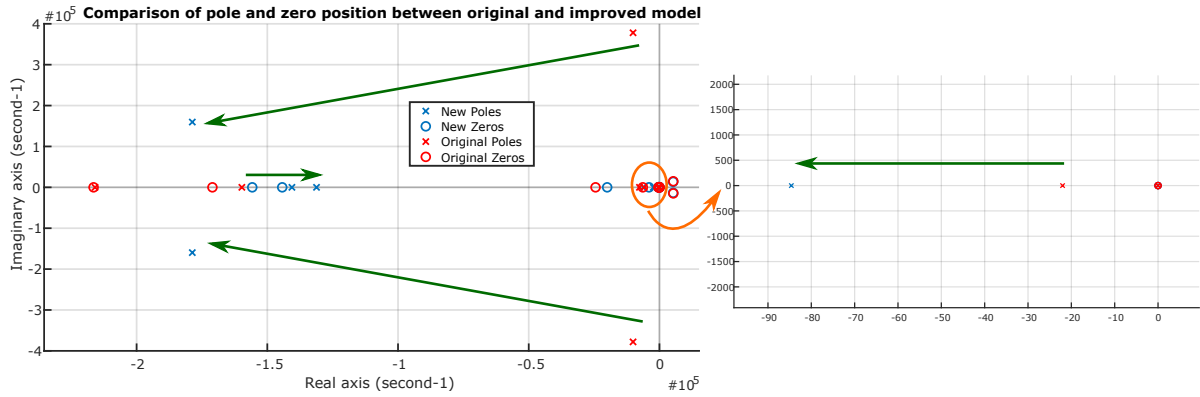


**Figure 8.4:** Comparison between the improved model (blue) and the original model (red). The green arrows signal the trend of change in position.

As can be seen in the figure, although the trend for the non-dominant poles located in the x-axis is to move towards the origin, the complex poles have decreased their complex value and increased their real value. This is beneficial as they will decay faster, hence they will influence less in the response. Also, since their complex value has been reduced, the frequency of their oscillations will be slower.

The final value of the the dominant pole located at  $p = -22 \text{ s}^{-1}$  has increased in magnitude until reaching the value of  $p = -84.6 \text{ s}^{-1}$ , which makes the system noticeably more stable. The final value of the the zeros on the RHS is similar to the one obtained in the previous model.

## 8.2 Improved nonlinear model

With the information gathered in Chapter 7, the nonlinear model can also be improved. The improvements in the nonlinear model are the following:

First, as in the improved linear model, the displacement per revolution of the gear set have been reduced to 500 ccm/rev.

Second, the maximum and minimum openings for the areas have been set to  $7 \text{ mm}^2$  and  $0.3 \text{ mm}^2$  respectively, except for the openings of the  $A_1$  orifice, since it is the gateway for the rest of orifices and thus needs to provide enough oil for all of them.

Finally, instead of reducing the areas, since for the nonlinear model an array of different dimensions are used, the slopes are the ones that were changed. Taking into account that the model has to perform equally great when the wheel is turned in both directions all slopes have been smoothed out and made overall less steep, thus providing a more progressive increase in flow when the steering wheel is turned, instead of the abrupt increase provided in the original model. A comparison between the areas from the original model and the areas from the improved model

can be seen in Fig.8.5. If the two plots are compared, it can be seen that the sudden changes in slope have been removed and that the area of the  $A_1$  orifice is always greater than any of the other areas, thus the flow in the steering unit does not decrease. Although for this first improvement the slope of areas  $A_{2L}$  and  $A_{3R}$  are equal (same for  $A_{2R}$  and  $A_{3L}$ ), in subsequent models this could be looked into in more depth.

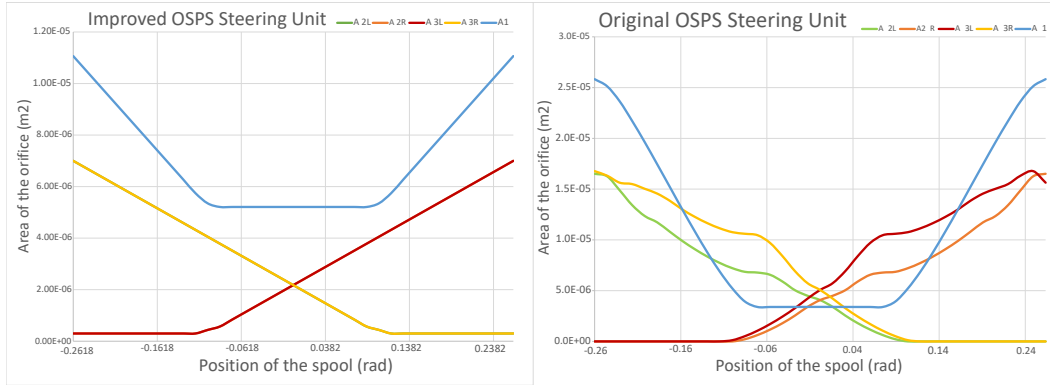


**Figure 8.5:** Left: plot showing the improved areas for the Steering Unit. The orifice  $A_{2L}$  follows the same path as  $A_{3R}$  and the orifice  $A_{2R}$  follows the same path as  $A_{3L}$ . Right: plot showing the original areas for the Steering Unit.

Once the new areas are obtained, a comparison of the response ( $\Delta P$ ) obtained with the different models is acquired. In this comparison the original model, the model obtained in Chapter 5 (so with equal areas as the original but different  $V_0$ ) and the improved model are going to be looked into. A plot showing these three responses can be seen in Fig.8.6.

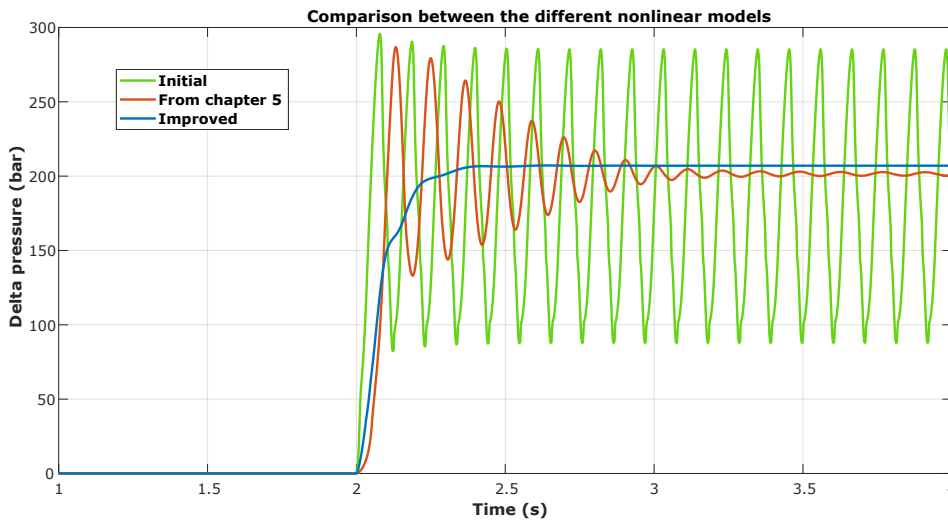


**Figure 8.6:** Comparison of the responses obtained with the original model (green), the model obtained in the validation chapter (orange) and the improved model (blue).

It can be seen in the figure how, for the original model, the system would become completely unstable when the required 210 bar pressure was trying to be obtained. This pressure was obtained with a  $V_0 = 135$  ccm/rev and a steering wheel velocity of 12.1 rad/s.

With the Chapter 5 method, which has the same areas as the original model but the displacement per revolution different, the response would have unwanted vibrations. However, instead of remaining constant as in the initial model, they would die out after some seconds, although some

remnants of the oscillations would prevail. This response was obtained with a  $\omega_{sp} = 2.06$  rad/s and a  $V_0 = 850$  ccm/rev.

The final improved response, obtained with the new areas and a  $V_0 = 500$  ccm/rev shows no vibration when the required pressure is obtained, although some lumps can be seen in the curved part of the plot. The velocity required to obtain this pressure is  $\omega_{sp} = 3.55$  rad/s, which is considerably less than the one needed for the original model.



## 9 | Conclusions and future work

The conclusions of this master thesis are:

- A mathematical model has been created from an experimental setup in order to better understand the system.
- A linearized model has been obtained from the nonlinear model in order to analyze the causes of the unwanted behaviour.
- A validation of the system has been performed in order to prove that the simulated system behaves in a logic way.
- An analysis of the relation between velocity input and pressure drop in the steering cylinder has been carried out in order to extract an initial guess of the input and displacement per revolution of the gear set used in the experimental setup.
- A sensitivity analysis has been conducted to gain a deep understanding of how each of the components of the real system affect the stability and response of the system. The sensitivity analysis has been done of both the pole and zero position and the response of the system.
- An improved model has been constructed in which, by changing the areas and displacement per revolution of the gear set, the unwanted behaviour is corrected.

As future work, the following ideas and recommendations are provided:

- A validation of the original steering system simulation with the experimental setup.
- A comparison between the results obtained with the improved model and the ones obtained once said changes have been implemented in the experimental setup.
- A more in depth analysis of the area openings to obtain a more realistic opening curve.
- An optimization analysis to find the best trade-off between velocity of the response and stability of the system.



# Bibliography

**Carsten Lund, 2002.** Morten Schack Søborg Carsten Lund. *Stabilization of a hydraulic steering unit: OSPF LS*, Aalborg University, 2002.

**Danfoss, July 2017.** Danfoss. *Steering. General, Steering Components*.  
[www.powersolutions.danfoss.com](http://www.powersolutions.danfoss.com), 2017. Downloaded: 10-11-2019.

**Danfoss, January 2015.** Danfoss. *Business Unit steering, training*.  
[www.powersolutions.danfoss.com](http://www.powersolutions.danfoss.com), 2015. Downloaded: 10-10-2019.

**Nielsen, 2018.** Torben Risager Nielsen. *Development, Validation and Optimization of a Speed Steering Dynamic Simulation Model*, Aalborg University, 2018.

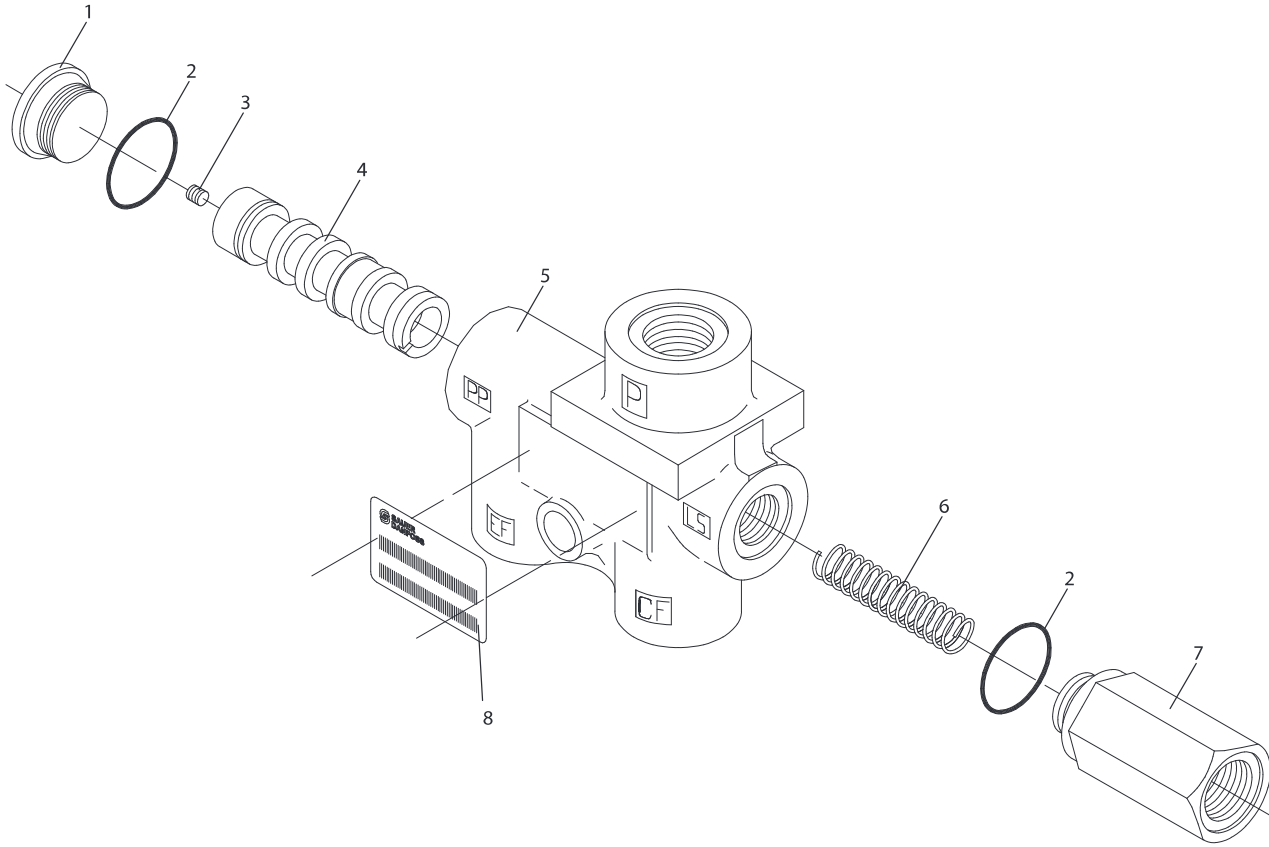
**Sauer-Danfoss, 2002.** Sauer-Danfoss. *OSPB, OSPC, OSPR, OSPD Open Center Steering units*. [www.sauer-danfoss.com](http://www.sauer-danfoss.com), 2002. Downloaded: 10-11-2019.



# A | Data Sheet OLS 40/80



Exploded View  
OLS 40/80



P301 162


**Spare Part List  
OLS 40/80**

Item	Spare parts	Code no	Orifice	Comments	No per unit	Tightening torque	
1	Internal PP – plug	152-0413		For seal ring (Al)	1	40 N-m +/- 10	
	External PP – plug	631X2046		For O-ring	1		
	G 1/4	152B0371	0.8 mm		1		
	M12 x 1.5	152B0314	0.8 mm		1		
	M12 x 1.5	11005127	1.0 mm		1		
	M12 x 1.5	152B0425	1.2 mm		1		
	PF 1/4	152B0434	0.8 mm		1		
2	Seals	O-ring	633B1457		2		
3	Orifice screw (PP)	155B8316	0.6 mm	M6	1	3.5 N-m +/- 0.5	
		631B1048	0.7 mm	M6	1		
		152B0380	0.8 mm	M6	1		
		631B1043	0.9 mm	M6	1		
		155B8320	1.0 mm	M6	1		
		631B1039	1.2 mm	M6	1		
4	Spool Static:	OLS 40	152B0302	Dynamic orifice:	Not sold separately info. Only		
		OLS 40	152B0310		Intern pp CF 2.5 - EF 4, 9, 18		1
		OLS 40	152B0326		Intern pp CF 0 - EF 4, 9, 18		1
		OLS 80	152B0462		Extern pp CF 2.5 - EF 4, 9, 18		1
		OLS 80	152B0304		Intern pp CF 8 - EF 4, 9		1
		OLS 80	152B0316		Intern pp CF 8 - EF 4, 9, 18		1
		OLS 80	152B0316		Intern pp CF 0 - EF 4, 9, 18		1
		OLS 80	152B0305		Extern pp CF 8 - EF 4, 9, 18		1
Dynamic:	OLS 40	152B0306	0.6 mm	Intern pp CF 2.5 - EF 4, 9, 18	1		
	OLS 40	152B0311	0.6 mm	Intern pp CF 2.5 - EF 2, 5, 10, 21	1		
	OLS 40	11059514	0.8 mm	Intern pp CF 2,5 - EF 2, 5, 10, 21	1		
	OLS 40	152B0307	0.9 mm	Intern pp CF 2.5 - EF 4, 9, 18	1		
	OLS 40	152B0442	0.9 mm	Intern pp CF 2.5 - EF 2, 5, 10, 21	1		
	OLS 80	152B0365	0.7 mm	Intern pp CF 8 - EF 4, 9, 19	1		
	OLS 80	152B0449	0.9 mm	Intern pp CF 8 - EF 4, 9, 19	1		
	OLS 80	152B0454	0.7 mm	Intern pp CF 8 - EF 4, 9	1		
	OLS 80	152B0441	1.0 mm	Intern pp CF 8 - EF 4, 9, 18	1		
	OLS 80	11035542	0.9 mm	Intern pp CF 8 - EF 2, 5, 10, 22	1		
	5	Housing			Not sold separately		1
6	Spring	4 bar	663X1088		1		
		5.5 bar	663X6208		1		
		7 bar	663X1087		1		
		10 bar	663X1084		1		
7	External LS – plug	G 1/4 Male	11005740	1.0 mm		40 N-m +/- 10	
		G 1/4	152B0372	0.7 mm			
		G 1/4 (external thread)	152B0426	0.7 mm			
		G 1/4	152B0370	0.8 mm			
		G 1/4	152B0448	1.0 mm			
		G 1/4	152B0378	1.2 mm			
		M12 x 1.5	152B0424	0.7 mm			
		M12 x 1.5	152B0369	0.8 mm			
		M12 x 1.5	11005126	1.0 mm			
		M12 x 1.5 for O-ring	152B0386	0.8 mm			
		M12 x 1.5 for O-ring	11028890	1.1 mm			
		PF 1/4	152B0435	0.7 mm			
		PF 1/4	11004288	1.2 mm			
		7/16 – 20 UNF	152B0368	0.7 mm			
		7/16 – 20 UNF	152B0376	0.8 mm			
		7/16 – 20 UNF	152B0431	1.0 mm			
		7/16 – 20 UNF	11003795	1.2 mm			
8	Name plate			Not available	1		
	Spare part bag	152B4015		Contains item 2			



## B | Linearized parameters

The linearized parameters for the priority valve are:

$$k_{qxCF} = \text{sgn}(P_{Pi} - P_{CFi}) \cdot Cd_1 \cdot \sqrt{\frac{2 \cdot |P_{Pi} - P_{CFi}|}{\rho}} \cdot \delta A_{CF} \quad (\text{B.1})$$

$$k_{qxEF} = \text{sgn}(P_{Pi} - P_{EFi}) \cdot Cd_1 \cdot \sqrt{\frac{2 \cdot |P_{Pi} - P_{EFi}|}{\rho}} \cdot \delta A_{EF} \quad (\text{B.2})$$

$$k_{qpCF} = \text{sgn}(P_{Pi} - P_{CFi}) \cdot \frac{Cd_1 \cdot A_{CFi} \sqrt{\frac{2}{\rho}}}{2 \cdot \sqrt{P_{Pi} - P_{CFi}}} \quad (\text{B.3})$$

$$k_{qpEF} = \text{sgn}(P_{Pi} - P_{EFi}) \cdot \frac{Cd_1 \cdot A_{EFi} \sqrt{\frac{2}{\rho}}}{2 \cdot \sqrt{P_{Pi} - P_{EFi}}} \quad (\text{B.4})$$

$$k_{qpLS} = \text{sgn}(P_{DYNi} - P_{LSi}) \cdot \frac{Cd_2 \cdot A_{LS} \sqrt{\frac{2}{\rho}}}{2 \cdot \sqrt{P_{DYNi} - P_{LSi}}} \quad (\text{B.5})$$

$$k_{qpDYN} = \text{sgn}(P_{CFi} - P_{DYNi}) \cdot \frac{Cd_2 \cdot A_{DYN} \sqrt{\frac{2}{\rho}}}{2 \cdot \sqrt{P_{CFi} - P_{DYNi}}} \quad (\text{B.6})$$

$$k_{qpPP} = \text{sgn}(P_{CFi} - P_{PPi}) \cdot \frac{Cd_2 \cdot A_{PP} \sqrt{\frac{2}{\rho}}}{2 \cdot \sqrt{P_{CFi} - P_{PPi}}} \quad (\text{B.7})$$

And for the steering unit and steering cylinder:

$$k_{xA1} = \text{sgn}(P_{CFi} - P_{LS'i}) \cdot Cd_2 \cdot \sqrt{\frac{2 \cdot |P_{CFi} - P_{LS'i}|}{\rho}} \cdot \delta A_1 \quad (\text{B.8})$$

$$k_{xA2L} = \text{sgn}(P_{LS'i} - P_{SCi}) \cdot Cd_2 \cdot \sqrt{\frac{2 \cdot |P_{LS'i} - P_{SCi}|}{\rho}} \cdot \delta A_{2L} \quad (\text{B.9})$$

$$k_{xA2R} = \text{sgn}(P_{LS'i} - P_{GSi}) \cdot Cd_2 \cdot \sqrt{\frac{2 \cdot |P_{LS'i} - P_{GSi}|}{\rho}} \cdot \delta A_{2R} \quad (\text{B.10})$$

$$k_{xA3L} = \text{sgn}(P_{SCi} - P_{suti}) \cdot Cd_2 \cdot \sqrt{\frac{2 \cdot |P_{SCi} - P_{suti}|}{\rho}} \cdot \delta A_{3L} \quad (\text{B.11})$$

$$k_{xA3R} = \text{sgn}(P_{GSi} - P_{suti}) \cdot Cd_2 \cdot \sqrt{\frac{2 \cdot |P_{GSi} - P_{suti}|}{\rho}} \cdot \delta A_{3R} \quad (\text{B.12})$$

$$k_{xA_T} = \text{sgn}(P_{suti} - P_T) \cdot Cd_2 \cdot \sqrt{\frac{2 \cdot |P_{suti} - P_T|}{\rho}} \cdot \delta A_{10} \quad (\text{B.13})$$

$$k_{qpA1} = \text{sgn}(P_{CFi} - P_{LS'i}) \cdot \frac{Cd_2 \cdot A_{1i} \sqrt{\frac{2}{\rho}}}{2 \cdot \sqrt{P_{CFi} - P_{LS'i}}} \quad (\text{B.14})$$

$$k_{qpLS'} = \text{sgn}(P_{LS'i} - P_{LS}) \cdot \frac{Cd_2 \cdot A_{LS'} \sqrt{\frac{2}{\rho}}}{2 \cdot \sqrt{P_{LS'i} - P_{LS}}} \quad (\text{B.15})$$

$$k_{qpA2L} = \text{sgn}(P_{LS'i} - P_{SCi}) \cdot \frac{Cd_2 \cdot A_{2Li} \sqrt{\frac{2}{\rho}}}{2 \cdot \sqrt{P_{LS'i} - P_{SCi}}} \quad (\text{B.16})$$

$$k_{qpA2R} = \text{sgn}(P_{LS'i} - P_{GSi}) \cdot \frac{Cd_2 \cdot A_{2Ri} \sqrt{\frac{2}{\rho}}}{2 \cdot \sqrt{P_{LS'i} - P_{GSi}}} \quad (\text{B.17})$$

$$k_{qpA3L} = \text{sgn}(P_{SCi} - P_{suti}) \cdot \frac{Cd_2 \cdot A_{3Li} \sqrt{\frac{2}{\rho}}}{2 \cdot \sqrt{P_{SCi} - P_{suti}}} \quad (\text{B.18})$$

$$k_{qpA3R} = \text{sgn}(P_{GSi} - P_{suti}) \cdot \frac{Cd_2 \cdot A_{3Ri} \sqrt{\frac{2}{\rho}}}{2 \cdot \sqrt{P_{GSi} - P_{suti}}} \quad (\text{B.19})$$

$$k_{qpAT} = \text{sgn}(P_{suti} - P_T) \cdot \frac{Cd_2 \cdot A_{10i} \sqrt{\frac{2}{\rho}}}{2 \cdot \sqrt{P_{suti} - P_T}} \quad (\text{B.20})$$

$$k_{qpB} = \text{sgn}(P_{Ri} - P_{SC}) \cdot \frac{Cd_B \cdot A_B \sqrt{\frac{2}{\rho}}}{2 \cdot \sqrt{P_{Ri} - P_{SC}}} \quad (\text{B.21})$$

# C | More sensitivity analysis

The pole and zero position when the value of  $V_{sut}$  is changed can be seen in Fig.C.1 and Fig.C.2 respectively.

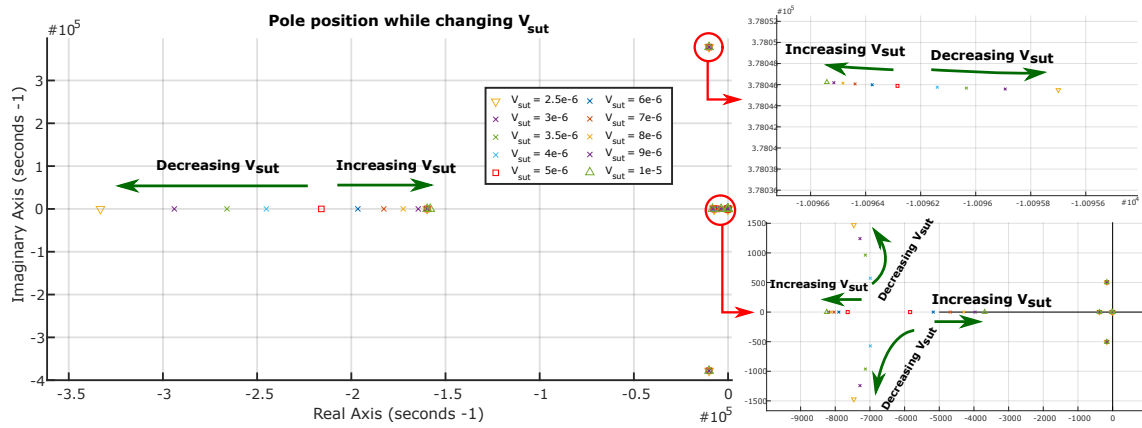


**Figure C.1:** Position and trend of variation of the poles when the value of  $V_{sut}$  is either increased or decreased. The original value is  $V_{sut} = 5e-6m^3$

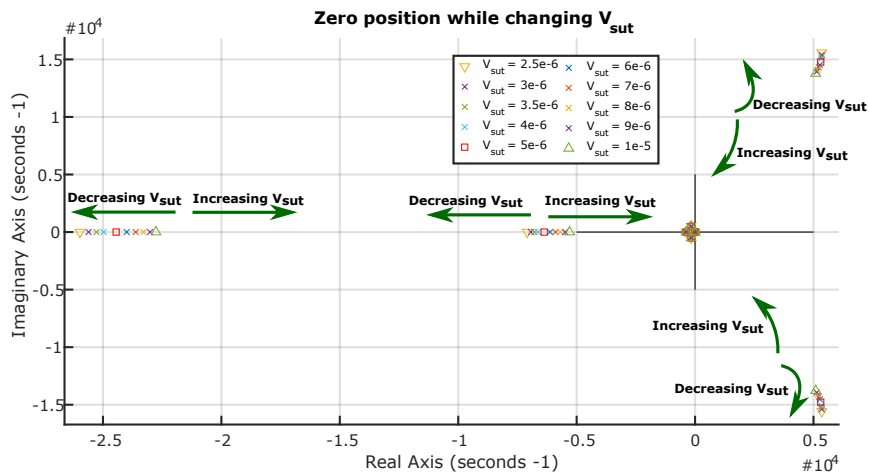


**Figure C.2:** Position and trend of variation of the zeros when the value of  $V_{sut}$  is either increased or decreased. The original value is  $V_{sut} = 5e-6m^3$

The changes in the response when  $V_{sut}$  is varied is plotted in Fig.C.3. The trend of change is shown with green arrows pointing the direction of the change.

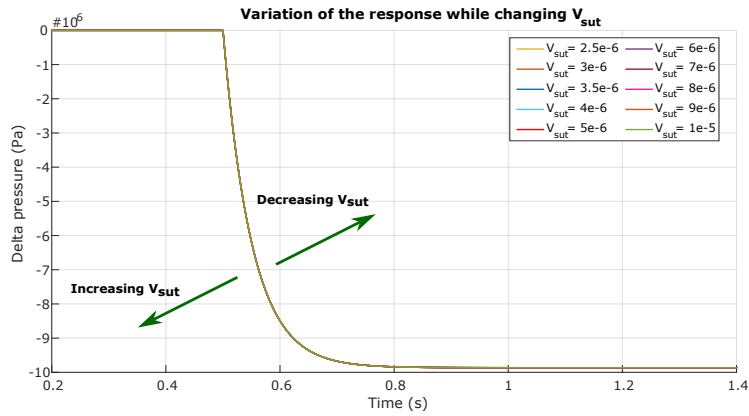


**Figure C.3:** Plot showing how the response of the system changes when  $V_{sut}$  is changed. The original response is represented with a red line.

The pole and zero position and the response when the value of  $V_{GS}$  is changed can be seen on Fig.C.4, Fig.C.5 and Fig.C.6 respectively.

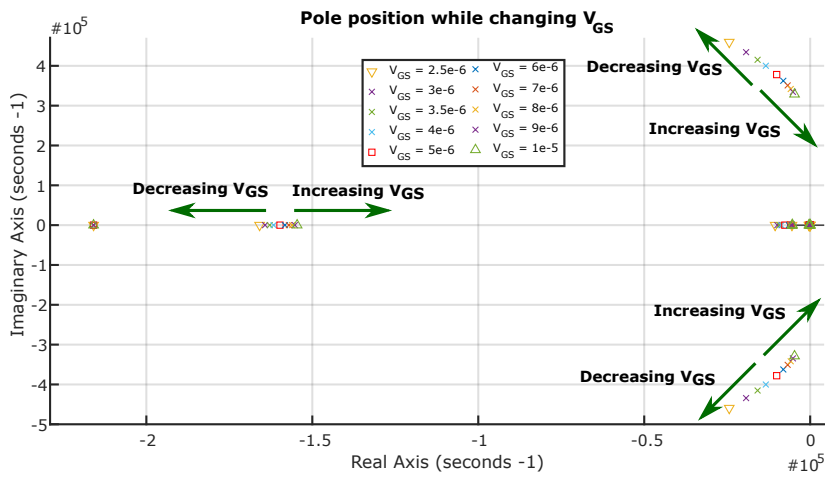


**Figure C.4:** Position and trend of variation of the poles when the value of  $V_{GS}$  is either increased or decreased. The original value is  $V_{GS} = 5e-6m^3$

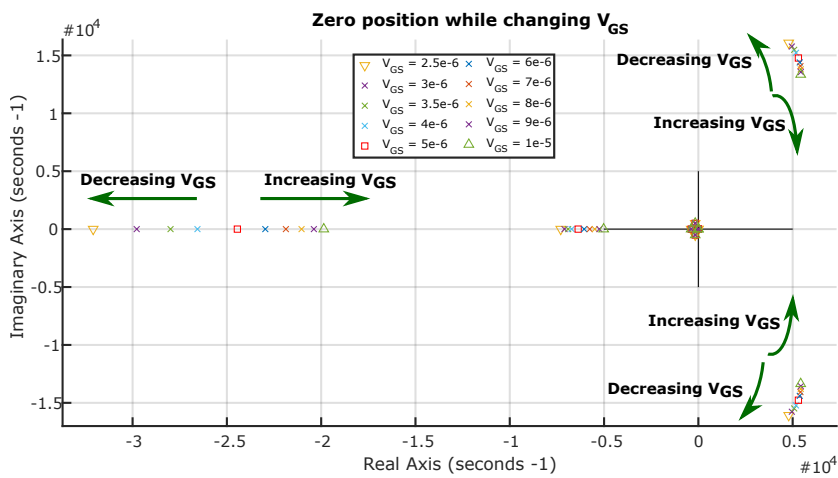


**Figure C.5:** Position and trend of variation of the zeros when the value of  $V_{GS}$  is either increased or decreased. The original value is  $V_{GS} = 5e-6m^3$

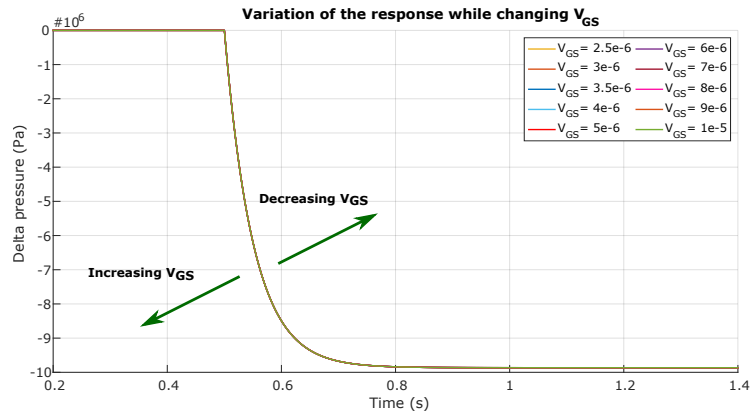


Figure C.6: Plot showing how the response of the system changes when  $V_{GS}$  is changed. The original response is represented with a red line.

$A_{2L}$  and  $\dot{A}_{2L}$

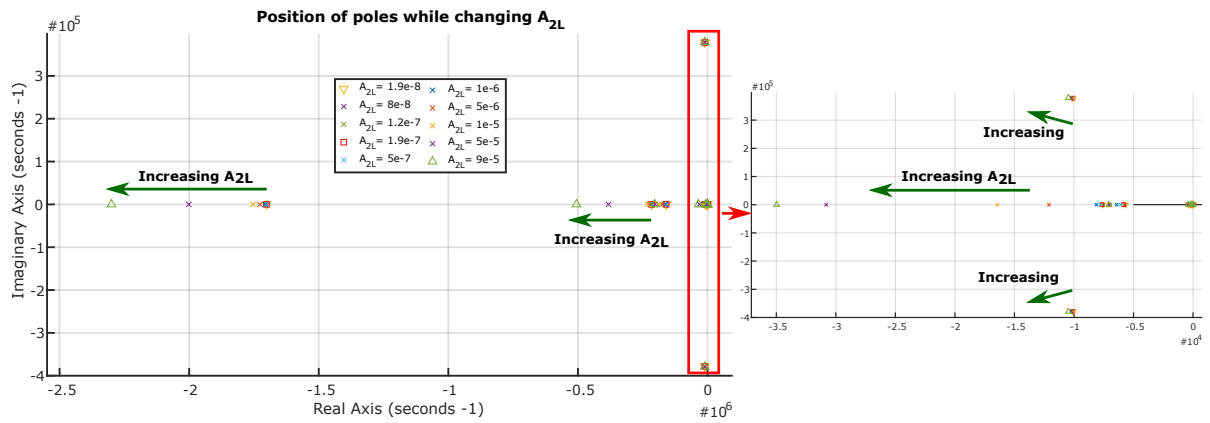


Figure C.7: Position and trend of variation of the poles when the value of  $A_{2L}$  is either increased or decreased. The original value is represented with a red square.

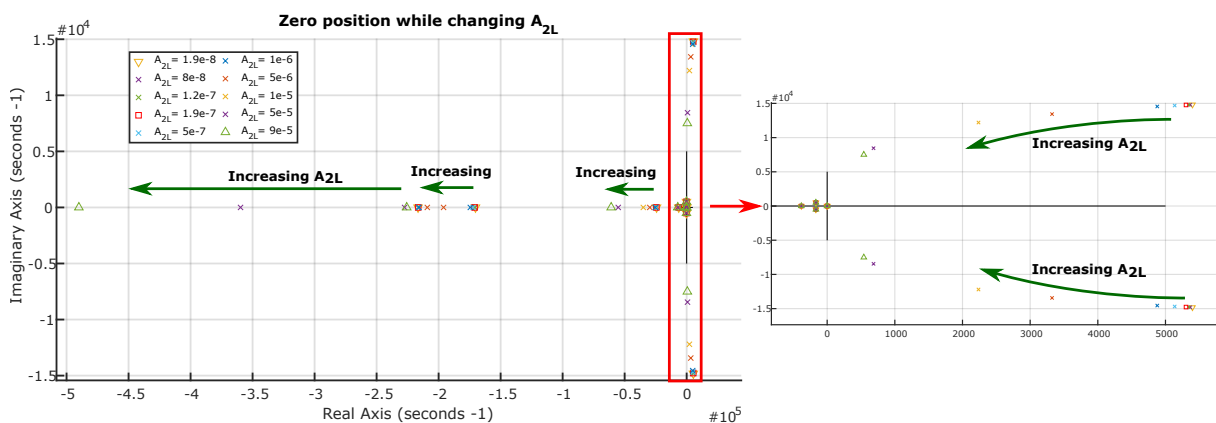


Figure C.8: Position and trend of variation of the zeros when the value of  $A_{2L}$  is either increased or decreased. The original value is represented with a red square.

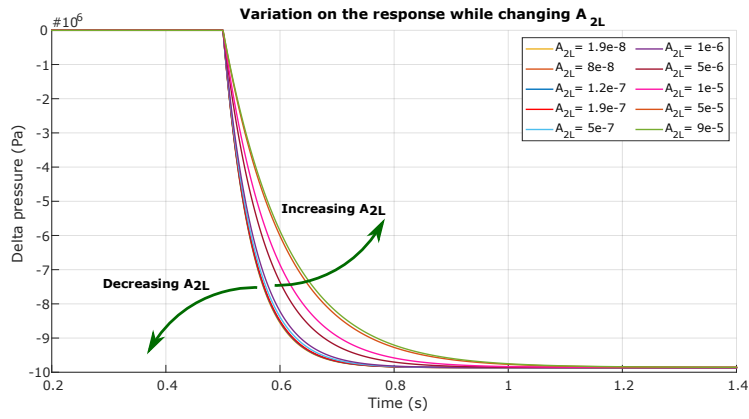


Figure C.9: Plot showing how the response of the system changes when  $A_{2L}$  is changed. The original response is represented with a red line.

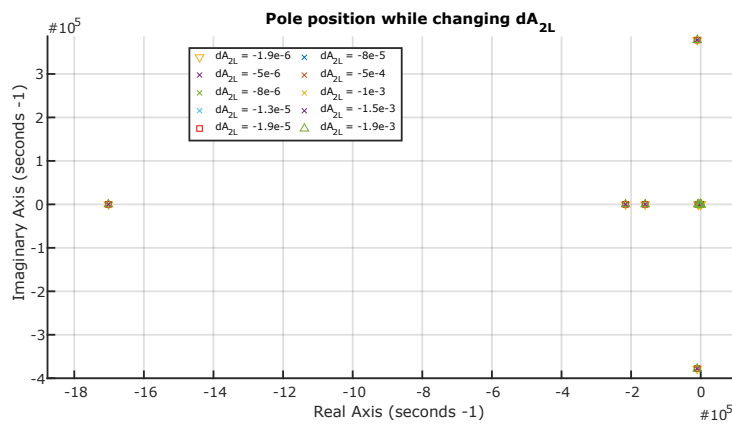


Figure C.10: Position and trend of variation of the poles when the value of  $\dot{A}_{2L}$  is either increased or decreased. The original value is represented with a red square.

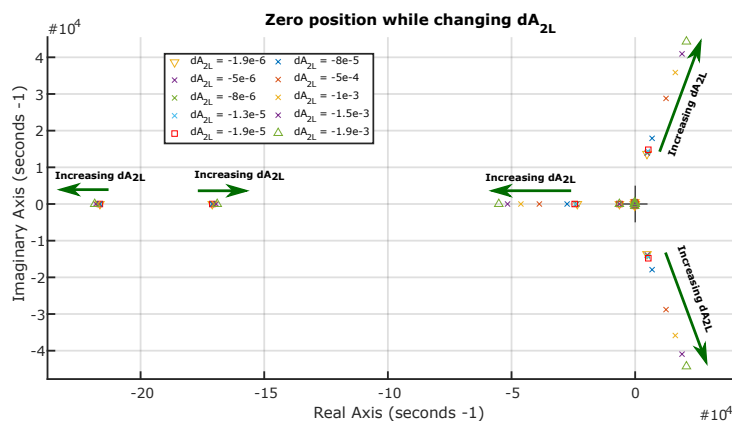


Figure C.11: Position and trend of variation of the zeros when the value of  $\dot{A}_{2L}$  is either increased or decreased. The original value is represented with a red square.

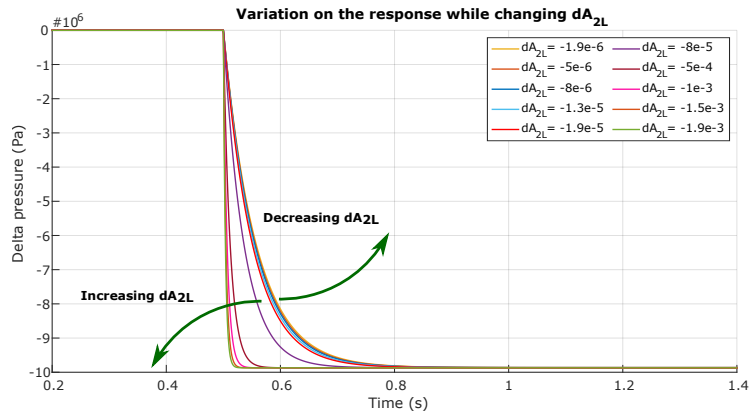


Figure C.12: Plot showing how the response of the system changes when  $\dot{A}_{2L}$  is changed. The original response is represented with a red line.

### $A_{3R}$ and $\dot{A}_{3R}$

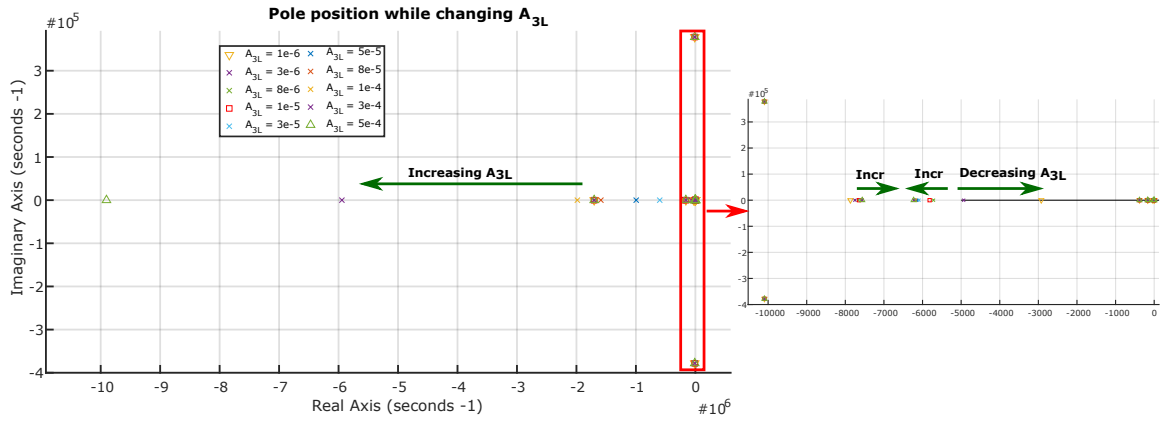


Figure C.13: Position and trend of variation of the poles when the value of  $A_{3R}$  is either increased or decreased. The original value is represented with a red square.

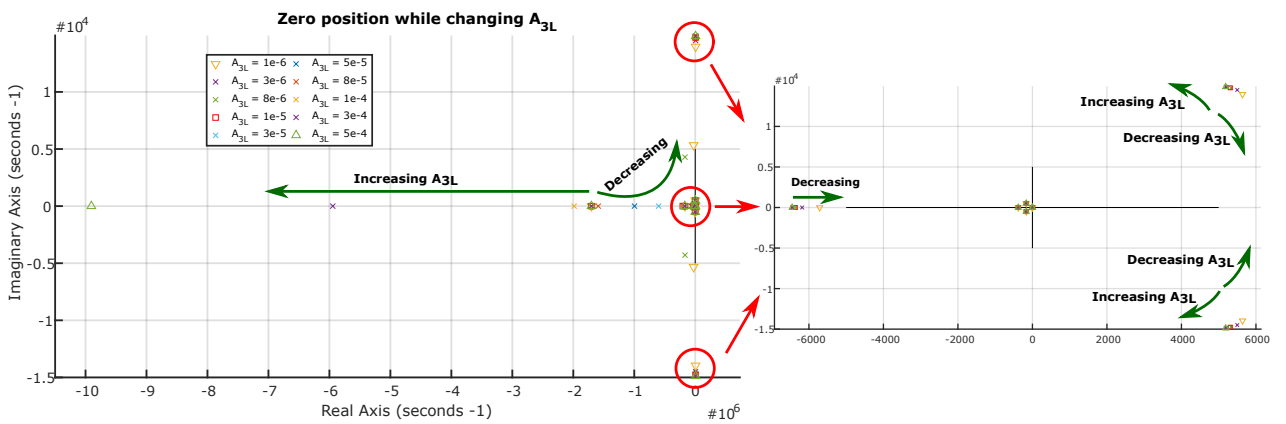


Figure C.14: Position and trend of variation of the zeros when the value of  $A_{3R}$  is either increased or decreased. The original value is represented with a red square.

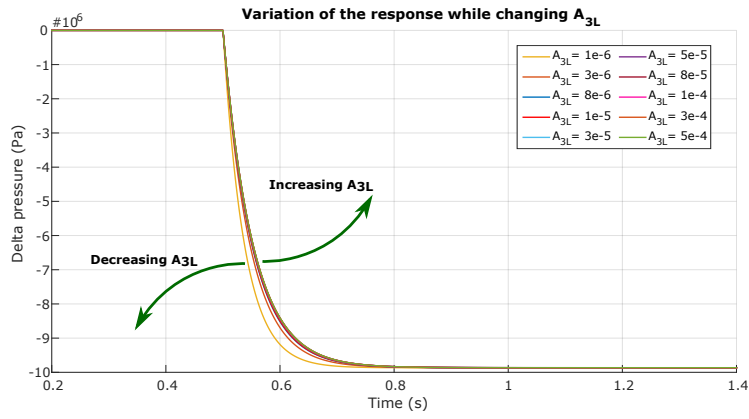


Figure C.15: Plot showing how the response of the system changes when  $A_{3L}$  is changed. The original response is represented with a red line.

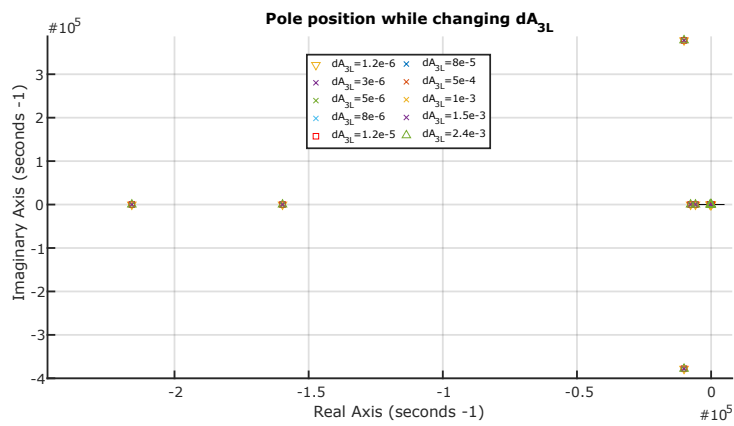


Figure C.16: Position and trend of variation of the poles when the value of  $\dot{A}_{3R}$  is either increased or decreased. The original value is represented with a red square.

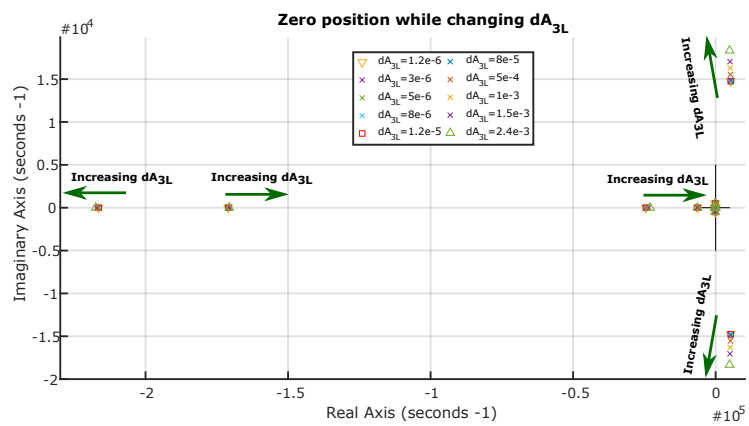


Figure C.17: Position and trend of variation of the zeros when the value of  $\dot{A}_{3R}$  is either increased or decreased. The original value is represented with a red square.

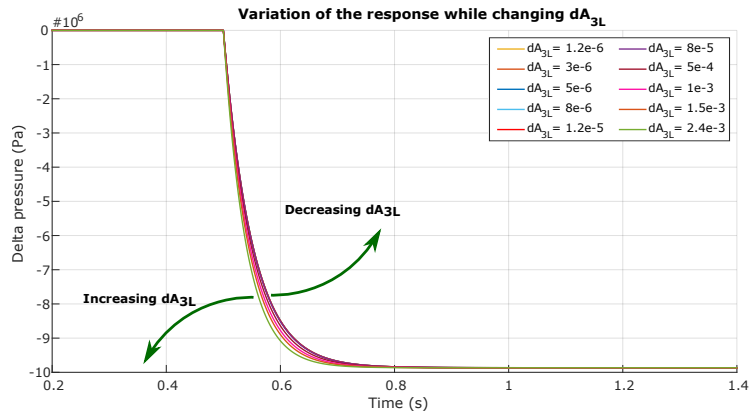


Figure C.18: Plot showing how the response of the system changes when  $\dot{A}_{3L}$  is changed. The original response is represented with a red line.

$A_{3R}$  and  $\dot{A}_{3R}$

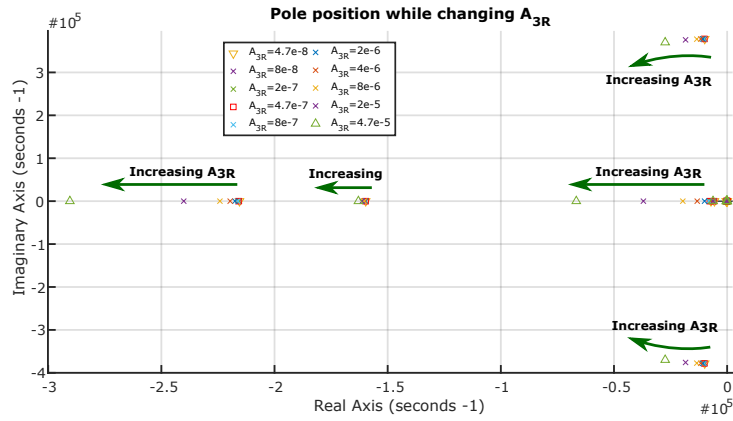


Figure C.19: Position and trend of variation of the poles when the value of  $A_{3R}$  is either increased or decreased. The original value is represented with a red square.

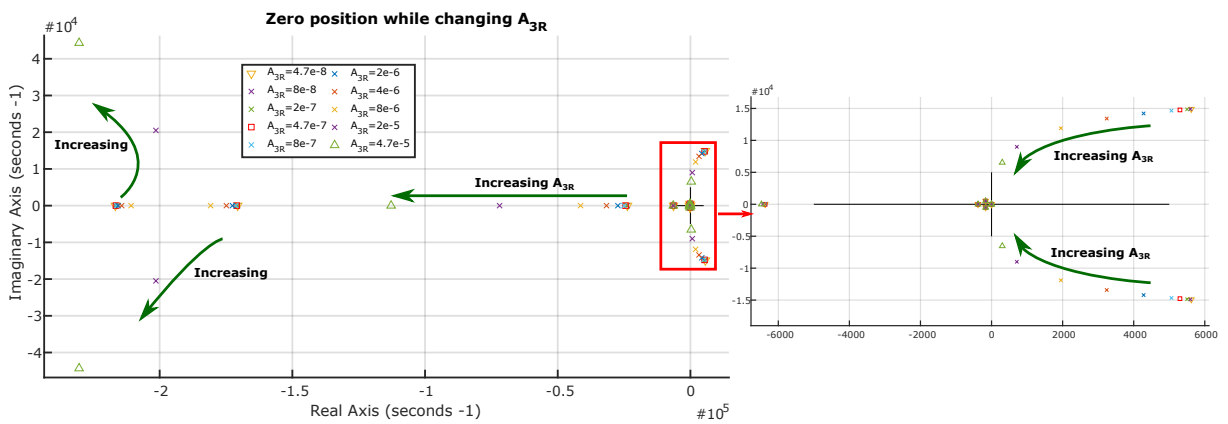


Figure C.20: Position and trend of variation of the zeros when the value of  $A_{3R}$  is either increased or decreased. The original value is represented with a red square.

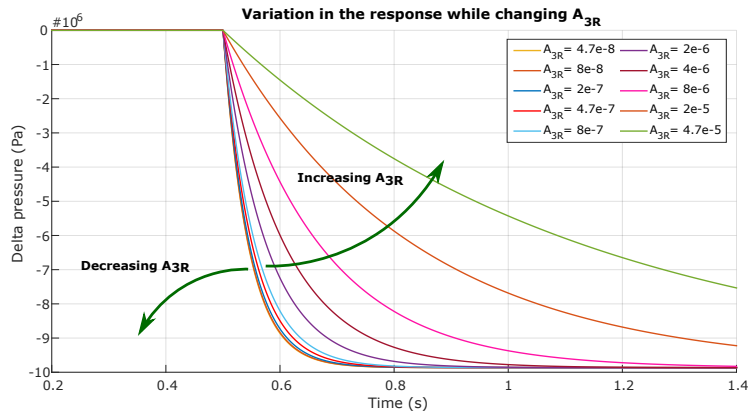


Figure C.21: Plot showing how the response of the system changes when  $A_{3R}$  is changed. The original response is represented with a red line.

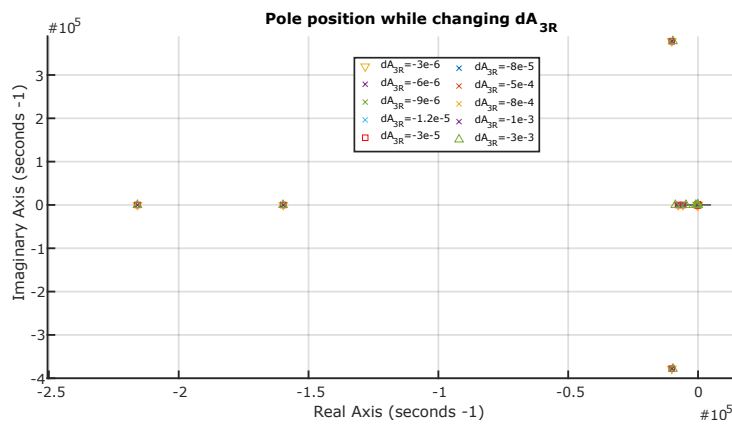


Figure C.22: Position and trend of variation of the poles when the value of  $\dot{A}_{3R}$  is either increased or decreased. The original value is represented with a red square.

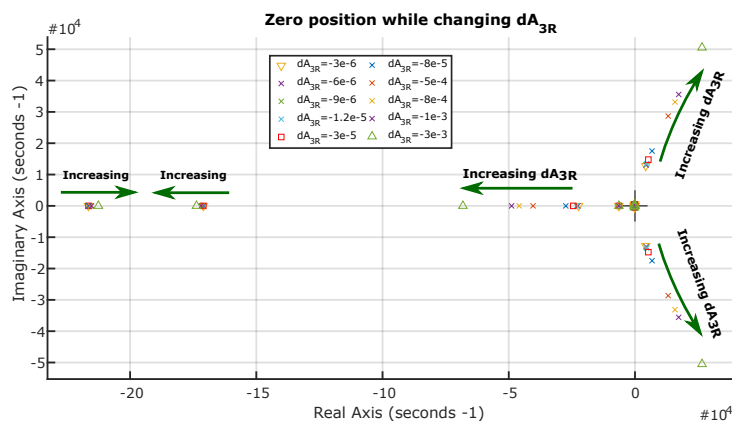


Figure C.23: Position and trend of variation of the zeros when the value of  $\dot{A}_{3R}$  is either increased or decreased. The original value is represented with a red square.

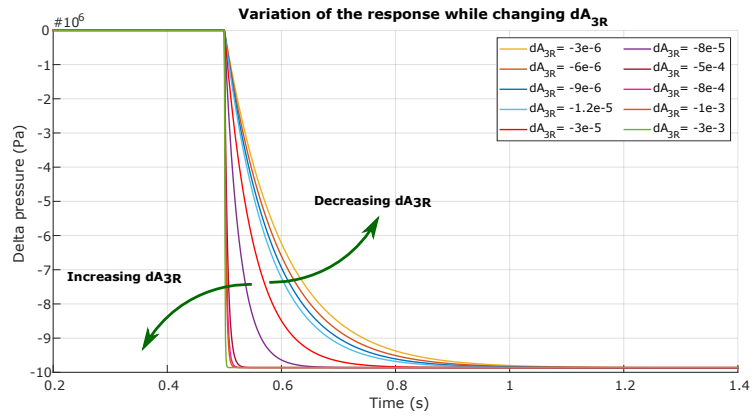


Figure C.24: Plot showing how the response of the system changes when  $\dot{A}_{3R}$  is changed. The original response is represented with a red line.

### $A_1$ and $\dot{A}_1$

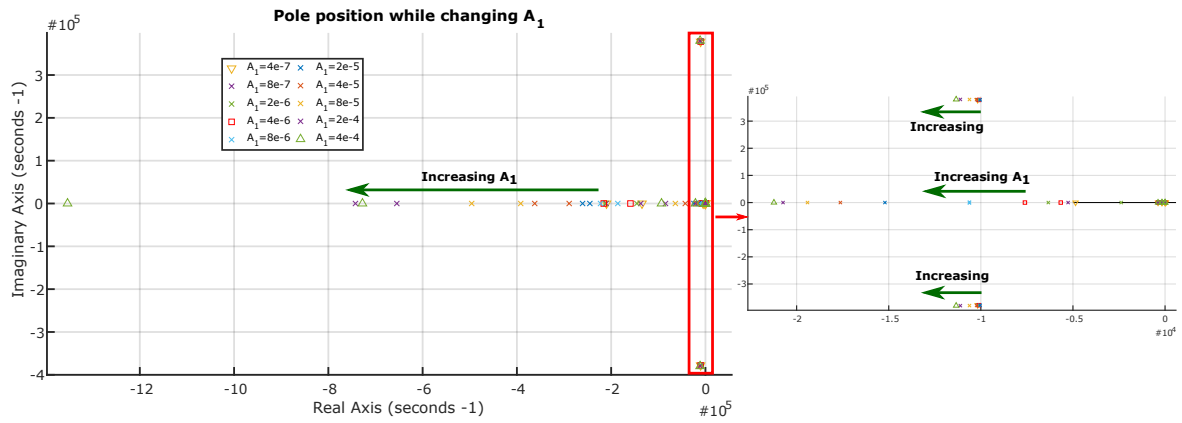


Figure C.25: Position and trend of variation of the poles when the value of  $A_1$  is either increased or decreased. The original value is represented with a red square.

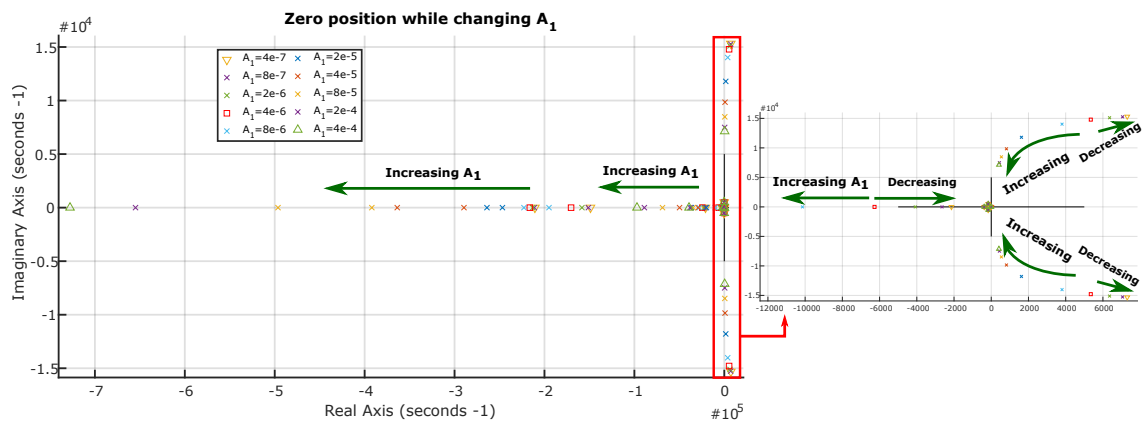


Figure C.26: Position and trend of variation of the zeros when the value of  $A_1$  is either increased or decreased. The original value is represented with a red square.

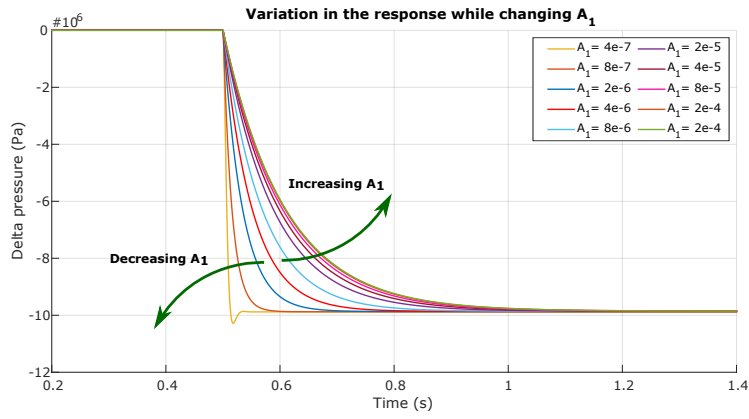


Figure C.27: Plot showing how the response of the system changes when  $A_1$  is changed. The original response is represented with a red line.

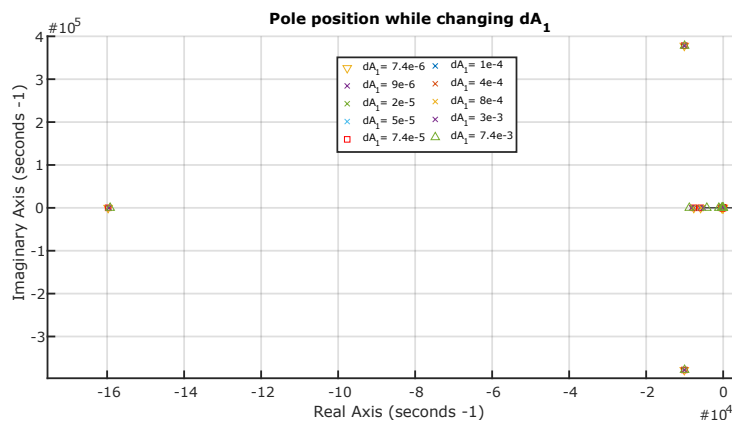


Figure C.28: Position and trend of variation of the poles when the value of  $\dot{A}_1$  is either increased or decreased. The original value is represented with a red square.

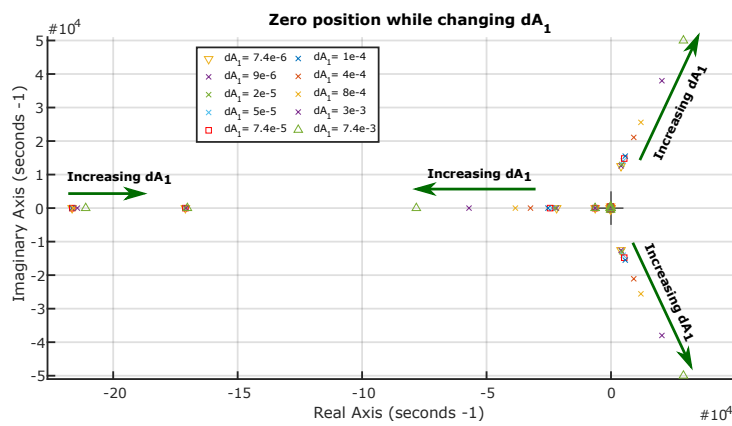
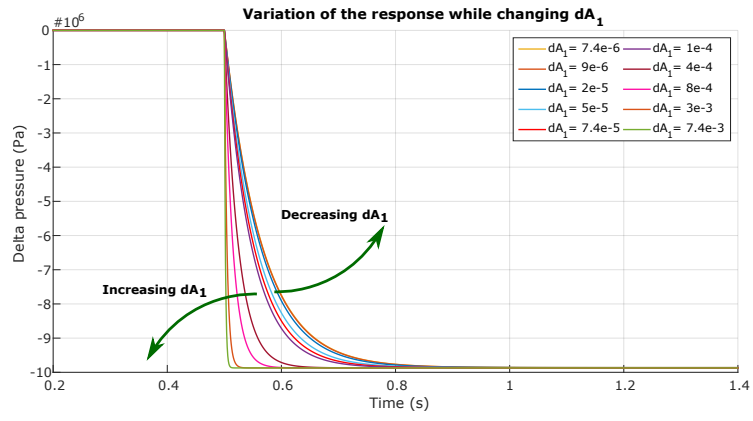


Figure C.29: Position and trend of variation of the zeros when the value of  $\dot{A}_1$  is either increased or decreased. The original value is represented with a red square.



**Figure C.30:** Plot showing how the response of the system changes when  $\dot{A}_1$  is changed. The original response is represented with a red line.